An *in Vitro* and *in Silico* Kinetic Study of a Viral RNA Silencing Suppressor

by

Renata Afi Rawlings

A dissertation submitted in partial fulfillment
of the requirements for the degree of
Doctor of Philosophy
(Biophysics)
in the University of Michigan
2010

Doctoral Committee:

Professor Nils G. Walter, Chair
Professor Hashim M. Al-Hashimi
Professor Ari Gafni
Professor Duncan G. Steel
Associate Professor Alice Telesnitsky

To the Lord Almighty who is my constant support.

ACKNOWLEDGMENTS

There are no words to describe the aid provided to me by my advisor Nils G. Walter, who has been an excellent mentor and scholar under which to train, allowing me into his lab, and giving me the tools to grow into a "true biophysicist". Nils, thank you for being instrumental in my development as a scientist and for always having an open door for questions and ideas.

To the members of my committee, Dr. Hashim Al-hashimi, Dr. Ari Gafni, Dr. Alice Telesnitsky, and Dr. Duncan Steel, I am sincerely grateful for the help and support of such excellent scientists and truly inspiring people. My experience has been enriched by your advice and your insights. Additional mentors include Dr. Patrick Nelson, Drs. Joseph and Lynette Johnson, Dr. Chameree DeSilva, Dr. John Hoertor, Dr. Meridith Newby, and the many others who have given of their time and talents to provide a space for me to pursue new challenges.

It is impossible to overstate the support of my family, loved ones, and friends who have been my foundation in all that I achieve. Specifically, my mother (Illona Sheffey-Rawlings, JD), brother (Michael Sheffey-Rawlings), father (Dr. Keith Rawlings), grandmother (Dr. Ruthe T. Sheffey), and grandfather (Marsden Rawlings), have been instrumental and awe-inspiring with all their help and love.

Without the unfailing support of Stanford C. Goss, Kyla McMullen, The Nottingham family, The McCoy Family, The Quinn family, The Jacobs family, The

CLFMI family, SMES-G, SCOR, AGEP, Debby Mitchell, Carol-Burell Jackson, Angelique Johnson, Charissa Clark, Anabel Rawlings, Vernon R. Sheffey, Lilyan Nottingham and many others, this journey would not have been the successful and rewarding experience it has been.

I would like to especially thank all past and current members of the Walter lab. You have made my experience immeasurably gratifying due to the gift of such a bright and wonderful group of current and future scientists as colleagues and as friends. The caliber of scholarship and support from all of those who have acted as mentors and friends have made Michigan truly live up to the motto "the Leaders and Best." I look forward to hearing about your auspicious careers and sharing in your lives in the years to come.

Renata Afi Rawlings

30 March 2010

TABLE OF CONTENTS

LIST OF FIGURES

LIST OF APPENDICES

LIST OF ABBREVIATIONS

RNA	ribonucleic acid
DNA	deoxyribonucleic acid
RNAi	RNA interference
RISC	RNA induced silencing complex
siRNA	small interfering RNA
miRNA	micro RNA
dsRNA	double-stranded RNA
ncRNA	non-coding RNA
mRNA	messenger RNA
RSS	RNA Silencing Suppression protein
UTR	untranslated region
RdRp	RNA dependent RNA polymerase
Ago2	Argonaute2
RLC	RISC loading complex
CIRV	Carnation Italian Ringspot Virus
SP	siRNA:p19 complex
SD	siRNA:Dicer complex
SDP	siRNA:Dicer:p19 complex
F	fluorescein
T	tetramethylrhodamine
FRET	fluorescence resonance energy transfer
RNase	ribonuclease
MD	molecular dynamics
tr-FRET	time-resolved FRET
EMSA	Electrophoretic mobility shift assay
HPLC	reversed phase high performance liquid chromatography
ELISA	Enzyme-linked immunosorbent assay
PAGE	poly-acrylamide gel electrophoresis
PCR	polymerase chain reaction
kDa	kilo-Dalton
WT	wild type
PNK	polynucleotide kinase
ATP	adenosine triphosphate
NTP	nucleotide triphosphate
DTT	dithiothreitol
EDTA	ethylenediaminetetraacetic
SDS	sodium dodecyl sulfate
TBE	tris-borate-EDTA buffer

ABSTRACT

An *in Vitro* and *in Silico* Kinetic Study of a Viral RNA Silencing Suppressor

by

Renata Afi Rawlings

Chair: Nils G. Walter

RNA interference (RNAi) is a conserved gene regulatory mechanism employed by higher eukaryotes to avert emergent viruses and retrotransposons. During viral infection, the RNase III-type endonuclease Dicer cleaves viral double-stranded RNA into small interfering RNAs (siRNAs), 21-24 nucleotides in length, and helps load them into the RNA-induced silencing complex (RISC) to guide cleavage of complementary viral RNA. As a countermeasure, many viruses have evolved viral RNA silencing suppressor (RSS) proteins that tightly, and presumably quantitatively, bind siRNAs to thwart RNAi-mediated degradation.

Here we report fluorescence quenching and electrophoretic mobility shift assays that probe siRNA binding by the dimeric RSS p19 from Carnation Italian Ringspot Virus (CIRV), as well as by Dicer and RISC assembly complexes. We find that the siRNA:p19 interaction is readily reversible, characterized by rapid binding ($(1.69 \pm 0.07)\times10^{8}$ $M^{-1}s^{-1}$) and marked dissociation ($k_{off} = 0.062 \pm 0.002$ s^{-1}). We also observe that p19 efficiently

competes with recombinant human Dicer and inhibits formation of RISC-related assembly complexes found in human cell extract.

Computational modeling based on these results provides evidence for the formation of a ternary complex between siRNA, p19, and human Dicer. The assumption of an obligatory transient ternary complex intermediate correlates well with the experimentally observed efficient shuttling of an siRNA toward the p19 bound state. A simple model based on this mechanism yields a greater than 20-fold bias in dissociation equilibrium constant for the ternary complex intermediate to dissociate into the siRNA:p19 complex rather than the siRNA:Dicer complex.

We explicitly model the time dependence of the RNAi complexes in response to p19 silencing suppression by monitoring the impact of exogenously introduced p19 on the expression of a messenger RNA targets. We find p19 action to be concentration dependent and able to significantly increase the peak amount of mRNA produced and extend the length of the viral replication phase. From our experimentation and mathematical modeling we can postulate fundamental principles for the optimization of p19 in conjunction with RNAi-based techniques and therapeutics.

Chapter 1:

THE CO-EVOLUTION OF RNA INTERFERENCE AND VIRAL SILENCING SUPPRESSION

1.1 Introduction

In recent decades, it has been hypothesized that the distinction between humans and other mammals is due to either an increased amount of genetic information (DNA) (1), an increased amount of DNA being translated into proteins (2), or the highly complex processing of DNA editing and remodeling (3, 4). Since the birth of molecular biology in 1952 with the famed Hershey – Chase heredity experiment (5) and the subsequent 1953 Watson-Crick DNA structure (6), DNA has been the *molécule de fascination* promising an explanation for disease susceptibility, genetic variation and the source of human complexity. In an influential 1957 presentation, James Crick announced his Central Dogma of Molecular Biology that further solidified DNA as the master molecule, stating essentially that DNA is copied or transcribed into RNA to be translated into proteins, which do the heavy lifting in the cell. If the manual of life, however, is encoded only in our DNA and worked out by our proteins, the initial publications of the Human Genome Project in 2000 should have functionally unlocked the approximately 20,000-25,000 human genes to give unprecedented understanding of genetic information.

Contrary to estimates based on relative size, where the human genome is 30-fold the size of the worm *C. elegans* and 600-fold that of the bacterium *E. coli*, the percentage of human DNA genes encoding proteins was found to be minuscule in comparison to other organisms, amounting to only ~2% (7, 8). The surprise in discovering that over 98.5% of the human genome does not code for proteins was only intensified by the discovery that the majority of this DNA is still being transcribed into RNA, now termed non-coding RNA (ncRNA) for distinction (8). More perplexing still, the amount of non-protein coding RNA, not that of protein coding RNA, is scaling with the complexity of different organisms (2).

The notion that RNA's role in the cell is passive was to be challenged over the next decade due to numerous discoveries that RNA is in fact effecting genetic control and is able to regulate gene expression in a number of ways. This new awareness led to *Science* hailing RNA discoveries as the Breakthrough of the Year in 2002, stating that, "these electrifying discoveries are prompting biologists to overhaul their vision of the cell and its evolution (9)." Since then the sheer number of identified non-coding RNAs has boomed, with varied functions in diverse cellular processes such as suppression of infecting viruses and transposons, cell differentiation, gene regulation, and formation of heterochromatin used to organize chromosomes (8, 10). Although we are closer than ever to dispelling the common misconception that "one gene equals one protein, equals one function", echoes of this central dogma are still found in studies of evolutionary biology.

1.2 The RNA World and Non-coding RNAs

Walter Gilbert, in a 1986 article for *Nature*, outlined a potential scenario for evolution he called the RNA World theory (11). In essence he proposed that RNA molecules, or molecules like them, were the original primordial genetic material and could act to both catalyze their own replication and undertake a wide range of enzymatic activities, including the synthesis of proteins (11). Subsequently, through the eventual processing of RNA into DNA, by reverse transcription, the much more versatile RNA would be finally superseded by the more stable DNA as the primary storehouse of genetic information (12).

Soon after Gilbert's article, Thomas Cech and Sidney Altman were awarded the 1989 Nobel Prize in Chemistry for the two-fold discovery that catalytic RNAs could cut themselves out of larger RNAs (self-splicing introns) and could cut the leader sequence off all transfer RNAs across different species through a protein-assisted RNA enzyme (ribonuclease P) (13, 14). These findings led to a rapid growth in the discovery and characterization of hundreds of diverse non-coding and catalytic RNAs, including self-splicing introns, self-cleaving ribozymes, riboswitches, ribosomal RNAs, and new classes of RNA interference inducers, all with functions outlined below (15).

Splicing occurs when sections of non-coding RNA termed introns are cut out of pre-messenger RNA transcripts resulting in mature mRNA that is translated into protein (16). A multimegadalton RNA-protein complex, called the spliceosome, catalyzes this reaction and is composed of 5 small nuclear ribonucleoprotein complexes that participate in the two transesterification reactions necessary to fully remove the intron and re-ligate

the exons to be translated (17). As a normal phenomenon in eukaryotes, mRNAs can undergo alternative splicing during which exons can be recombined in multiple ways to increase protein diversity. Over 80% of human genes are alternatively spliced with numerous modes of alternative splicing observed (18). Rare introns, classified as group I, and II, have been observed to perform self-splicing through the formation of an RNA enzyme or ribozyme that can do the job of the splicosome while requiring no (or only few) proteins, providing a glimpse into a possible evolutionary cousin to the modern splicosome (14, 17).

Ribozymes are found not only in self-splicing introns but in the genomes of some RNA viruses. For example, the human hepatitis delta virus (HDV) encodes a ribozyme crucial to viral replication (19). The Varkud satellite (VS) ribozyme, found in the bread mold Neurospora, catalyzes the self-cleavage and ligation reactions necessary for the life cycle of the VS RNA (20). Other such molecules, including the hairpin and hammerhead ribozymes, are found in RNA satellites of plant viruses and function to cleave sense and antisense genomic copies of the virus during rolling circle replication (20, 21). The glucosamine-6-phosphate activated *glmS* ribozyme occurs in certain gram-positive bacteria and regulates cellular production of glucosamine-6-phosohate (GlcN6P) by controlling the production of the enzyme in charge of GlcN6P production (22). When concentrations of GlcN6P become elevated, the ribozyme will bind GlcN6P to catalyze its own cleavage, leading to mRNA degradation and ultimately a reduction in the amount of enzyme and indirectly GlcN6P (22, 23). In this way, the ribozyme acts as a negative feedback loop regulating the amount of available enzyme, based on the GlcN6P concentration. Due to the fact that the *glmS* ribozyme can control gene expression in

response to the concentration of a metabolite (i.e., GlcN6P) it is also considered a riboswitch.

Riboswitches in general use the binding of small metabolites to directly regulate the activity of the mRNA they are embedded within (24-26). Mostly contained in feedback loops of bacteria, riboswitches are generally classified by the small ligands they bind and regulate. The TPP riboswitch binds directly to thiamin pyrophosphate (TPP) to regulate genes involved in thiamin biosynthesis and transport, and is the only riboswitch reported in eukaryotes (27, 28). SAM riboswitches bind S-adenosylmethione (SAM) to regulate the expression of proteins involved in sulfur metabolism including the metabolism of methionine, cysteine and SAM (29). PreQ1 riboswitches bind pre-queuosine$_1$ (PreQ1), to regulate the synthesis or transport of this precursor to queuosine (30). The Glycine riboswitch binds glycine to regulate protein components of the glycine cleavage system and metabolism (31). The number and variety of biochemically identified riboswitches is steadily growing due to high conservation of structure and the development of computational identification tools to recognize specific RNA motifs (32).

Arguably the most widespread and abundant enzyme on earth, the ribosome is another powerhouse of RNA. It is composed of two ribonucleoprotein subunits responsible for universal translation of mRNAs into proteins through transfer RNA adapters (33). Assembly of both subunits into a mature ribosome initiates translation on the mRNA template (34). The ribosome then builds the nascent polypeptide chain by binding an aminoacyl-tRNA (aa-tRNA) and checking for a match between the three-nucleotide anticodon of the tRNA and the first codon of the mRNA sequence (35). Transfer of the growing peptide chain from one tRNA onto the next aminoacyl-tRNA

(aa-tRNA) requires high-fidelity proofreading and large dynamic conformational changes with multiple co-factors (34-38).

At the modern forefront, a newly discovered immune and gene regulatory pathway dominates the RNA landscape. First identified in *C. elegans*, RNA interference (RNAi) is a pathway that can use small non-coding RNA fragments as triggers to either destroy invading RNA (i.e., from viruses or transposons) or regulate endogenous gene expression (39). The implications of this discovery led to RNAi being used as a new approach to manipulate gene expression in mammalian cells (40). Researchers have effectively knocked down genes of interest by introducing into a cell small RNAs targeted against that gene. For functional genetics this has offered a wide variety of applications spanning almost all classes of eukaryotes. Also, RNAi is gaining interest as a potential therapeutic strategy with drug design on the horizon (41).

Today the evolutionary theory of the RNA World still has its supporters and detractors, however, it has sparked decades of research into these fascinating molecules and uncovered ever more varied functions. RNA has been risen from relative obscurity, and from being regarded as a simple facilitator of protein translation to a major player in gene regulation, not only in ancient times, but in modern organisms. We now know that RNA molecules can act as enzymes (i.e., ribozymes) (22, 23), regulators of splicing (group I and II introns) (14, 17), genetic switches (riboswitches) (27, 28), universal participants in protein translation (ribosome) (34-38), and complex regulators of massive gene networks as seen in RNAi (39-41). These and other increasingly elaborate biological functions continue to emerge and stand as proof of the varied capabilities of RNA and the relevance of RNA biology.

1.3 RNA Interference

The newest RNA revolution, RNA interference, has sparked a Nobel Prize of its own in 2006, a billion dollar business, and is yet another illustration of the meteoric journey of RNA into the public awareness. The discovery of RNAi began with the research of Rich Jorgensen, a plant biologist, who observed an irregular phenotype in petunias. In his attempts to make a more pigmented petunia Jorgensen observed that he was actually producing non-pigmented white samples. His strategy was to add genes that encoded for additional pigmentation in the hopes of up-regulating the pigment production in the plant (42). Initially his white samples were considered an aberration; however, we now know he was witness to early evidence of the RNA interference pathway.

Since Jorgensen, the role and function of RNAi has been further illuminated. First, in a 1998 *Nature* paper Fire and Mello observed that double-stranded RNA triggers RNAi and stated that, "To our surprise, we found that double-stranded RNA was substantially more effective at producing interference than was either strand individually" (39). In 2000, Zamore *et al.* reported that long double-stranded RNAs (dsRNAs) are processed into smaller fragments in intervals of 21-24 nucleotides by the RNase III type enzyme, Dicer (43). Tuschl and co-workers then arrived at a more biochemical understanding by demonstrating that the functional units of RNAi are small double stranded RNAs and by first describing RNAi in mammalian cells (44).

Presently the understanding of one RNAi pathway is that long double-stranded RNA enters the cytoplasm of a cell and is cleaved by the RNase III type enzyme, Dicer, into small interfering RNA or siRNAs (45-48). These siRNAs are then loaded into an

RNA-induced silencing complex (RISC) that selectively uses one strand of the siRNA as a guide to identify other complementary RNAs in the cell. Once the target RNA is found, the RISC complex works to degrade all targets complementary to the original siRNA sequence (49, 50). In this way, the original message is silenced. It turned out that this silencing was the reason for Jorgensen's white petunias, as he added to his plant samples genes that encoded for more pigmentation he inadvertently triggered Dicer cleavage and the RNAi pathway. RISC used the siRNAs produced by Dicer to suppress or destroy all RNA encoding for pigment, not only the original additions.

Dicer enzymes are thought to play a crucial dual role in RNAi by not only generating mature small interfering RNAs, but by participating in handing them off to the RISC complex. Minimally, RISC is composed of Argonaute proteins, which in both humans and the fruitfly *Drosophila* have been reported to bind siRNA duplexes, degrade one of the two RNA strands (the passenger strand), and initiate sequence-specific cleavage of the target mRNAs using the other strand, the guide strand (51, 52). There are, however, many protein partners of Argonaute that are necessary for full *in vivo* RNA silencing functions (53). Human Dicer is one among the Argonaute protein partners (54) and binds directly to the PIWI domain of human Ago2 (55). This direct binding supports a role for Dicer in siRNA handoff (53) and, consequently, Dicer has been reported to be a key component in several RISC loading complexes (56-59). The importance of handoff has been demonstrated by the work of John Rossi (City of Hope) and Greg Hannon (Cold Spring Harbor), who independently found that longer Dicer substrates (60) or small hairpin RNAs (61) could induce more potent knockdown, by over 100-fold, when compared to mature siRNAs introduced to the cell.

The fundamental steps in RNAi are outlined above, however, there are expanding groups of subfamilies that perform different variations on this theme. The two initially described classes of non-coding RNAs involved in RNAi are the siRNA and micro-RNA (miRNA) pathways. Micro-RNAs, unlike siRNAs, are endogenous products originating in the nucleus of the cell and containing selective non-complementary regions. Once cleaved by Dicer, these molecules are of the same size as siRNAs, but suppress translation as opposed to promoting targeted cleavage of messenger RNAs. MicroRNAs have the added benefit to the host organism of requiring only limited base pairing with a target, enabling them to down-regulate many targets based on short recognition (seed) sequences.

From a bench-top point of view, functional genomics has taken a giant leap forward in that researchers can now knockdown genes of interest and examine their phenotype by introducing siRNAs or a plasmid producing short hairpin RNAs (shRNAs) that mimic the precursor step in miRNA biogenesis. Forms of the RNAi pathway have been found in yeast, plants, invertebrates, and mammals, allowing RNAi tools to be extended to most model systems. Diverse processes from characterizing mouse gene products, to aging and HIV are being studied using RNAi knockdown or silencing, therefore RNAi has rapidly become recognized as a gold standard for manipulating gene expression (62-64).

With RNAi research being applicable to such auspicious targets as HIV and cancer, the major progression of the field has shifted naturally toward therapeutics. Several major companies have been recently founded around this endeavor, and big pharmaceutical companies are eager to get into the market early, as evidenced by the fact

that Merck bought the San Francisco based start up Sirna in 2006 for close to a billion dollars. Clinical trials have begun for an RNAi drug to treat macular degeneration, less than a decade from the technology's discovery. By scientific standards this is remarkably fast, again attesting to the weight given to RNAi's potential impact on the future of science and medicine.

1.4 Viral Suppression of RNAi

Due to the progression of RNAi toward therapeutics, the interactions between RNAi and potentially invading viruses are of central importance to the field. Although RNAi is thriving as a laboratory technique, a 2007 review article states that "the path toward RNAi therapeutics is not as straightforward as initially hoped. The drawbacks with delivery and toxicity that have plagued earlier antisense-based technologies may prove to be an issue for RNAi therapeutics as well (65)." There are numerous *in vitro* approaches and chemical modifications being actively evaluated that show differences in relative merit in animal systems as well as in *in vivo* applications, leaving open questions as to the viability of RNAi techniques for human subjects.

Additionally, viruses have evolved specific mechanisms for evading RNAi knockdown. Induced RNAi resistance involves active viral mRNA rearrangement in the presence of the RNAi pathway, including partial or complete deletion of target sequences, or insertions and mutations within a target (65). Some point mutations outside of the target site can induce a conformational change, rendering the target sequence inaccessible to RISC cleavage (65). Also, there can be intrinsic viral RNAi resistance

where viruses enclose their messenger RNA within a sub-cellular compartment to deny the RNAi machinery access (65). Viral produced proteins can bind mRNA targets and sterically block target sites (65). Lastly, some viruses encode RNA silencing suppressor proteins (RSSs). These proteins act to inhibit or compete with Dicer and/or other RNAi components to decrease the amount of viably loaded RISC complexes (65, 66). Many potent and hazardous viruses produce an RSS either solely or in conjunction with other methods of RNAi resistance to increase infection length and systemic effects. Examples of this counter-defense include the HIV-1 tat protein, Influenza NS1, Ebola VP35, and a host of other plant-based viruses (67-69).

Considered the most ubiquitous mechanism of RSS suppression is the binding or sequestering of small RNA products. Viruses that encode an RSS of this type include HC-Pro of Tobacco etch virus (TEV), p21 of Beet yellows virus (BYV), p122 of Tobacco mosaic virus (cr-TMV), p15 of clump virus, gB of Barley stripe mosaic virus, as well as p19 of the tombusvirus Carnation Italian Ringspot Virus (CIRV) (70-73). All members of the plant virus family tombusviridae produce a small RNA binding, dimeric RSS protein of ~19 kDa molecular weight per monomer (p19). Sequestration and binding of Dicer substrates (small RNAs) by p19 has been observed to correlate with reduced viral mRNA degradation, systemic symptom spread and the sustainability of the viral phenotype after infection observed from *in vivo* studies performed in human cells as well as plants (74-78).

1.5 The Role of the p19 Protein in RNAi Suppression

p19 binds small double-stranded RNAs, and this binding is considered to be a widespread method of viral RNAi suppression (70-73). As one of the earliest examples of this type of RSS, p19 has been used in efforts to boost production of plant-based vaccines for human diseases as well as in conjunction with classical gene therapy vectors to increase protein production levels in lenti- and adenovirus vectors (40, 79).

p19 is a required protein for viral toxicity and spread of symptoms in CIRV and other tombusviruses. It forms soluble homodimers that bind specifically to siRNAs, 19 base pairs in length with 2-nucleotide 3' overhangs (80-82). Independently solved crystal structures (80, 81) and molecular dynamics simulations (82) of p19 dimers in complex with siRNAs show the protein's binding to be length dependent, due to caliper-like stacking on terminal tryptophans, but independent of siRNA sequence, due to nonspecific binding between residues in the protein groove of the dimer and the sugar-phosphate backbone of the RNA duplex. *In vitro* assays, measuring p19 binding, report a tight apparent dissociation equilibrium constant of 0.17 nM for the siRNA:p19 complex (80). In conjunction with the experimentally observed correlation between siRNA binding ability and p19's silencing suppression efficiency, the prevailing description of p19's suppression mechanism is to sequester siRNAs away from the RISC machinery (74-78).

In its natural host, p19 has to compete with an siRNA signal that can be amplified due to the presence of RNA dependent RNA polymerases (RdRp's), increasing the concentration demands on p19 protein production. *In vivo* assays show that p19, due to its sequence independent binding, also associates with miRNAs and possibly any small

duplex RNA of the required length (78, 83). Without additional parameters, this would require stoichiometric binding of a large number of intracellular small RNAs by p19 and would substantially increase the necessary p19 concentration requirements for future applications. Gel-based assays can, however, only give relative affinities for protein binding and will not shed light on the solution kinetics of p19 for its various targets, so to further test the sequestration hypothesis solution-based biophysical techniques are needed.

1.6 Physics in Biology

For decades, physical techniques such as X-ray cystallography, nuclear magnetic resonance, Raman spectroscopy, circular dichroism, and fluorescence resonance energy transfer (FRET) have been staples of molecular research. Some of the founders of molecular biology were originally trained as physicists, including Francis Crick, who co-discovered the double helical structure of DNA with James Watson in 1958, and Max Delbrück, who became a 1969 Nobel laureate in physiology for his discovery that viruses reproduce in a one-step process as opposed to exponentially as cellular organisms. These discoveries and others sparked a movement of physically trained scientists into molecular biology, bolstered by the then recent successes in physics, such as the advent of radar during World War II.

Molecular biologists, over the approximately half century since Watson and Crick deciphered the double-helical structure of DNA, have amassed a truly impressive amount of data regarding the interactions of biological systems, however, with the advent of the

genomic era and increasing discoveries regarding RNAi and large-scale gene regulatory networks, renewed effort has been placed on the search for interesting RNA phenomena. In fact, the field has become so apt in this search that it is experiencing a deluge of information, from which some are now trying to take a step back to examine the larger conclusions. Physicists, accustomed to reducing complex systems to fundamental principles, are in a unique position to help with this effort. Their background in theory and experience in model building can be applied to the explanation of these massive datasets, and the interaction between individual elements.

1.7 The Advantages of Computational Modeling: Speed and Cost

Attempts to bridge the gap between physics and molecular biology have sparked the creation of a relatively new field within biophysics, coined computational biology, which now includes several long-standing branches of collaborative approaches. Computational biology uses advances in physics, computer science, statistics, and applied mathematics to simulate and model complex biological interactions and datasets. Historically, computational biology got its start as systems biology, analogous to systems engineering, due to its overlap in techniques and relation to biological systems. This did not, however, have the same defined scope in biology as it once had in engineering. *Nature Insights* put it best in saying, "When biology ceases to concern itself with the 'systems' of organisms it ceases to be biology (84))." To avoid this confusion, the term computational biology was adopted to more accurately describe the role of predictive mathematics in defining the discipline.

Computational biology has expanded under its new definition and now encompasses a number of subfields, which include bioinformatics, mathematical biology, molecular dynamics, protein structure prediction, and computational biomodeling. Bioinformatics uses statistics and algorithms to sift through large sets of data to make classifications and predict trends, such as aligning sequences for protein homolog comparisons. Mathematical biology aims to mathematically describe these biological systems and has produced new equation sets to describe population growth, cancer, and other intricate processes. Molecular dynamics is the use of extensive structural modeling for observing molecules at an atomic level in simulated environments. Protein, RNA and DNA structure prediction software, such as M-fold, allows for 3-D molecular structures to be generated from only the knowledge of their one-dimensional sequence. Lastly, computational biomodeling focuses on the building of computer models that synthesize and visualize the interactions between molecules to provide a comprehensive view of how distinct changes in individual components affect the outcome of large and/or complex biological networks.

Biomodeling has the benefit of being extremely applicable to the study of human systems. One of the first emerging large-scale studies featured mapping and studying the human brain at a molecular level. The Blue Brain Project founded in 2005 by The Brain and Mind Institute of Switzerland is attempting to reverse-engineer the mammalian brain using biologically realistic neuro-networks to gain insight into the nature of consciousness. Later, a significant amount of work was done in ecology modeling, fueled by advances in descriptive equations from mathematical biology. Large numbers of species interactions were able to be determined, and famously, the effect of wolves or any

large predator on the concentration of prey was predicted by the Lotka-Volterra model equations to be periodic (85, 86).

Complementary to experimental work, the appropriate use of computational modeling to describe and in some ways predict biological outcomes is a powerful tool for research and therapeutic applications. Without computational tools the pace and the expense of ongoing laboratory tests and of subsequent clinical trials become prohibitive, with the average cost of bringing a drug to market exceeding 900 million dollars. Using mathematical tools to potentially model these systems in advance of such trials reduces the cost and increases the speed of conventional drug design, which is becoming restrictive if not impossible.

1.8 Chapter Overviews

Here physical and computational techniques are used to probe the interactions of the viral suppressor p19 on the RNA interference pathway. In Chapter 2, a ratiometric fluorescence quenching assay is reported that probes siRNA binding by the dimeric RSS p19 from Carnation Italian Ringspot Virus (CIRV). The siRNA:p19 interaction is observed to be reversible, characterized by rapid binding ($(1.69 \pm 0.07)\times10^{8}$ $M^{-1}s^{-1}$) and noticeable dissociation (k_{off} = 0.062 ± 0.002 s^{-1}) (Figure 2.2). In Drosophila extract, competition between p19 and siRNA-containing complexes is shown to be time dependent and potent (87). p19 efficiently competes with recombinant human Dicer and inhibits formation of RISC-related assembly complexes found in human cell extract. We also find evidence of a ternary complex between p19, siRNA and human Dicer and,

based on these results, the possible modes of Dicer/p19 competition are tested using computational modeling.

In Chapter 3 we develop two independent models, first, to determine the time-dependent impact of p19 on the RNAi pathway and, second, to assess the mechanism of p19 competition with human Dicer by an alternative steady-state approach. We explicitly investigate the time dependence of the RNAi complexes in response to p19 silencing suppression, and the outcomes of exogenous protein introduction on mRNA accumulation. We observe that high p19 can increase the yield of a virally introduced gene of interest by up to 10-fold for the concentrations tested, but has a much more significant effect on the infection, increasing the effective length of infection by over 100-fold. Additionally, p19 is observed to reinitiate mRNA accumulation even after suppression has been achieved, suggesting active RNAi is needed to maintain viral repression. We confirm evidence of a ternary complex between p19, siRNA, and human Dicer and numerically determine rate constants for this interaction that reproduces experimental competition data. Using these rates we can achieve viral accumulation levels consistent with previous experimental literature data from using p19 in support of gene therapy vectors.

Additionally, Chapter 4 discusses miRNA binding experiments in human cytosolic extract as well as the potential use of miRNAs for *in vivo* localization experiments. We measure equivalent p19 binding affinities for siRNA and miRNA substrates, highlighting the substrate diversity of p19 *in vivo*. Chapter 5 summarizes and discusses all results and provides future directions for both models and experiments.

1.9 References

1. Fields C, Adams MD, White O, & Venter JC (1994) How many genes in the human genome? *Nat Genet* **7**(3):345-346
2. Pennisi E (2007) Genomics. DNA study forces rethink of what it means to be a gene. *Science* **316**(5831):1556-1557
3. Neely KE & Workman JL (2002) The complexity of chromatin remodeling and its links to cancer. *Biochim Biophys Acta* **1603**(1):19-29
4. Turelli P & Trono D (2005) Editing at the crossroad of innate and adaptive immunity. *Science* **307**(5712):1061-1065
5. Hershey AD & Chase M (1952) Independent functions of viral protein and nucleic acid in growth of bacteriophage. *J. Gen Physiol.* **36**:39-56.
6. Waston JD & Crick FHC (1953) A Structure for Deoxyribose Nucleic Acid. *Nature* **171**:737-738.
7. Hahn MW & Wray GA (2002) The g-value paradox. *Evol Dev* **4**(2):73-75
8. Szymanski M, Barciszewska MZ, Zywicki M, & Barciszewski J (2003) Noncoding RNA transcripts. *J Appl Genet* **44**(1):1-19
9. Couzin J (2002) Breakthrough of the year. Small RNAs make big splash. *Science* **298**(5602):2296-2297
10. Kurth HM & Mochizuki K (2009) Non-coding RNA: a bridge between small RNA and DNA. *RNA Biol* **6**(2):138-140
11. Gilbert W (1986) The RNA World. *Nature* **319**: 618.

12. Klyce B (The RNA World.) (web).

13. Altman S*, et al.* (1989) Catalysis by the RNA subunit of RNase P--a minireview. *Gene* **82**(1):63-64

14. Cech TR (1990) Self-splicing of group I introns. *Annu Rev Biochem* **59**:543-568

15. Walter NG & Engelke DR (2002) Ribozymes: catalytic RNAs that cut things, make things, and do odd and useful jobs. *Biologist (London)* **49**(5):199-203

16. Crick F (1979) Split genes and RNA splicing. *Science* **204**(4390):264-271

17. Ritchie DB, Schellenberg MJ, & MacMillan AM (2009) Spliceosome structure: piece by piece. *Biochim Biophys Acta* **1789**(9-10):624-633

18. Matlin AJ, Clark F, & Smith CW (2005) Understanding alternative splicing: towards a cellular code. *Nat Rev Mol Cell Biol* **6**(5):386-398

19. Asif-Ullah M, Levesque M, Robichaud G, & Perreault JP (2007) Development of ribozyme-based gene-inactivations; the example of the hepatitis delta virus ribozyme. *Curr Gene Ther* **7**(3):205-216

20. Cochrane JC & Strobel SA (2008) Catalytic strategies of self-cleaving ribozymes. *Acc Chem Res* **41**(8):1027-1035

21. Doherty EA & Doudna JA (2001) Ribozyme structures and mechanisms. *Annu Rev Biophys Biomol Struct* **30**:457-475

22. Winkler WC, Nahvi A, Roth A, Collins JA, & Breaker RR (2004) Control of gene expression by a natural metabolite-responsive ribozyme. *Nature* **428**(6980):281-286

23. Cochrane JC, Lipchock SV, & Strobel SA (2007) Structural investigation of the GlmS ribozyme bound to Its catalytic cofactor. *Chem Biol* **14**(1):97-105

24. Tucker BJ & Breaker RR (2005) Riboswitches as versatile gene control elements. *Curr Opin Struct Biol* **15**(3):342-348

25. Vitreschak AG, Rodionov DA, Mironov AA, & Gelfand MS (2004) Riboswitches: the oldest mechanism for the regulation of gene expression? *Trends Genet* **20**(1):44-50

26. Batey RT (2006) Structures of regulatory elements in mRNAs. *Curr Opin Struct Biol* **16**(3):299-306

27. Sudarsan N, Barrick JE, & Breaker RR (2003) Metabolite-binding RNA domains are present in the genes of eukaryotes. *RNA* **9**(6):644-647

28. Kubodera T*, et al.* (2003) Thiamine-regulated gene expression of Aspergillus oryzae thiA requires splicing of the intron containing a riboswitch-like domain in the 5'-UTR. *FEBS Lett* **555**(3):516-520

29. Montange RK & Batey RT (2006) Structure of the S-adenosylmethionine riboswitch regulatory mRNA element. *Nature* **441**(7097):1172-1175

30. Roth A*, et al.* (2007) A riboswitch selective for the queuosine precursor preQ1 contains an unusually small aptamer domain. *Nature structural & molecular biology* **14**(4):308-317

31. Mandal M*, et al.* (2004) A glycine-dependent riboswitch that uses cooperative binding to control gene expression. *Science* **306**(5694):275-279

32. Bengert P & Dandekar T (2004) Riboswitch finder--a tool for identification of riboswitch RNAs. *Nucleic Acids Res* **32**:W154-159

33. Ditzler MA, Aleman EA, Rueda D, & Walter NG (2007) Focus on function: single molecule RNA enzymology. *Biopolymers* **87**(5-6):302-316

34. Rodnina MV, Beringer M, & Wintermeyer W (2006) Mechanism of peptide bond formation on the ribosome. *Q Rev Biophys* **39**(3):203-225

35. Ogle JM & Ramakrishnan V (2005) Structural insights into translational fidelity. *Annu Rev Biochem* **74**:129-177

36. Ramakrishnan V (2002) Ribosome structure and the mechanism of translation. *Cell* **108**(4):557-572

37. Blanchard SC, Kim HD, Gonzalez RL, Jr., Puglisi JD, & Chu S (2004) tRNA dynamics on the ribosome during translation. *Proc Natl Acad Sci U S A* **101**(35):12893-12898

38. Munro JB, Altman RB, O'Connor N, & Blanchard SC (2007) Identification of two distinct hybrid state intermediates on the ribosome. *Mol Cell* **25**(4):505-517

39. Fire A, *et al.* (1998) Potent and specific genetic interference by double-stranded RNA in Caenorhabditis elegans. *Nature* **391**:806-881.

40. de Vries W, *et al.* (2008) Increased virus replication in mammalian cells by blocking intracellular innate defense responses. *Gene Ther* **15**(7):545-552

41. Tiemann K & Rossi JJ (2009) RNAi-based therapeutics-current status, challenges and prospects. *EMBO Mol Med* **1**(3):142-151

42. Napoli C, Lemieux C, & Jorgensen R (1990) Introduction of a Chimeric Chalcone Synthase Gene into Petunia Results in Reversible Co-Suppression of Homologous Genes in trans. *Plant Cell* **2**(4):279-289

43. Zamore PD, Tuschl T, Sharp PA, & Bartel DP (2000) RNAi: Double-stranded RNA directs the ATP-dependent cleavage of mRNA at 21-23 nucleotide intervals. . *Cell* (101):25-33.

44. S. M. Elbashir JH, W. Lendeckel, A. Yalcin, Klaus Weber, T. Tuschl, (2001) Duplexes of 21-nucleotide RNAs mediate RNA interference in cultured mammalian cells. *Nature* **411**:494-498.

45. Carthew RW & Sontheimer EJ (2009) Origins and Mechanisms of miRNAs and siRNAs. *Cell* **136(**4):642-655

46. Chellappan P, Vanitharani R, & Fauquet CM (2005) MicroRNA-binding viral protein interferes with Arabidopsis development. *Proc Natl Acad Sci U S A* **102**(29):10381-10386

47. Baulcombe D (2004) RNA silencing in plants. *Nature* **431**:356-363

48. Ding SW & Voinnet O (2007) Antiviral immunity directed by small RNAs. *Cell* **130**(3):413-426

49. Ji X (2008) The mechanism of RNase III action: how dicer dices. *Curr Top Microbiol Immunol* **320**:99-116

50. Siomi H & Siomi MC (2009) On the road to reading the RNA-interference code. *Nature* **457**(7228):396-404

51. Liu J, *et al.* (2004) Argonaute2 is the catalytic engine of mammalian RNAi. *Science* **305**(5689):1437-1441

52. Meister G, *et al.* (2004) Human Argonaute2 mediates RNA cleavage targeted by miRNAs and siRNAs. *Mol Cell* **15**(2):185-197

53. Yang J & Yuan YA (2009) A structural perspective of the protein-RNA interactions involved in virus-induced RNA silencing and its suppression. *Biochim Biophys Acta* **1789**(9-10):642-652

54. Hammond SM, Boettcher S, Caudy AA, Kobayashi R, & Hannon GJ (2001) Argonaute2, a link between genetic and biochemical analyses of RNAi. *Science* **293**(5532):1146-1150

55. Tahbaz N, *et al.* (2004) Characterization of the interactions between mammalian PAZ PIWI domain proteins and Dicer. *EMBO Rep* **5**(2):189-194

56. Liu Q, *et al.* (2003) R2D2, a bridge between the initiation and effector steps of the Drosophila RNAi pathway. *Science* **301**(5641):1921-1925

57. Liu X, *et al.* (2007) Dicer-1, but not Loquacious, is critical for assembly of miRNA-induced silencing complexes. *RNA* **13**(12):2324-2329

58. Gregory RI, Chendrimada TP, Cooch N, & Shiekhattar R (2005) Human RISC couples microRNA biogenesis and posttranscriptional gene silencing. *Cell* **123**(4):631-640

59. Chendrimada TP, *et al.* (2005) TRBP recruits the Dicer complex to Ago2 for microRNA processing and gene silencing. *Nature* **436**(7051):740-744

60. Kim DH, *et al.* (2005) Synthetic dsRNA Dicer substrates enhance RNAi potency and efficacy. *Nat Biotechnol* **23**(2):222-226

61. Siolas D, *et al.* (2005) Synthetic shRNAs as potent RNAi triggers. *Nat Biotechnol* **23**(2):227-231

62. Lee SK & Kumar P (2009) Conditional RNAi: towards a silent gene therapy. *Adv Drug Deliv Rev* **61**(7-8):650-664

63. Grimm D (2009) Small silencing RNAs: state-of-the-art. *Adv Drug Deliv Rev* **61**(9):672-703

64. Umbach JL & Cullen BR (2009) The role of RNAi and microRNAs in animal virus replication and antiviral immunity. *Genes Dev* **23**(10):1151-1164

65. Haasnoot J, Westerhout EM, & Berkhout B (2007) RNA interference against viruses: strike and counterstrike. *Nat Biotechnol* **25**(12):1435-1443

66. Li F & Ding SW (2006) Virus counterdefense: diverse strategies for evading the RNA-silencing immunity. *Annu Rev Microbiol* **60**:503-531

67. Qu F & Morris TJ (2005) Suppressors of RNA silencing encoded by plant viruses and their role in viral infections. *FEBS Lett* **579**(26):5958-5964

68. Roth BM, Pruss GJ, & Vance VB (2004) Plant viral suppressors of RNA silencing. *Virus Res* **102**(1):97-108

69. Voinnet O (2001) RNA silencing as a plant immune system against viruses. *Trends Genet* **17**(8):449-459

70. Csorba T, Bovi A, Dalmay T, & Burgyan J (2007) The p122 subunit of Tobacco Mosaic Virus replicase is a potent silencing suppressor and compromises both small interfering RNA- and microRNA-mediated pathways. *J Virol* **81**(21):11768-11780

71. Lakatos L*, et al.* (2006) Small RNA binding is a common strategy to suppress RNA silencing by several viral suppressors. *EMBO J* **25**(12):2768-2780.

72. Lozsa R, Csorba T, Lakatos L, & Burgyan J (2008) Inhibition of 3' modification of small RNAs in virus-infected plants require spatial and temporal co-expression of small RNAs and viral silencing-suppressor proteins. *Nucleic Acids Res* **36**(12):4099-4107

73. Merai Z, *et al.* (2006) Double-stranded RNA binding may be a general plant RNA viral strategy to suppress RNA silencing. *J Virol* **80**(12):5747-5756

74. Chu M, Desvoyes B, Turina M, Noad R, & Scholthof HB (2000) Genetic dissection of tomato bushy stunt virus p19-protein mediated host-dependent symptom induction and systemic invasion. *Virology* (266):79-87.

75. Omarov R, Sparks K, Smith L, Zindovic J, & Scholthof HB (2006) Biological relevance of a stable biochemical interaction between the tombusvirus-encoded P19 and short interfering RNAs. *J Virol* **80**(6):3000-3008

76. Silhavy D, *et al.* (2002) A viral protein suppresses RNA silencing and binds silencing-generated, 21- to 25-nucleotide double-stranded RNAs. *EMBO J.* **21**:3070-3080.

77. Havelda Z, Hornyik C, Valoczi A, & Burgyan J (2005) Defective Interfering RNA Hinders the Activity of a Tombusvirus-Encoded Posttranscriptional Gene Silencing Suppressor. *J Virol* (79):450-457.

78. Dunoyer P, Lecellier CH, Parizotto EA, Himber C, & Voinnet O (2004) Probing the microRNA and small interfering RNA pathways with virus-encoded suppressors of RNA silencing. *Plant Cell* **16**(5):1235-1250

79. Zheng N, *et al.* (2009) Boosted expression of the SARS-CoV nucleocapsid protein in tobacco and its immunogenicity in mice. *Vaccine* **27**(36):5001-5007

80. Vargason JM, Szittya G, Burgyan J, & Hall TM (2003) Size selective recognition of siRNA by an RNA silencing suppressor. *Cell* (115):799-811.

81. Ye K, Malinina L, & Patel DJ (2003) Recognition of siRNA by a viral suppressor of RNA silencing. *Nature* (426):874-878.

82. Xia Z, Zhu Z, Zhu J, & Zhou R (2009) Recognition mechanism of siRNA by viral p19 suppressor of RNA silencing: a molecular dynamics study. *Biophys J* **96**(5):1761-1769

83. Chapman EJ, Prokhnevsky AI, Gopinath K, Dolja VV, & Carrington JC (2004) Viral RNA silencing suppressors inhibit the microRNA pathway at an intermediate step. *Genes Dev* **18**(10):1179-1186

84. Surridge C (2002) Computational Biology. *Nature* 420(6912).

85. Jost C, Devulder G, Vucetich JA, Peterson R, & Arditi R (2005) The wolves of Isle Royale display scale-invariant satiation and density dependent predation on moose. *Amimal Ecology* **74**(5):809-816.

86. Lotka AJ (1910) Contribution to the Theory of Periodic Reaction. *J. Phys. Chem* **14**(3):271-274.

87. Lakatos L, Szittya G, Silhavy D, & Burgyan J (2004) Molecular mechanism of RNA silencing suppression mediated by p19 protein of tombusviruses. *EMBO J* **23**(4):876-884.

Chapter 2:

CATCH AND RELEASE: VIRAL RNA SILENCING SUPPRESSOR COMPETES WITH HUMAN DICER AND IMPAIRS RISC ASSEMBLY BY REVERSIBLY BINDING SIRNA

2.1 Introduction

Over the past decade, RNA interference (RNAi) has become recognized as both an innate eukaryotic immune response against viral pathogens or transposons, and a benchmark laboratory and potentially clinical tool to control gene expression (1-6). During viral infection, eukaryotes activate RNAi where viral RNA is specifically recognized by the cytoplasmic RNase III-type endonuclease Dicer and degraded by an RNA-induced silencing complex (RISC). Dicer cleaves exposed stretches of double-stranded RNA into small interfering RNAs (siRNAs) 21-24 nucleotides in length (depending on species). Dicer then delivers the double-stranded siRNA to the RNA-induced silencing complex (RISC) (7, 8), where the passenger strand of the duplex is cleaved and released while the guide strand is retained to guide specific cleavage of complementary viral RNA genomes or transcripts (9, 10). Dicer is thus thought to play a critical dual role in RNAi by both generating virus-specific siRNA duplexes and assembling them with the necessary protein components into active RISC (11).

To subvert the host RNAi response many viruses have evolved small proteins that act as RNA silencing suppressors (RSSs) (12-14). One of the best characterized RSSs is exemplified in the plant pathogen Carnation Italian Ringspot Virus (CIRV), which encodes a 19 kDa protein termed p19, an important pathogenicity factor that is highly conserved among all tombusviruses (15). Crystal structures (16, 17) and recent molecular dynamics simulations (18) show that homodimers of p19 bind a single siRNA duplex in a positively charged surface cleft (Figure 2.1*A*). Pairs of tryptophan residues stack on both terminal base pairs to establish a sequence-independent, caliper-like size selection for siRNA duplexes with 19 base pairs and 2-nucleotide long 3′-overhangs. Sequestration and binding of Dicer-generated siRNAs by p19 has been observed to correlate with reduced viral RNA degradation, systemic symptom spread, and sustainability of the viral phenotype after infection (19-24). Previous electrophoretic mobility shift assays (EMSAs) have suggested that the affinity of dimeric p19 for siRNA is high with an apparent equilibrium dissociation constant of $K_{D,app}$ = 0.17 ± 0.02 nM (16). These findings are consistent with a widely accepted sequestration model wherein the p19 dimer more or less quantitatively binds siRNA duplexes to suppress RNAi (15, 21). Such double-stranded RNA binding is considered to be the most common RSS mechanism (26-29), yet measurements of siRNA binding and dissociation kinetics to directly test the quantitative sequestration model have not been reported for any RSS protein.

Here we develop solution-based fluorescence quenching assays that observe siRNA:p19 (SP) binding to be readily reversible with not only a rapid binding rate constant ($(1.69 \pm 0.07)\times10^8$ $M^{-1}s^{-1}$), but also a dissociation rate constant (k_{off} = 0.062 ± 0.002 s^{-1}) markedly faster than those of slow-release nucleic acid binding proteins (30,

31). Our results are consistent, within error, with the high apparent affinity measured in EMSAs, yet also call into question a simple sequestration model. Where irreversible binding would require the virus to generate sufficient quantities of p19 dimer to quantitatively bind (nearly) all small RNAs produced enzymatically by either Dicer cleavage or the amplification effected in a plant cell through RNA-dependent RNA polymerase (3), reversibility of SP complex formation opens the possibility that multiple turnover may potentiate p19's efficacy as RSS. In particular, if p19 were to disrupt the siRNA:Dicer (SD) interaction via multiple turnover, it would potently interfere with the role of Dicer as obligatory RISC assembly factor.

Consistent with such a mechanism of p19 action, we observe efficient competition of p19 with recombinant human Dicer for siRNA binding, and prominent disruption of RISC assembly complexes observed in human HeLa cell extract. Mathematical modeling demonstrates that the Dicer competition data are only accurately reproduced assuming the formation of a transient ternary complex, siRNA:Dicer:p19 (SDP). Taken together, a multiple-turnover "catch and release" mechanism emerges where p19 repeatedly promotes dissociation of SD complexes to efficiently suppress Dicer-mediated RISC assembly.

2.2 Materials and Methods

Sources of p19, Dicer, and RNA. Purified p19 protein was prepared as previously described (16), and its dimer concentration was measured by Bradford assay. Active recombinant human Dicer in a crude extract was obtained from Genlantis at a

purity of 5%; it is not known what other RISC related components this extract may contain. The concentration of total protein was verified by Bradford assay. All RNAs were synthesized by the HHMI Biopolymer/Keck Foundation Biotechnology Resource Laboratory at the Yale University School of Medicine, then deprotected and purified as previously described (34, 35). Sequences were derived from the firefly luciferase gene (36) and were as follows: Sense strand 5′-P-CGU ACG CGG AAU ACU UCG AAA-3′; antisense strand 5′-P-UCG AAG (Fluorescein-dT)AU UCC GCG (Amino C6-dT)AC GUG-3′, where P denotes a 5′-phosphate, and Fluorescein-dT and Amino C6-dT denote the phosphoramidites of the same name from Glen Research; the antisense strand was also synthesized with only one or no modification wherein U replaced the modified dT. Where needed, tetramethylrhodamine was coupled to the Amino C6 linker and the RNA purified as described (34).

Steady-State Fluorescence Spectroscopy. Standard fluorescence measurements were performed on an Aminco Bowman spectrofluorometer (Thermo Scientific) at 37 ^{o}C. siRNA duplexes were formed by mixing an excess of 100 nM of unlabeled sense strand with 50 nM labeled sense strand in near-physiologic standard buffer (50 mM Tris-Acetate, pH 7.4, 80 mM KCl, 20 mM NaCl, 1 mM $MgCl_2$, 1 mM DTT, 0.02% (v/v) Tween 20), heat annealing for 2 min at 70 ^{o}C, and cooling to room temperature over 5 min. Fluorescein/tetramethylrhodamine doubly-labeled siRNAs were excited at 490 nm (4 nm slit width) and emission alternately detected at 520 nm (for fluorescein, F) and 585 nm (8 nm slit width, for tetramethylrhodamine, T) to calculate the T/F ratio; F or T singly-labeled siRNAs were excited/detected at 490/520 nm or 565/585nm, respectively.

In a typical experiment, p19 was added to 50 nM labeled siRNA and mixed manually to a final concentration of 500 nM unless otherwise indicated. For a chase experiment, unmodified siRNA duplex (formed through annealing the unlabeled composite sense and antisense RNA strands in a 2:1 ratio in standard buffer) was added to a final concentration of 3 μM. Saturation by the chase was ensured by triplicate trials using 500 nM, 750 nM, 1.5 μM, and 3 μM (Figure A1).

To observe fast SP complex formation, siRNA samples were prepared as above in standard buffer to a final concentration of 40 nM. In standard buffer p19 was added to varying (at least 8-fold) final excess concentrations (0.32 – 1.76 μM) at 37 ^{o}C in a KinTek PMA23B stopped-flow spectrofluorometer while exciting at 520 nm and detecting emission at 585 nm. All time course were fit with single-exponential increase or decrease functions in Origin (OriginLab) as described (37).

Time-Resolved FRET. Time-resolved donor (fluorescein, F) fluorescence decays were collected in the presence and absence of acceptor (tetramethylrhodamine, T) using time-correlated single-photon counting, as previously described (38, 39). As before, the donor decay in the presence of acceptor was modeled as a weighted average of the decays for each donor-acceptor distance in the ensemble of molecules assuming a three-dimensional Gaussian distance distribution with a Förster distance of 54 Å between F and T (38, 39).

EMSA. For radioactive EMSAs the non-phosphorylated antisense strand was first 5′-^{32}P labeled with T4 polynucleotide kinase (PNK) and γ-^{32}P-ATP at an RNA

concentration of 800 nM. PNK was inactivated by heating to 90 °C for 10 min, then the 5′ phosphorylated complementary strand was added in 2-fold molar excess and the reaction slowly cooled to room temperature to anneal the two strands. The siRNA duplex was further purified by nondenaturing, 20% (w/v) polyacrylamide gel electrophoresis. The duplex siRNA was cut out, eluted overnight into 1 mM EDTA at 4 ^{o}C, ethanol precipitated, and dissolved in RNase-free water. Scintillation counting was done on a Beckman LS6500 Multipurpose Scintillation Counter. EMSAs were performed as described previously (16) on 10-cm non-denaturing 12% (w/v) polyacrylamide gels in 0.5x TBE (44.5 mM Tris-Borate, 1 mM EDTA) and run at 500 V and 4 ^{o}C for 2 h. Dicer and p19 at varying final concentrations were added to radiolabeled siRNA duplex (50,000 cpm, < 400 pM of 5′-^{32}P labeled duplex) in 10 μL standard buffer and incubated for 0.5 hrs. Next, 10 μL non-denaturing loading buffer (10% glycerol, 0.5x TBE, 0.025% bromophenol blue, and 0.025% xylene cyanol) was added and each sample loaded into a well of the EMSA gel. Competition experiments were performed by preincubating < 400 pM siRNA duplex (prepared as above) in standard buffer either with 140 nM Dicer and increasing concentrations of p19, or with 0.17 nM or 2.5 nM p19 and increasing concentrations of Dicer. Gels were wrapped in plastic wrap and exposed to phosphor screens, which were scanned on a Storm 840 PhosphorImager and quantified using Image Quant software (Molecular Dynamics). The relative fraction f of relevant protein complexes was fit with the following hyperbolic binding isotherm to extract saturation point f_{max} and half-titration point $K_{D,app}$:

$$f = f_{\max} \frac{[protein]}{[protein] + K_{D,app}}$$

RISC Assembly Complex Formation. To observe RISC assembly complexes 15, 50, 75% (v/v) cytosolic HeLa cell extract (Jena Bioscience) was incubated with < 400 pM siRNA duplex (prepared as above) in a final volume of 10 μL HeLa buffer [8% (v/v) Lysis Buffer (23.7 mM HEPES, pH 7.5, 79 mM potassium acetate, 1.58 mM magnesium acetate, 5 mM DTT, and 1 mg/ml Perabloc SC (Roche)), supplemented with 20% (v/v) 5x RNAi mix (125 mM creatine phosphate, 5 mM ATP, 25 mM DTT), 2% (w/v) creatine kinase, and 20% (v/v) RNA guard RNase Inhibitor (GE Bioscience)] for 2 h at 4 ^{o}C, unless otherwise specified. For competition experiments, p19 was added in increasing concentrations to the HeLa cell extract/siRNA mixture either immediately or after a 2 h preincubation. Time courses were stopped by direct loading onto a running nondenaturing 4% (w/v) polyacrylamide gel in 0.5x TBE (44.5 mM Tris-Borate, 1 mM EDTA), run at ~50 mW/cm^2 and 4 ^{o}C. For comparison with a previous assay, 50 and 75% (v/v) Hela cell extract was incubated with siRNA as described in (40) for 1 h at 4 ^{o}C to 37 ^{o}C and analyzed by EMSA, yielding similar results (Fig S3). 15% (v/v) extract was preferred for most of our work due to the better pH control afforded by this lower concentration and to better conserve material. For antibody supershift EMSA, 24 μg of cytosolic HeLa cell extract was pre-incubated with 0.8 μg or 1.6 μg of anti-Dicer rabbit polyclonal antibody (Santa Cruz Biotechnology, Inc.) and 0.8 μg or 1.6 μg of an unrelated control antibodies namely anti- DsRed rabbit polyclonal antibody (Clonetech Laboratories, Inc.) and anti-β actin mouse monoclonal antibody (Sigma-Aldrich, Inc.) for 2 hr, at 4 ^{o}C prior to the RISC assembly assay. Final volume was (60) μL per lane. Nondenaturing 4% (w/v) polyacrylamide gel electrophoresis was used to resolve these complexes as described above. Time courses and titration curves were fit as above.

Western Blots for Dicer Detection. RISC assembly complexes were formed as described above, but scaled up 6-fold. Gels were soaked in 0.1% (w/v) SDS for 15 min and then electroblotted in Tris-Glycine transfer buffer (25 mM Tris, 25 mM Glycine) onto a PVDF (Polyvinylidene Fluoride) membrane (Immobilon-P Membrane, Millipore) over 75 min at 300 mA, using a Bio-Rad Trans-Blot SD semi-dry transfer cell per the manufacturer's instructions. After transfer, the proteins were fixed to the membrane by incubating in 5-10% (v/v) acetic acid, rinsing with deionized water, and air drying. The membrane was probed with a rabbit primary antibody against Dicer (Santa Cruz Biotechnology), followed by a goat anti-rabbit secondary antibody, conjugated with horseradish peroxidase (Zymed, Invitrogen). The blot was developed using a peroxide/enhancer solution (ECL-Plus detection, Amersham), and visualized on a Typhoon 9410 Variable Mode Imager.

Mathematical Model Description. Details of the model used to describe p19's interaction with the RNAi machinery is found in Appendix B.

2.3 Results

Fluorescence Assays to Observe siRNA:p19 Complex Formation

We site-specifically labeled the antisense (guide) strand of an established luciferase-targeting siRNA duplex (35, 36) with either fluorescein or tetramethylrhodamine as fluorescence quenching probes in positions not expected to interfere with p19 binding (Figure 2.1*A*). We found that only the tetramethylrhodamine label was efficiently quenched upon p19 addition (Figure 2.1*B*). Addition of buffer or other proteins such as recombinant Dicer caused no such quenching (Appendix A Figure A1). To observe a robust quenching signal upon p19 addition, we proceeded to label with both fluorophores together, allowing us to monitor a normalized tetramethylrhodamine:fluorescein (T/F) fluorescence ratio that is insensitive to dilution effects and other perturbations of an otherwise relative fluorescence signal. Next, we tested by EMSA p19 binding of this doubly-labeled siRNA against that of the unlabeled siRNA and detected no interference from the fluorophores ($K_{D,app}$ = 0.17 ± 0.03 nM in both cases, consistent with earlier EMSA studies (16) (Figure 2.1*C*). Time-resolved fluorescence resonance energy transfer (trFRET) between the two fluorophores revealed only a small increase in fluorophore distance distribution upon p19 addition (with the mean distance increasing from 43.4 to 44.5 Å; (Figure 2.1*D*), indicating that formation of the SP complex leads to only a minor deformation of the siRNA duplex, as expected from X-ray crystallography (16). We conclude that the doubly-labeled siRNA duplex is a suitable reporter for formation of the siRNA:p19 interaction in solution.

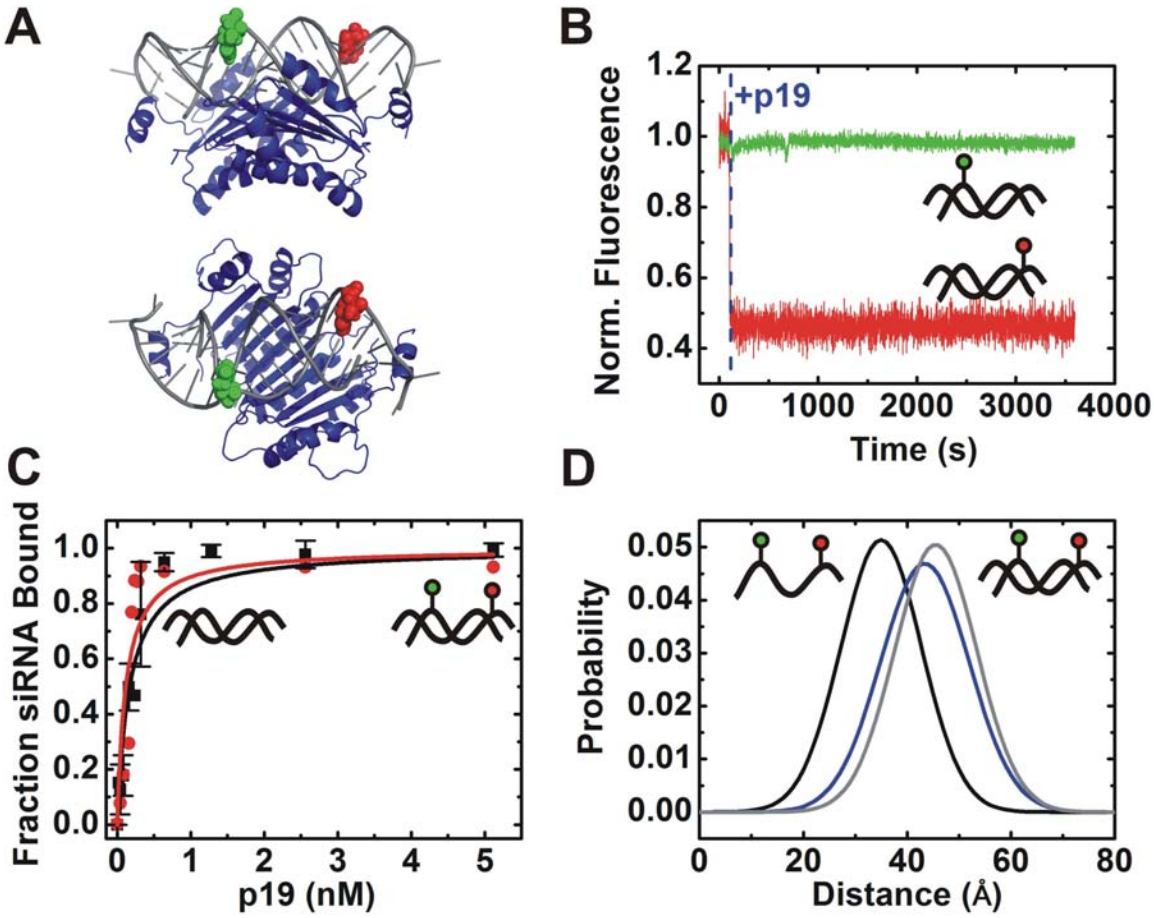

Figure 2.1 Fluorescence assays to detect siRNA:p19 complex formation. (*A*) Crystal structure of p19 (blue) bound to an siRNA (grey). The nucleotides to which the fluorophores fluorescein (F) and tetramethylrhodamine (T) are attached are highlighted in green and red, respectively. (*B*) The T-only labeled siRNA (red) is quenched upon p19 addition, while the F-only labeled siRNA (green) is unaffected by p19. (*C*) EMSA analysis shows that the doubly-labeled ft-siRNA (red) binds to p19 with the same affinity as the unlabeled siRNA (black). (*D*) Time-resolved FRET measures the F:distances for the single-stranded, protein-free double-stranded, and p19-bound double-stranded siRNA 35 Å, 43.4 Å, and 44.5 Å, respectively.

p19 Binds siRNA Rapidly and Reversibly

Addition of increasing excess concentrations of p19 to the doubly-labeled siRNA led to an increase in the pseudo-first order rate constant of tetramethylrhodamine quenching as monitored by the T/F ratio, yielding a bimolecular binding rate constant of $k_{on} = (1.69 \pm 0.07) \times 10^8\ M^{-1}s^{-1}$ (Figure 2.2*A*,*B*). Next, dissociation of the preformed SP complex was monitored upon addition of a large excess of unlabeled siRNA (chase), yielding a dissociation rate constant of $k_{off} = 0.062 \pm 0.002\ s^{-1}$ (Figs. 2*C* and S1). Together with the rapid k_{on}, a solution-based dissociation equilibrium constant of $k_{off}/k_{on} = K_D = 0.37 \pm 0.08$ nM is obtained, within 2-fold of the EMSA predicted value (0.17 nM), attesting to a high-affinity, yet also notably reversible siRNA:p19 binding mode.

p19 Efficiently Competes with Recombinant Human Dicer for siRNA Binding

The critical dual role of Dicer in RNAi as both the enzyme that produces siRNAs and as a RISC assembly factor (11) suggests the siRNA:Dicer (SD) interaction as a particularly vulnerable step during RNA silencing. Previous studies in embryo extracts of the fruitfly Drosophila have shown that p19 suppresses RNA silencing by competing with the Dcr2-R2D2 complex (21, 27). To determine whether p19 also competes with human Dicer for siRNA, we employed EMSA using radio-labeled siRNA duplexes and recombinant human Dicer (available as an active crude extract from Genlantis, see Methods). We measured the apparent equilibrium dissociation constant of the human SD complex as $K_{D,app} = 3.7 \pm 0.4$ nM (Figs. 3A and S2A).

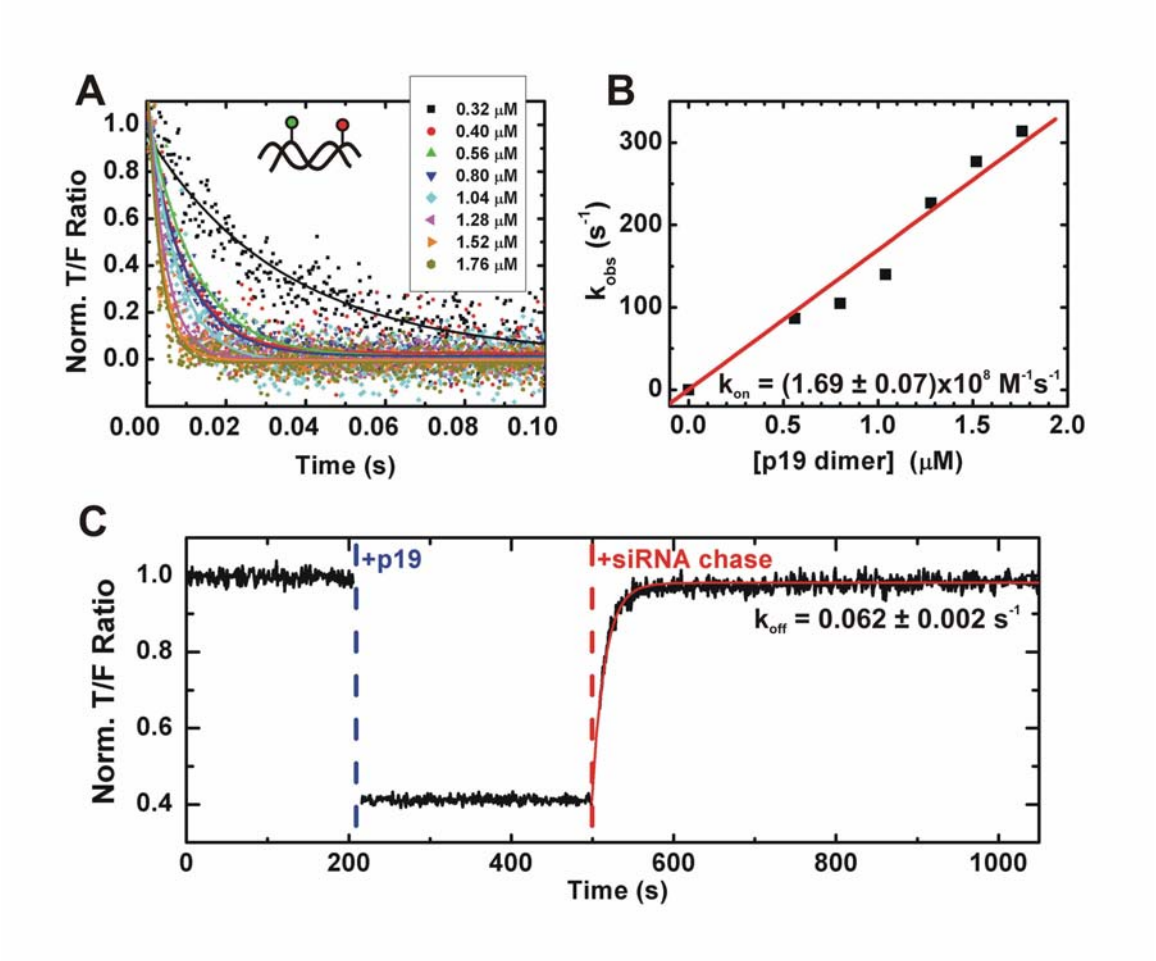

Figure 2.2 Kinetics of formation and dissociation of the siRNA:p19 complex. (*A*) Pseudo-first order kinetics of the binding of doubly-labeled siRNA (50 nM) to excess p19, measured through the T/F ratio during stopped-flow mixing. Scatter points denote raw data; lines denote single-exponential fits to extract rate constants. (*B*) Plot of the observed pseudo-first rate constants from panel A over the p19 concentration. The linear fit yields the indicated bimolecular binding rate constant, k_{on}. (*C*) Fluorescence detection of the binding of doubly-labeled siRNA (50 nM) to p19 (500 nM) and of complex dissociation upon addition of an unlabeled siRNA chase (3 μM). A single-exponential fit (red line) yields the indicated dissociation rate constant, k_{off}.

The presence of a low concentration of p19 (0.17 nM), equivalent to the $K_{D,app}$ of the SP complex, weakened this interaction by >25-fold to ~100 nM (Figs. 3A and S2B). The presence of a saturating concentration of p19 (2.5 nM) weakened the interaction still further by >270-fold to an estimated lower limit of ~1.0 μM (Figs. 3A and S2C). These findings led us to hypothesize that p19 can function to inhibit RNAi in humans by interrupting the SD complex before Dicer can hand off siRNA to RISC. Reciprocal competition experiments showed that the presence of even saturating concentrations (140 nM) of Dicer lowered the apparent affinity of p19 for siRNA only marginally (~4-fold from 0.17 ± 0.03 nM to 0.81 ± 0.06 nM; Figs. 3B and S2D,E), further supporting the hypothesis that strong competition with the SD complex is an important mode of action for p19 inhibition of RNAi in human cells.

Human siRNA-Containing Complexes Formed in Cytosolic Cell Extract are Vulnerable to p19 Challenge

Previous studies with *Drosophila* extracts have shown that p19 inhibits RISC assembly while disrupting preassembled RISC to a lesser extent (27). Our result that p19 disrupts the complex of recombinant human Dicer with siRNA suggests that p19 may also be effective in suppressing RISC assembly in mammals. To test this hypothesis and probe p19's effect on the formation of human RISC-related complexes, we used a modified *in vitro* RISC assembly assay (40, 41), wherein we incubated radio-labeled siRNA duplex with 15% (v/v) cytosolic HeLa cell extract and analyzed the products by EMSA and autoradiography (Figure 2.4*A*,*B*).

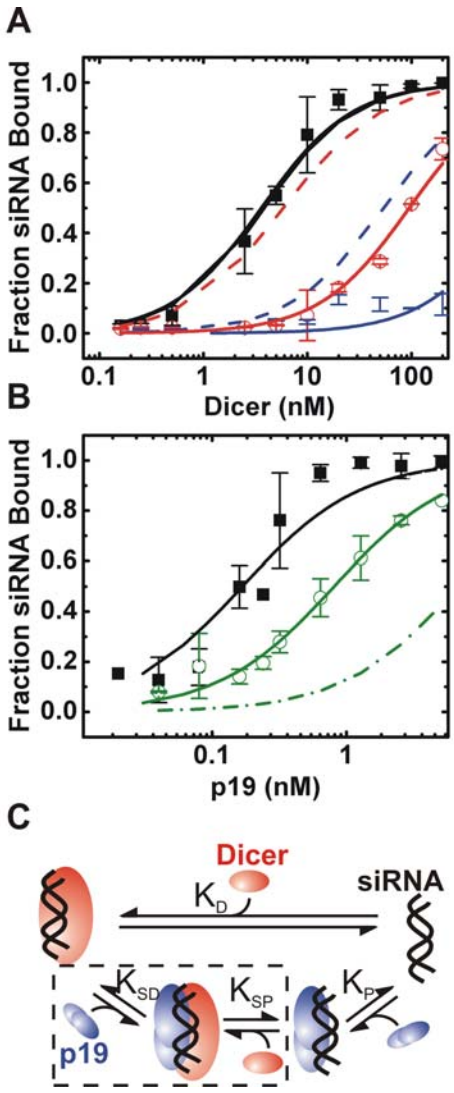

Figure 2.3 Competition of p19 with human Dicer for siRNA binding as detected by EMSA. (*A*) Fraction of siRNA bound to Dicer over increasing Dicer concentrations in the absence (black squares) and presence of p19 at 0.17 nM (open red circles) or 2.5 nM (blue dots). The solid lines are hyperbolic fits and dashed lines indicate calculated curves predicting p19 competition for an indirect equilibrium shift mechanism. (*B*) Fraction of siRNA bound to p19 over increasing p19 concentrations in the absence (black squares) or presence of a saturating Dicer concentration of 140 nM (open green circles). The solid

(Figure 2.3 continued) lines are hyperbolic fits and the dashed-dotted line indicates the calculated curve assuming p19 and Dicer competition is an indirect equilibrium shift only. Representative EMSA gel images are shown in (Figure A2). (C) Steady-state two protein competition model.

Three distinct siRNA-containing complexes were observed that correspond to those previously observed, including a slowly-migrating complex D that is thought to contain Dicer, as well as two faster migrating bands termed C1 and C2 (21, 42) (Figure 2.4*B*). The normalized fraction of complex C2 decreases over a 2-h period, whereas the complex C1 and D fractions increase (with estimated rate constants of 2×10^{-3} s^{-1}, 0.8×10^{-3} s^{-1}, and 0.4×10^{-3} s^{-1}, respectively, (Figure 2.4*A*).To test for the presence of Dicer we performed supershift assays with anti-Dicer polyclonal antibody and found that only complex D specifically supershifts with this antibody (Figure 2.4*C*). Similarly, Dicer is detected by Western blot in complex D only (Figure A4). Notably, adding increasing p19 concentrations to the cell extract prior to siRNA addition increasingly impairs the formation of all three siRNA-containing complexes, concomitant with an accumulation of the competing SP complex (Figure 2.4*D,E*). When p19 is added to the RISC assembly assay after 2 h of pre-incubation with siRNA, the formation of particularly the Dicer-containing complex D is inhibited to a lesser extent (Figure 2.4*F,G*). Similar results were obtained at higher HeLa cell extract concentrations and temperatures (Figure A3).

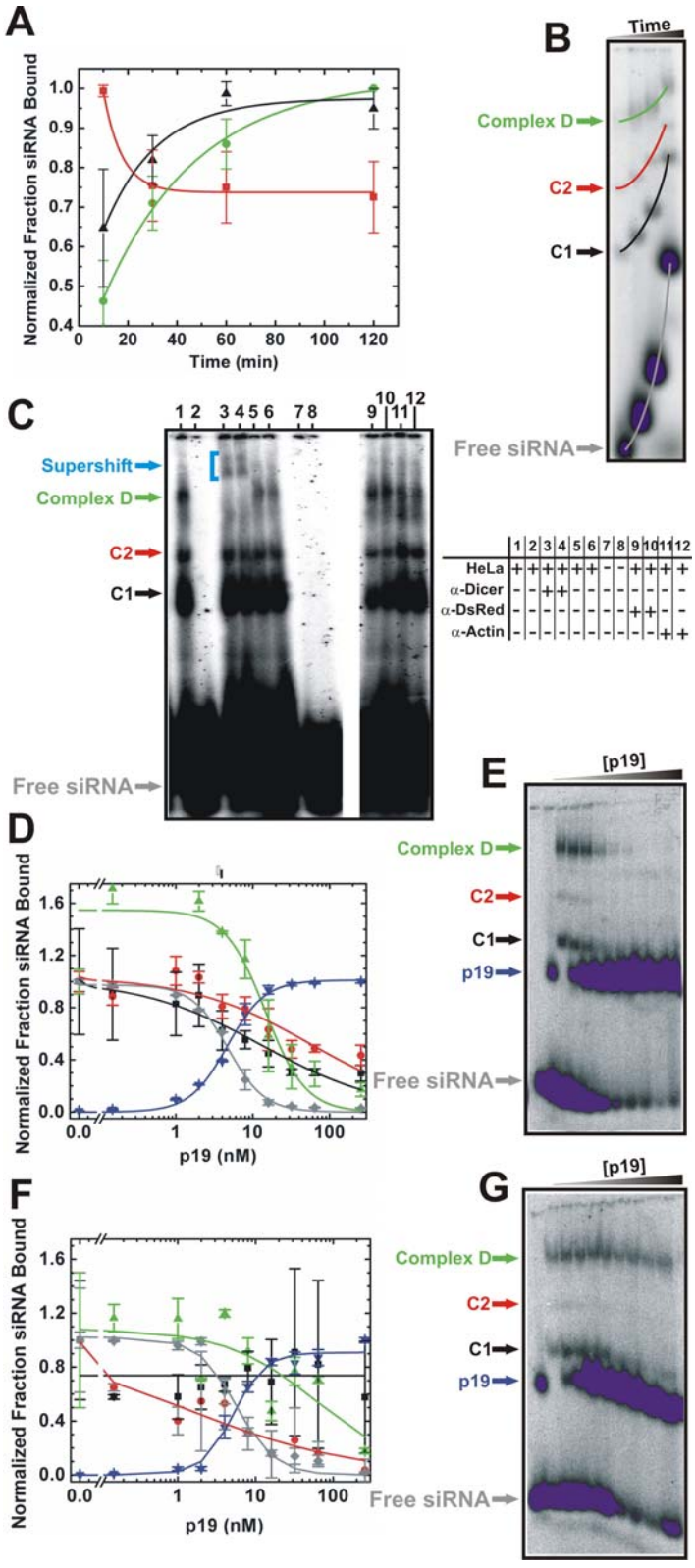
A
Normalized Fraction siRNA Bound
Time (min)
B
Time
Complex D
C2
C1
Free siRNA
C
1 2 3 4 5 6 7 8 9 10 11 12
Supershift
Complex D
C2
C1
Free siRNA
HeLa
α-Dicer
α-DsRed
α-Actin
D
Normalized Fraction siRNA Bound
p19 (nM)
E
[p19]
Complex D
C2
C1
p19
Free siRNA
F
Normalized Fraction siRNA Bound
p19 (nM)
G
[p19]
Complex D
C2
C1
p19
Free siRNA

Figure 2.4 Competition of p19 with human siRNA-containing complexes found in cytosolic HeLa cell extract. (*A*) Normalized fraction of siRNA bound to complexes D (green), C2 (red), and C1 (black), where the highest point is normalized to unity in each complex over time, as derived from the gel in panel B. The relative abundances of C1 and complex D increase over time at estimated rate constants of 8×10^{-4} s^{-1} and 4×10^{-4} s^{-1}, respectively, whereas C2 decreases in relative abundance at a rate constant of 2×10^{-3} s^{-1}. (*B*) Formation of complexes D, C2, and C1 after 10, 30, 60 and 120 min incubation of siRNA in cytosolic HeLa cell extract. Samples were loaded onto a running 4% native polyacrylamide gel, leading to the indicated differences in migration. (*C*) Supershift assay of 5′ end labeled siRNA incubated with cytosolic HeLa cell extract. Dicer containing complex D, shifts in the presence of an anti-Dicer antibody (lanes 3 and 4), where 0.8 μg or 1.6 μg of antibody is added respectively. Lanes 1, 5 and 6 indicate the mobility of the complexes in the absence of any antibody. Lanes 9-12 are the negative controls with 0.8 μg or 1.6 μg of □- actin (9-10) and DsRed (11-12) antibodies respectively. (*D*) Quantification of the normalized fraction of siRNA bound in each complex, as derived from gels as in panel E. Fractions were normalized to the zero time point. (*E*) Formation of complexes after 2.5 h incubation of siRNA in cytosolic HeLa cell extract, and increasing concentrations of p19. (*F*) Quantification of the normalized fraction of siRNA bound in each complex, as derived from gels as in panel E, normalized as in D. (*G*) Formation of complexes D, C1, and C2 after 2 h incubation of siRNA in cytosolic HeLa cell extract, followed by the addition of increasing concentrations of p19 and further incubation for 30 min.

Modeling Supports Formation of a Transient Ternary siRNA:Dicer:p19 Complex

The mechanism of competition between p19 and human Dicer can be determined from mathematically modeling the two possible modes of competition for a two-protein-single-substrate system. First, competition may occur through a dissociative binding mode, where the higher affinity protein shifts the relative equilibrium of the system by binding all available substrate as it dissociates from the competitor, thus establishing a new equilibrium position (Figure 2.3*C*). In the case of p19 and Dicer, siRNAs are pre-associated with Dicer at the onset, due to their cleavage from longer RNAs, making such dissociative binding by p19 relatively fast only if spontaneous dissociation from Dicer is rapid. Second, competition may occur through formation of a ternary complex intermediate involving siRNA, Dicer, and p19 (Figure 2.3*C*). Using the previously determined gel-based apparent dissociation equilibrium constants for p19 ($K_{D,app}$ = 0.17 ± 0.02 nM) and Dicer ($K_{D,app}$ = 3.7 ± 0.4 nM), we can discriminate between these two possible modes of competition by calculating the resulting expected siRNA:Dicer and siRNA:p19 complex fractions and comparing them to experiments for a given set of equilibrium conditions (43).

Assumption of the dissociative binding mechanism shows poor correlation with experiment as the change upon adding Dicer is consistently overestimated (Figure 2.3*A*), while the change upon adding p19 is consistently underestimated (Figure 2.3*B*). This poor correlation suggests that ternary complex formation is needed to explain the observed efficient disruption of the siRNA:Dicer complex in the presence of p19. The addition of ternary complex formation creates a thermodynamic cycle that requires the

ratio of dissociation constants K_D/K_{SP} to equal that of K_P/K_{SD} (44). Rearranging and using the values of K_D and K_P we find that $K_{SP}/K_{SD} = K_D/K_P = 21.6$ and therefore $K_{SP} = 21.6\ K_{SD}$. This result suggests that the dissociation of the ternary complex into the binary siRNA:p19 complex is >20-fold more likely than dissociation into the siRNA:Dicer complex, indicating that siRNAs can indeed be effectively shuttled toward the p19 bound state by assuming transient formation of a ternary siRNA:Dicer:p19 complex. This result correlates well with experiment and explains both the weak effect that Dicer addition has on the siRNA:p19 complex and the large effect that p19 addition has on the siRNA:Dicer complex (Figure 2.3*A*,*B*). A similar result is observed when p19 is placed in the context of the RNAi pathway (Appendix B: Model Description).

2.4 Discussion

The small, positive-sense, single-stranded RNA genome of tombusviruses encodes p19, a RSS thought critical for symptom spread and cytotoxicity of this class of plant pathogens (19, 20, 23, 24) through its ability to bind and thus sequester Dicer-generated siRNAs (15, 21). To better understand the basis of the cytotoxicity of CIRV's p19, we studied its siRNA binding properties through fluorescence quenching assays in combination with radioactive EMSAs. Noticeable dissociation of an siRNA from p19 ($k_{off} = 0.062 \pm 0.002\ s^{-1}$) is counterbalanced by fast association to yield a solution based dissociation equilibrium constant ($K_D = 0.37 \pm 0.08$ nM; Figure 2.2), within 2.2-fold of the high affinity previously deduced in EMSAs (16). The off rate for p19 binding of siRNA is considerably faster than some proteins considered to 'irreversibly bind' their

nucleic acid binding partners with dissociation rate constants on the order of 10^{-4} s^{-1} (30, 31, 45, 46).

The rate and equilibrium constants for p19 resemble those of HIV-1 protein Rev for interaction with Rev Response Element (RRE) RNA (k_{on} = 5.3 x10^{8} M^{-1} s^{-1}, k_{off} = 0.14 s^{-1}, perhaps due to the similar relatively non-sequence specific binding of a small protein to a (partially) base paired RNA duplex (47).

The presence of low concentrations of p19 dramatically weakens the interaction of human Dicer with its siRNA product (25 to >270-fold, depending on the p19 concentration, Figure 2.3*A*). Conversely, the presence of saturating concentrations of Dicer only slightly lowers (~4-fold) the affinity of p19 for siRNA (Figure 2.3*B*), supporting the hypothesis that strong competition with the SD complex is an important mode of p19 action in mammals *in vivo*. Assembly assays show that p19 also significantly disrupts RISC-related human siRNA-protein complexes (Figure 2.4). Our experimental results inform mathematical modeling of p19-Dicer competition and the steady-state kinetic interactions involving p19, siRNA, Dicer, RISC, and viral (m)RNA. We determine that the minimal model necessary to achieve p19 suppression and Dicer competition includes a ternary complex between Dicer, p19, and siRNA substrates (Figure 2.3).

Several implications for the struggle between the viral p19 and the cellular RNAi machinery arise from our work. First, our experimental data suggest that the observed efficient competition of p19 with the siRNA:Dicer complex (Figure 2.3) and thus resulting Dicer-containing RISC assembly complexes (Figure 2.4) targets a particularly critical step on the path to an activated RISC. Recent 3D reconstructions from negatively-

stained electron microscopy images of human Dicer complexes depict it as a fist-like shape with a central flat surface that is thought to bind the siRNA (48, 49). This architecture along with the known binding mode of p19 leaves open the possibility that p19 could bind the opposite face of the siRNA in a ternary complex with Dicer. Notably, we did not observe formation of a super-shifted band as indicative of such a ternary complex in our EMSAs with siRNA, p19, and human Dicer (Figure 2.4*D*,*G*), however, the complex may be too short-lived or our EMSA too low in resolution for the complex to be detected.

Second, the previously proposed simple sequestration model would require stoichiometric p19 concentrations relative to all siRNA duplexes, native to CIRV or not, that are generated by Dicer, as well as all miRNA duplexes (22, 25), defective interfering RNAs (23), and the siRNA amplification products generated in plant cells by RNA-dependent RNA polymerase activity (3). Our finding that formation of the high-affinity siRNA:p19 complex is readily reversible (Figure 2.2) while still interfering with siRNA binding by Dicer and RISC-related assembly complexes *in vitro* (Figures 2.3 and 2.4) raises the possibility that sub-stoichiometric p19 concentrations may suffice *in vivo* to efficiently prevent siRNAs from assembling into RISC, enabling the virus to keep pace with the amplified host response during systemic RNAi self-defense of the plant host against CIRV (50).

Third, while our results have an immediate impact on our understanding of the physicochemical properties and biological function of p19, a more practical consideration also arises from our work. The future of RNAi based strategies may well be dependent on the ability to control and predict the relative intracellular expression levels of RISC

components and potential therapeutics (51, 52). CIRV p19 and other RSS's have been shown to aid in the transfection and difficult over-expression of alpha-, adeno-, and lentiviruses used in gene therapy and in plant based vaccines, through their ability to suppress the intracellular RNAi immune response (51). For such immunosuppression to be effective, dosing of the RSS is important, analogous to immunosuppressants in modern organ transplant surgery.

2.5 Acknowledgements

I would like to thank Vishalakshi Krishnan for all her hard work and contributions to (Figure 2.4) and (Figure A4). We thank Jeffrey Vargason and Traci Hall for the generous provision of purified p19 protein as well as Patrick Nelson for helpful discussions on mathematical modeling. Also we appreciate Jennifer Doudna's lab for providing analytical amounts of purified Dicer and Ago 2 protein.

2.6 References

1. Fire A, *et al.* (1998) Potent and specific genetic interference by double-stranded RNA in Caenorhabditis elegans. *Nature* **391**:806-881.
2. Castanotto D & Rossi JJ (2009) The promises and pitfalls of RNA-interference-based therapeutics. *Nature* **457**(7228):426-433
3. Carthew RW & Sontheimer EJ (2009) Origins and Mechanisms of miRNAs and siRNAs. *Cell* **136**(4):642-655
4. Lee SK & Kumar P (2009) Conditional RNAi: towards a silent gene therapy. *Adv Drug Deliv Rev* **61**(7-8):650-664
5. Grimm D (2009) Small silencing RNAs: state-of-the-art. *Adv Drug Deliv Rev* **61**(9):672-703
6. Umbach JL & Cullen BR (2009) The role of RNAi and microRNAs in animal virus replication and antiviral immunity. *Genes Dev* **23**(10):1151-1164
7. Collingwood MA, *et al.* (2008) Chemical modification patterns compatible with high potency dicer-substrate small interfering RNAs. *Oligonucleotides* **18**(2):187-200
8. Kim DH, *et al.* (2005) Synthetic dsRNA Dicer substrates enhance RNAi potency and efficacy. *Nat Biotechnol* **23**(2):222-226
9. Ji X (2008) The mechanism of RNase III action: how dicer dices. *Curr Top Microbiol Immunol* **320**:99-116
10. Siomi H & Siomi MC (2009) On the road to reading the RNA-interference code. *Nature* **457**(7228):396-404

11. Jaskiewicz L & Filipowicz W (2008) Role of Dicer in posttranscriptional RNA silencing. *Curr Top Microbiol Immunol* **320**:77-97

12. Qu F & Morris TJ (2005) Suppressors of RNA silencing encoded by plant viruses and their role in viral infections. *FEBS Lett* **579**(26):5958-5964

13. Roth BM, Pruss GJ, & Vance VB (2004) Plant viral suppressors of RNA silencing. *Virus Res* **102**(1):97-108

14. Voinnet O (2001) RNA silencing as a plant immune system against viruses. *Trends Genet* **17**(8):449-459

15. Scholthof H (2006) The Tombusvirus-encoded P19: from irrelevance to elegance. *Nat Rev Microbiol* (4):405-411.

16. Vargason JM, Szittya G, Burgyan J, & Hall TM (2003) Size selective recognition of siRNA by an RNA silencing suppressor. *Cell* (115):799-811.

17. Ye K, Malinina L, & Patel DJ (2003) Recognition of siRNA by a viral suppressor of RNA silencing. *Nature* (426):874-878.

18. Xia Z, Zhu Z, Zhu J, & Zhou R (2009) Recognition mechanism of siRNA by viral p19 suppressor of RNA silencing: a molecular dynamics study. *Biophys J* **96**(5):1761-1769

19. Chu M, Desvoyes B, Turina M, Noad R, & Scholthof HB (2000) Genetic dissection of tomato bushy stunt virus p19-protein mediated host-dependent symptom induction and systemic invasion. *Virology* (266):79-87.

20. Silhavy D, *et al.* (2002) A viral protein suppresses RNA silencing and binds silencing-generated, 21- to 25-nucleotide double-stranded RNAs. *EMBO J.* **21**:3070-3080.

21. Lakatos L, Szittya G, Silhavy D, & Burgyan J (2004) Molecular mechanism of RNA silencing suppression mediated by p19 protein of tombusviruses. *EMBO J* **23**(4):876-884.

22. Dunoyer P, Lecellier CH, Parizotto EA, Himber C, & Voinnet O (2004) Probing the microRNA and small interfering RNA pathways with virus-encoded suppressors of RNA silencing. *Plant Cell* **16**(5):1235-1250

23. Havelda Z, Hornyik C, Valoczi A, & Burgyan J (2005) Defective Interfering RNA Hinders the Activity of a Tombusvirus-Encoded Posttranscriptional Gene Silencing Suppressor. *J Virol* (79):450-457.

24. Omarov R, Sparks K, Smith L, Zindovic J, & Scholthof HB (2006) Biological relevance of a stable biochemical interaction between the tombusvirus-encoded P19 and short interfering RNAs. *J Virol* **80**(6):3000-3008

25. Chapman EJ, Prokhnevsky AI, Gopinath K, Dolja VV, & Carrington JC (2004) Viral RNA silencing suppressors inhibit the microRNA pathway at an intermediate step. *Genes Dev* **18**(10):1179-1186

26. Csorba T, Bovi A, Dalmay T, & Burgyan J (2007) The p122 subunit of Tobacco Mosaic Virus replicase is a potent silencing suppressor and compromises both small interfering RNA- and microRNA-mediated pathways. *J Virol* **81**(21):11768-11780

27. Lakatos L, *et al.* (2006) Small RNA binding is a common strategy to suppress RNA silencing by several viral suppressors. *EMBO J* **25**(12):2768-2780.

28. Lozsa R, Csorba T, Lakatos L, & Burgyan J (2008) Inhibition of 3' modification of small RNAs in virus-infected plants require spatial and temporal co-expression

of small RNAs and viral silencing-suppressor proteins. *Nucleic Acids Res* **36**(12):4099-4107

29. Merai Z*, et al.* (2006) Double-stranded RNA binding may be a general plant RNA viral strategy to suppress RNA silencing. *J Virol* **80**(12):5747-5756

30. Mitsis PG & Wensink PC (1989) Identification of yolk protein factor 1, a sequence-specific DNA-binding protein from Drosophila melanogaster. *J Biol Chem* **264**(9):5188-5194

31. Ramsden JJ & Dreier J (1996) Kinetics of the interaction between DNA and the type IC restriction enzyme EcoR124II. *Biochemistry* **35**(12):3746-3753

32. Voinnet O, Rivas S, Mestre P, & Baulcombe D (2003) An enhanced transient expression system in plants based on suppression of gene silencing by the p19 protein of tomato bushy stunt virus. *Plant J* **33**(5):949-956

33. Zheng N*, et al.* (2009) Boosted expression of the SARS-CoV nucleocapsid protein in tobacco and its immunogenicity in mice. *Vaccine* **27**(36):5001-5007

34. Walter NG (2002) Probing RNA structural dynamics and function by fluorescence resonance energy transfer. *Curr. Protocols Nucleic Acid Chem*, pp 11.10.11-11.10.23.

35. Hoerter JA & Walter NG (2007) Chemical modification resolves the asymmetry of siRNA strand degradation in human blood serum. *RNA* **13**(11):1887-1893

36. Martinez J, Patkaniowska A, Urlaub H, Luhrmann R, & Tuschl T (2002) Single-stranded antisense siRNAs guide target RNA cleavage in RNAi. *Cell* **110**:563-574.

37. Gondert ME, Tinsley RA, Rueda D, & Walter NG (2006) The catalytic core structure of the trans-acting HDV ribozyme is subtly influenced by sequence variation outside the core. *Biochemistry* **45**:7563-7573.

38. Rueda D, Wick K, McDowell SE, & Walter NG (2003) Diffusely bound Mg2+ ions slightly reorient stems I and II of the hammerhead ribozyme to increase the probability of formation of the catalytic core. *Biochemistry* **42**(33):9924-9936

39. Gerczei T, Shah BN, Manzo AJ, Walter NG, & Correll CC (2009) RNA chaperones stimulate formation and yield of the U3 snoRNA-Pre-rRNA duplexes needed for eukaryotic ribosome biogenesis. *J Mol Biol* **390**(5):991-1006

40. Pellino JL, Jaskiewicz L, Filipowicz W, & Sontheimer EJ (2005) ATP modulates siRNA interactions with an endogenous human Dicer complex. *RNA* **11**(11):1719-1724

41. Pham JW & Sontheimer EJ (2005) Separation of Drosophila RNA silencing complexes by native gel electrophoresis. *Methods Mol Biol* **309**:11-16

42. Pham JW, Pellino JL, Lee YS, Carthew RW, & Sontheimer EJ (2004) A Dicer-2-dependent 80s complex cleaves targeted mRNAs during RNAi in Drosophila. *Cell* **117**(1):83-94

43. Sigurskjold BW (2000) Exact analysis of competition ligand binding by displacement isothermal titration calorimetry. *Anal Biochem* **277**(2):260-266

44. Wreggett KA & De Lean A (1984) The ternary complex model. Its properties and application to ligand interactions with the D2-dopamine receptor of the anterior pituitary gland. *Mol Pharmacol* **26**(2):214-227

45. Mougel M, Ehresmann B, & Ehresmann C (1986) Binding of Escherichia coli ribosomal protein S8 to 16S rRNA: kinetic and thermodynamic characterization. *Biochemistry* **25**(10):2756-2765

46. Seimiya M & Kurosawa Y (1996) Kinetics of binding of Antp homeodomain to DNA analyzed by measurements of surface plasmon resonance. *FEBS Lett* **398**(2-3):279-284

47. Pond SJ, Ridgeway WK, Robertson R, Wang J, & Millar DP (2009) HIV-1 Rev protein assembles on viral RNA one molecule at a time. *Proc Natl Acad Sci U S A* **106**(5):1404-1408

48. Wang HW, *et al.* (2009) Structural insights into RNA processing by the human RISC-loading complex. *Nature structural & molecular biology* **16**(11):1148-1153

49. Lau PW, Potter CS, Carragher B, & MacRae IJ (2009) Structure of the human Dicer-TRBP complex by electron microscopy. *Structure* **17**(10):1326-1332

50. Baulcombe D (2004) RNA silencing in plants. *Nature* **431**:356-363

51. de Vries W, *et al.* (2008) Increased virus replication in mammalian cells by blocking intracellular innate defense responses. *Gene Ther* **15**(7):545-552

52. Grimm D, *et al.* (2006) Fatality in mice due to oversaturation of cellular microRNA/short hairpin RNA pathways. *Nature* **441**(7092):537-541

Chapter 3:

EXPLICIT MODELING: TIME DEPENDENT AND ALTERNATIVE STEADY STATE *IN VIVO* INTERACTIONS BETWEEN RNA INTERFERENCE AND P19

3.1 Introduction

Computational modeling in infectious disease has been used mostly to elucidate disease mechanisms, model the progression of infection and to determine the spread of epidemics. Recently, the immune system has come under considerable scrutiny as a target for biomodeling. In the post-genomic era, the discovery of siRNAs, miRNAs, and huge networks of non-coding RNAs that act as genetic regulators against disease has forced scientists to question their previous understanding of the immune response to infection. With RNA interference (RNAi) impacting essentially all invading viruses in most species, from fission yeast to plants and mammals, the possibilities are expanding for genomic modeling.

The RNAi pathway is activated during viral infection to degrade exposed stretches of double-stranded viral mRNA. These mRNAs are specifically recognized and cleaved by the cytoplasmic RNase III-type endonuclease Dicer into small interfering RNAs (siRNAs) 21-24 nucleotides in length depending on species (1-9). Dicer has a second role, after cleavage, to deliver the double-stranded siRNA to the RNA Induced

Silencing Complex (RISC) (10-12). RISC cleaves and releases the passenger strand of the duplex while the guide strand is retained to direct specific cleavage of complementary viral RNA genomes or transcripts (13, 14).

Within the last five years, the modeling community has begun to address this largely unexplored territory. Bergstrom et. al (2003) used a time dependent compartmental model of RNAi to examine several key features of the RNAi pathway including synthesis, cleavage, and degradation of mRNA. They focused on the effect of siRNA amplification by RNA dependent RNA polymerases and the mechanism behind the reduced off target self-cleavage of host mRNA (15). Marshall (2005) used a steady-state compartmental model to study the effect of so-called recursive RNAi, targeting Dicer and RISC, on viral protein accumulation (16). Bartlett and Davis (2006) employed a more comprehensive model of RNAi in response to HIV infection and included the delivery of therapeutic siRNAs in viral production (17). Goutsias and Lee (2007) used experimental RNAi as a validation tool for gene regulatory models and designed reverse engineered algorithms for transcriptional regulatory networks by gene perturbations in colon cancer progression (18). Groenenboom and Hogeweg (2005, 2008) suggested extensions to the current view of RNAi that would unify the diversity of data presented on viral growth patterns and observed siRNA ratios in response to RNAi (19, 20).

To combat host RNAi suppression, many viruses have evolved small proteins that act as RNAi silencing suppressors or RSSs (21-23). Protein 19 (p19) is an RSS encoded by all members of the tombusviridae viral family that has been observed to correlate with reduced viral mRNA degradation, systemic symptom spread and the sustainability of the viral phenotype after infection (24-28). p19 has been shown to bind single siRNA

duplexes forming stacking interactions with the terminal base pairs of the siRNA to prevent reintroduction into the RNAi pathway (29-31). Currently, there are no available models that explicitly address the interaction of a viral suppressor protein with the RNAi pathway.

Here we report two sections of computational modeling; in section one we develop a time-dependent RNAi model that incorporates the effect of exogenously introduced p19 on viral mRNA levels. We find p19 to be able to increase either the amount of mRNA production or the length of the viral replication phase. Also, our model predicts p19 to time invariantly reinitiate viral replication after a steady-state level of suppression has been reached. In section two, we expand on the steady-state models presented previously to provide new information on the ternary complex described between siRNAs, Dicer, and p19. We can calculate through an alternative Jacobian-based method that indirect binding of siRNA substrates, by p19 or Dicer, is insufficient to reproduce experimental data reiterating the necessity of a ternary complex (see Model Description: Indirect Equilibrium Shift). We also numerically estimate rate constants for each individual reaction in the closed system by dynamic ranging and obtain results comparable to experiment (see Model Description: Direct Binding and Ternary Complex Formation).

3.2 Model Description(s):

Explicit Time-Dependence of RNA Interference

The RNA interference pathway depicted in (Figure 3.1) is described by a system of seven ordinary differential equations. The rates of change for viral messenger RNA (M), two products of mRNA cleavage by Dicer (ds2) and (ds1), free siRNA (S), Dicer bound siRNA (SD), p19 bound siRNA (SP), and the RISC complex (R) are given below.

- **d[M]/dt = h - k_7*[R]*[M]**
- **d[ds2]/dt = V_{max}*([M]/(K_m+[M]))-Vmax*([ds2]/(Km+[ds2])) + k7*[R]*[M]**
- **d[ds1]/dt = Vmax*([ds2]/(Km+[ds2]))-Vmax*([ds1]/(Km+[ds1]))**
- **d[S]/dt = -k3*[S]*[p19] + k4*[SP] - k1*[S]*[Dicer] + k1*Kd*[SD]**
- **d[SD]/dt = Vmax*([M]/(Km+[M]))+Vmax*([ds1]/(Km+[ds1]))+ Vmax*([ds2]/(Km+[ds2]))+k1*[S]*[Dicer]-k1*Kd*[SD]-k5*[SD]*[p19]-k6*[SD]*[Ago]**
- **d[SP]/dt = k3*[S]*[p19]-k4*[SP]+k5*[SD]*[p19]**
- **d[R]/dt = k6*[SD]*[Ago]-k8*[R]**

We describe these terms as follows:

a) **Messenger RNA (M)**: mRNAs are produced at a constant rate (h) and degraded by their interaction with the mature RISC complex (k7*[R]*[M]).

b) **Double-stranded RNA2 (ds2)**: ds2 is formed from messenger RNA after one round of cleavage by either Dicer or RISC (Vmax*([M]/(Km+[M])) + k7*[R]*[M]), respectively. (ds2) remains a substrate for Dicer and is further processed into ds1 by (Vmax*([ds2]/(Km+[ds2])).

c) **Double-stranded RNA1 (ds1)**: (ds1) is the product of (ds2) cleavage by Dicer described by the term (Vmax*([ds2]/(Km+[ds2]))) and is again a Dicer substrate (Vmax*([ds1]/(Km+[ds1]))).

d) **Free siRNA (S)**: siRNAs are accumulated in the cell by dissociation from either the SD or SP complex (k1*Kd*[SD] + k4*[SP]) and depleted by the binding of both proteins (k3*[S]*[p19]+ k1*[S]*[Dicer]).

e) **Dicer:siRNA (SD)**: The complex between Dicer and siRNAs is formed through the direct cleavage of either mRNA, (ds2), or (ds1) by Dicer (Vmax*([M]/(Km+[M]))+Vmax*([ds1]/(Km+[ds1]))+Vmax*([ds2]/(Km+[ds2])). The complex is then depleted through the binding of RISC proteins to form the mature RISC, natural dissociation, or facilitated dissociated by p19 (k6*[SD]*[Ago]+ k1*Kd*[SD]+k5*[SD]*[p19]), respectively.

f) **p19:siRNA (SP)**: The complex between p19 and siRNAs is formed by p19 binding of free or Dicer bound siRNAs (k3*[S]*[p19]) + k5*[SD]*[p19]), respectively, and dissociated at a rate of (k4*[SP]).

g) **Mature RISC (R)**: Mature RISC is formed through Ago proteins binding to the SD complex (k6*[SD]*[Ago]), and degraded at a rate of (k8*[R]).

We assume Dicer, and Ago proteins are kept constant in the cell and are produced at sufficient levels to not inhibit the reaction rates. Additionally, p19 is assumed to be expressed stably in all cases. Parameter values, intended to illustrate the qualitative features of this model and give insight into its dynamics, are as follows:

- h = 0.6; Rate of mRNA production (nM/hour)
- k7 = 0.001; Rate constant for RISC mRNA cleavage ($nM^{-1}hour^{-1}$)
- Vmax = 792; Maximum velocity of Dicer cleavage (nM/hour)*
- Km = 2800; Concentration of half maximal Dicer cleavage (nM)*
- k3 = 608.4; Rate constant for p19-siRNA binding ($nM^{-1}hour^{-1}$)*
- k4 = 363.6; Rate constant for SP dissociation ($hour^{-1}$)*
- k1 = 0.01476; Rate constant for Dicer-siRNA binding ($nM^{-1}hour^{-1}$)*
- Kd = 3.67; Dissociation constant for SD (nM)*
- k5 = 0.04446; Rate constant for p19-SD binding ($nM^{-1}hour^{-1}$)*
- k6 = 0.001; Rate constant for RISC-SD binding ($nM^{-1}hour^{-1}$)

- k8 = 0.1; Rate constant for RISC dissociation ($hour^{-1}$)

Those parameters that are derived or estimated from experimental results are indicated with an asterisk.

Steady-State Two Protein Model(s)

Ternary Complex Formation

Addition of a possible ternary complex between Dicer, p19 and siRNA increased the complexity beyond explicit solving methods. Rate equations were treated as a set of coupled ordinary differential equations and were numerically solved using Matlab 2007b.

- **SD' [t] = k1*S [t]*D [t] - k2*SD [t] - k5*SD [t]*P [t] + k6*SDP [t]**

- **S' [t] = -k4/ K_{Dp}*S [t]*P [t] +k4*SP [t] -k1*S [t]*D [t] +k2*SD[t]**

- **D' [t] = -k1*S [t]*D [t] + k2*SD [t] - k8*SP [t]*D [t] + k7*SDP[t]**

- **P' [t] = -k4/ K_{Dp} *S [t]*P [t] + k4*SP [t] - k5*SD [t]*P [t] + k6*SDP [t];**

- **SP' [t] = k4/ K_{Dp} *S [t]*P [t] - k4*SP [t] - k8*SP [t]*D [t] + k7*SDP [t];**

- **SDP' [t] = k5*SD [t]*P [t]-k6*SDP [t]+k8*SP [t]*D [t]-k7*SDP [t]** (1)

where the concentrations S, D, P, SD, SP and SDP are siRNA, free Dicer, free p19, Dicer:siRNA complex, p19:siRNA complex and the ternary complex (Dicer:p19:siRNA), respectively. Unknown constants (k_3, k_{-3}, k_4, k_{-4}) were simultaneously ranged and allowed to converge onto a best fit to the experimental data determined by residual least square analysis.

Dissociative Equilibrium Shift

The set of time dependent rate equations for the model depicted in (Figure 3.3C) are represented below:

$$SD'[t] = k1*S[t]*D[t] - k1*K_{Dd}\,SD[t]$$
$$SP'[t] = k3*S[t]*P[t] - k3*K_{Dp}\,SP[t] \qquad (2)$$

and

$$S[t] = So - SP[t] - SD[t]$$
$$D[t] = Do - SD[t] \qquad (3)$$
$$P[t] = Po - SP[t]$$

where the concentrations S, D, P, SD, and SP are siRNA, free Dicer, free p19, Dicer:siRNA complex, and p19:siRNA complex respectively. Initial conditions are represented as So, Do, and Po. After substituting equations (3) into equations (2) the two

unique rate equations (SD and SP) are non-dimensionalized or rescaled by substituting the concentrations SD and SP for scalar multiples multiplied by a unit carrying vectors.

$$SD\,[t] = x*Do$$
$$SP\,[t] = y*Po \qquad (4)$$

For a steady state analysis equations (1) are set to zero and x is represented in terms of y and solved for explicitly. The solutions for y are extensive; we get three values of y for x1 and three values of y for x2 for a total of six possible steady states for a given value of Po.

Summarized below :

$$x1 = A\,(y), \text{ and } y11 = a,\ y12 = b,\ y13 = c$$
$$x2 = B\,(y), \text{ and } y21 = d,\ y22 = e,\ y23 = g \qquad (5)$$

The steady states are :

$$[A\,(a), a],\ [A\,(b), b],\ [A\,(c), c],$$
$$[B\,(d), d],\ [B\,(e), e],\ [B\,(g), g] \qquad (6)$$

Next we must evaluate the stability of these steady states and look into their relevance. Negative values of x or y would mean negative concentrations and are meaningless. Values of SD or SP that are complex or greater than So (the amount of

initial siRNA) are meaningless as well. For stability we find the Jacobian of the system and evaluate it at the steady states.

$$\text{Jacobian} = \begin{matrix} \partial SD/\partial x & \partial SD/\partial y \\ \partial SP/\partial x & \partial SP/\partial y \end{matrix} \qquad (7)$$

When the Trace of the Jacobian is less than zero and the determinant is greater than zero the steady state is stable. We find the steady state values to be complex or non-biologically relevant at all explored values of p19 suggesting the need for additional complexity. Explicit indirect model was computed use Mathematica 7.0.0 Wolfram Research copyright 1988-2008. Below is a table of the six non-dimensionalized steady states for all values of p19 used in this study.

p19	Calculated Steady State for Dicer:siRNA	Calculated Steady State for p19:siRNA	Stability
0.04	0.00692274+0. i	1.00119+0. i	TRUE
0.04	-0.0488272+1.98287*10^-18 i	1.00119+0. i	TRUE
0.04	0.0066805+0. i	1.00119+0. i	TRUE
0.04	1.0264+0. i	1.00119+0. i	FALSE
0.04	1.02499+4.72524*10^-20 i	1.00119+0. i	FALSE
0.04	1.02639+0. i	1.00119+0. i	FALSE
0.08	0.00688667-1.97756*10^-17 i	1.00119-3.90799*10^-14 i	TRUE
0.08	-0.0490833+9.91446*10^-19 i	1.00119-3.90799*10^-14 i	TRUE
0.08	0.00640185+2.17537*10^-17 i	1.00119-3.90799*10^-14 i	TRUE
0.08	1.0264-5.25618*10^-19 i	1.00119-3.90799*10^-14 i	FALSE
0.08	1.02499+2.3615*10^-20 i	1.00119-3.90799*10^-14	FALSE

		i	
0.08	1.02638+5.7763*10^-19 i	1.00119-3.90799*10^-14 i	FALSE
0.16	0.00681551-5.9327*10^-18 i	1.00119-8.88178*10^-15 i	TRUE
0.16	-0.0495966-9.91469*10^-19 i	1.00119-8.88178*10^-15 i	TRUE
0.16	0.00584453+9.88834*10^-18 i	1.00119-8.88178*10^-15 i	TRUE
0.16	1.02639-1.57663*10^-19 i	1.00119-8.88178*10^-15 i	FALSE
0.16	1.02498-2.35924*10^-20 i	1.00119-8.88178*10^-15 i	FALSE
0.16	1.02637+2.62272*10^-19 i	1.00119-8.88178*10^-15 i	FALSE
0.24	0.00674562+5.93272*10^-18 i	1.00119+0. i	FALSE
0.24	-0.0501111-1.48724*10^-18 i	1.00119+0. i	TRUE
0.24	0.00528719+0. i	1.00119+0. i	TRUE
0.24	1.02639+1.57642*10^-19 i	1.00119+0. i	FALSE
0.24	1.02496-3.53547*10^-20 i	1.00119+0. i	FALSE
0.24	1.02635+0. i	1.00119+0. i	FALSE
0.32	0.00667699-1.97758*10^-18 i	1.00119-3.55271*10^-15 i	FALSE
0.32	-0.0506269+0. i	1.00119-3.55271*10^-15 i	TRUE
0.32	0.00472984+7.91113*10^-18 i	1.00119-3.55271*10^-15 i	TRUE
0.32	1.02639-5.25402*10^-20 i	1.00119-3.55271*10^-15 i	FALSE
0.32	1.02495+0. i	1.00119-3.55271*10^-15 i	FALSE
0.32	1.02634+2.0936*10^-19 i	1.00119-3.55271*10^-15 i	FALSE
0.64	0.00641443-1.97761*10^-18 i	1.00119-1.77636*10^-15 i	FALSE
0.64	-0.0527022-3.96642*10^-18 i	1.00119-1.77636*10^-15 i	TRUE
0.64	0.00250029+7.91204*10^-18 i	1.00119-1.77636*10^-15 i	TRUE
0.64	1.02638-5.25131*10^-20 i	1.00119-1.77636*10^-15	FALSE

		i	
0.64	1.0249-9.38265*10^-20 i	1.00119-1.77636*10^-15 i	FALSE
0.64	1.02628+2.0845*10^-19 i	1.00119-1.77636*10^-15 i	FALSE
1.28	0.00594131+5.93297*10^-18 i	1.00118+0. i	FALSE
1.28	-0.0569055-1.98357*10^-18 i	1.00118+0. i	TRUE
1.28	-0.00195954+0. i	1.00118+0. i	TRUE
1.28	1.02637+1.57393*10^-19 i	1.00118+0. i	FALSE
1.28	1.0248-4.65494*10^-20 i	1.00118+0. i	FALSE
1.28	1.02616+0. i	1.00118+0. i	FALSE
2.15	0.00539179-1.66097*10^-17 i	1.00118-1.55431*10^-15 i	FALSE
2.15	-0.0627148-4.99892*10^-18 i	1.00118-1.55431*10^-15 i	TRUE
2.15	-0.00802368+2.32695*10^-17 i	1.00118-1.55431*10^-15 i	TRUE
2.15	1.02636-4.40145*10^-19 i	1.00118-1.55431*10^-15 i	FALSE
2.15	1.02467-1.16033*10^-19 i	1.00118-1.55431*10^-15 i	FALSE
2.15	1.02601+6.0032*10^-19 i	1.00118-1.55431*10^-15 i	FALSE
5.12	0.0040705-1.38449*10^-17 i	1.00115-6.66134*10^-16 i	FALSE
5.12	-0.0831145-7.943*10^-18 i	1.00115-6.66134*10^-16 i	TRUE
5.12	-0.0287384+2.37726*10^-17 i	1.00115-6.66134*10^-16 i	TRUE
5.12	1.02632-3.65908*10^-19 i	1.00115-6.66134*10^-16 i	FALSE
5.12	1.0242-1.7749*10^-19 i	1.00115-6.66134*10^-16 i	FALSE
5.12	1.02548+5.88851*10^-19 i	1.00115-6.66134*10^-16 i	FALSE

3.3 Results

Enhancement of Free siRNA by p19

In the current model (Figure 3.1), RNAi is initiated by the production of messenger RNAs (mRNAs) from an infectious agent. mRNAs are cleaved sequentially by Dicer to produce a Dicer bound siRNA complex (SD) and a shorter double-stranded RNA product (ds2 or ds1). SD complexes recruit Argonaute and other RISC proteins to form the mature RISC, which then degrades one strand of the bound siRNA to use as a guide for selective mRNA degradation (Figure 3.1). The protein p19 can suppress RNAi by binding siRNAs either freely in the cytoplasm or by facilitating the dissociation of the SD complex. For simplicity it is assumed that plasmids containing p19 are stably transfected in the cell to produce the protein in constant amounts (Figure 3.1).

Before the introduction of p19, infected mRNA reaches its peak in ~48 h and is fully suppressed in ~96 h, after which it remains in constant equilibrium (Figure 3.2*A*). The SD complex accumulates to a high level with the peak concentration correlating with the lowest point of mRNA accumulation and the onset of equilibrium. Once the equilibrium concentration of mRNA has been reached the levels of SD, RISC, and free siRNA are also reduced. All three species remain, however, at a relatively high steady-state level (Figure 3.2*A*).

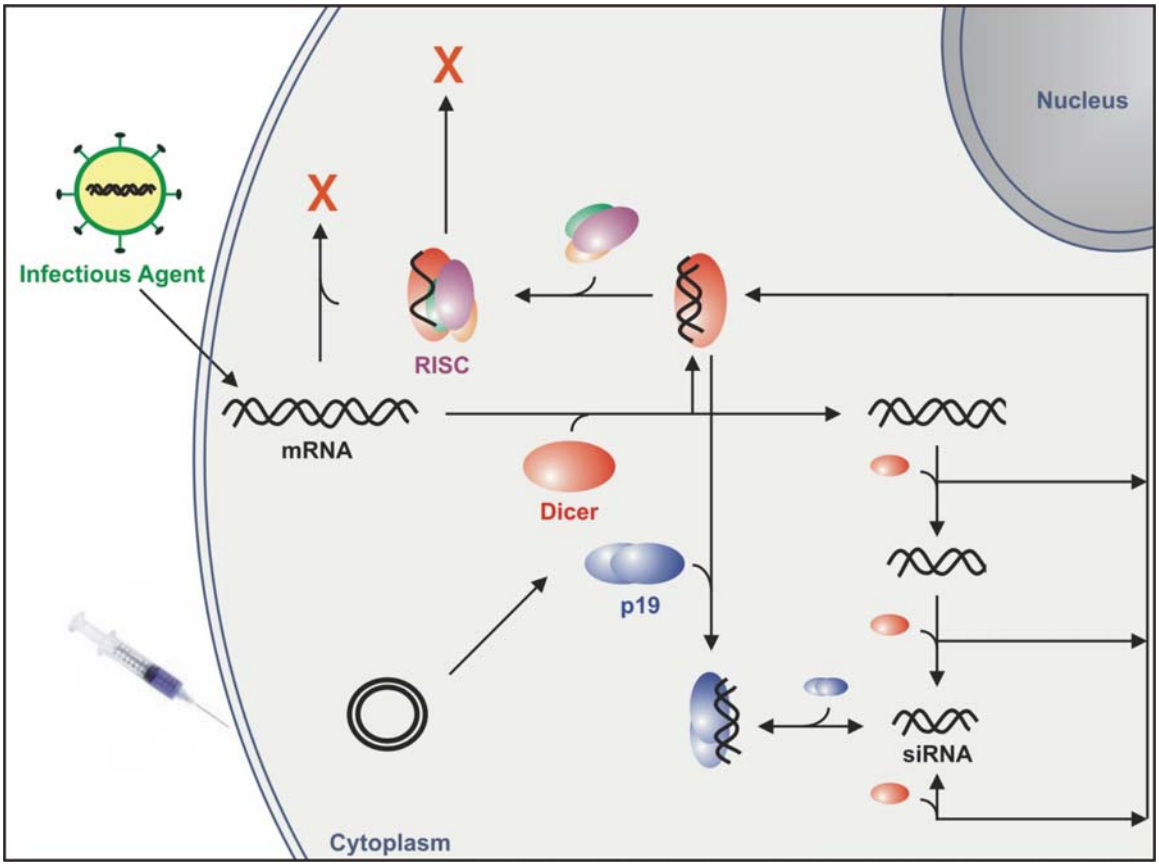

Figure 3.1 Model Diagram.

When the p19 plasmid is introduced, and assumed to express at a rate sufficient to produce a constant 5 nM of protein in the cell, the peak levels of SD and RISC are markedly reduced, with SD reduced by half (Figure 3.2*B*). Conversely, the level of free siRNA increases with the addition of p19, and accumulates to a much higher steady state level (Figure 3.2*B*). Messenger RNA levels are increased by 40% in the presence of 5 nM p19 and the time before suppression is increased by 50% (Figure 3.2 *C*,*D*).

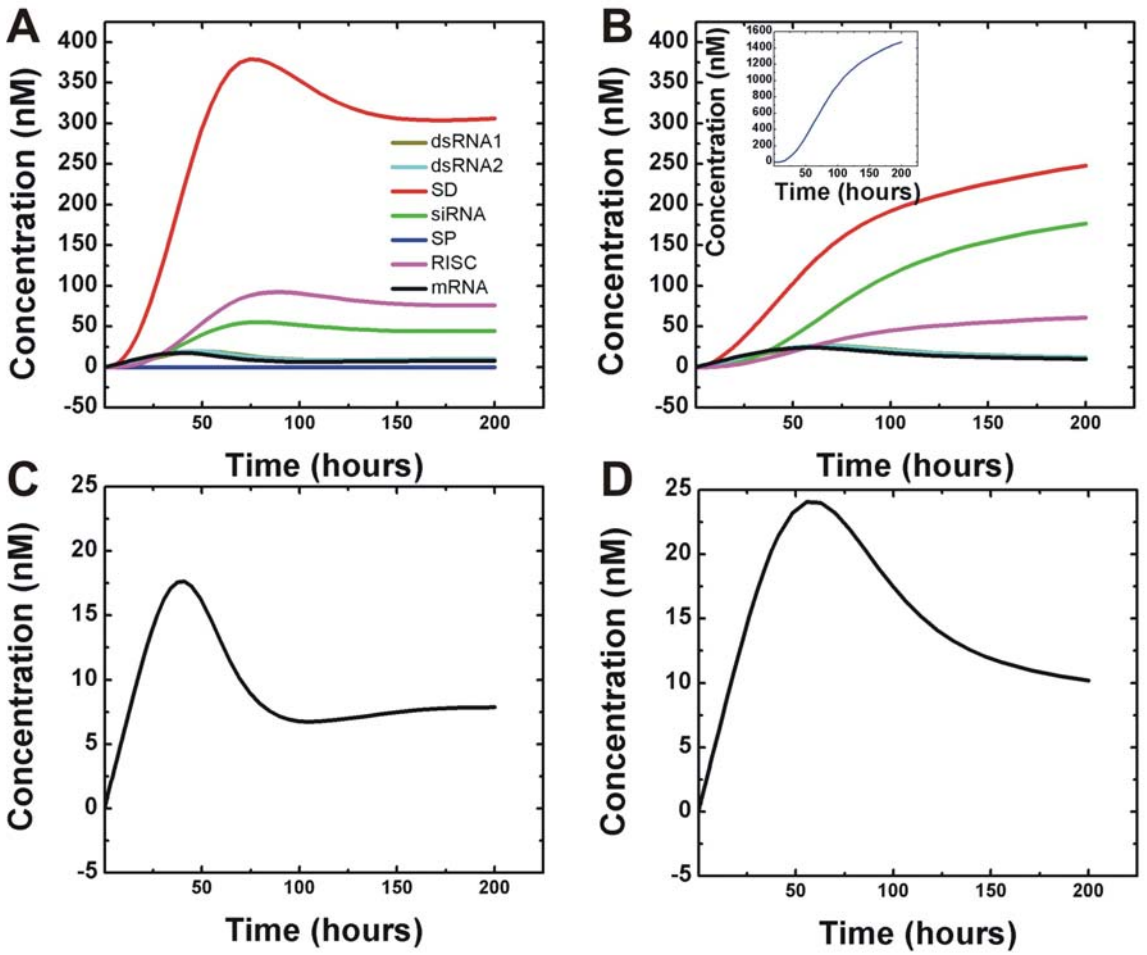

Figure 3.2 The effect of p19 on RNAi complexes. (*A*) Suppression of mRNA in the absence of p19. (*B*) Suppression of mRNA in the presence of 5 nM p19. The siRNA:Dicer complex (SD) and RISC are reduced in the presence of p19 while free siRNA concentration is increased. (*Insert*) Concentration of p19 bound siRNA over time. (*C*) Blowup of the mRNA concentration curve from panel *A* (*D*) Blowup of the mRNA concentration curve from panel *B*, showing a 40% increase in peak mRNA accumulation.

P19 Reinitiates Dormant mRNA Replication

Increasing the concentration of p19 from 0 to 250 nM, linearly increases the time spent in the replication phase and the peak mRNA accumulation. Peak mRNA accumulation increased by 1.5, 2.2, 5, and 8.7-fold in the presence of 5, 25, 125, and 250 nM of p19, respectively (Figure 3.3*A*). A larger effect, however, is seen on the duration of infection. At the highest p19 concentration, the time to fully suppress the infection is increased by over 100-fold (Figure 3.3*A*). Such substantial gains in infection duration may produce varied effects over the course of an infection. We probed effects of timing by introducing p19 to the cell at 24, 48, 72, 96, and 300 h after infection. Addition of p19 at 24 h increases the peak height only marginally over other time points. Interestingly, p19 is able to induce mRNA replication at all time-points observed even after equilibrium has been reached (Figure 3.3*B*).

Timed Introduction of p19 Increases Length of mRNA Replication Phase

Due to the apparent reactivation of infection with p19, we probed p19's effect on rising phase duration by increasing p19 concentration at intervals of 200 h. By increasing the p19 concentration stepwise, the mRNA replication phase is extended from 48 h to 900 h, compared to wild-type infection (Figure 3.4). Compared with p19 added at the onset of infection, rising phase duration is increased by ~ 200% (Figure 3.3*A*).

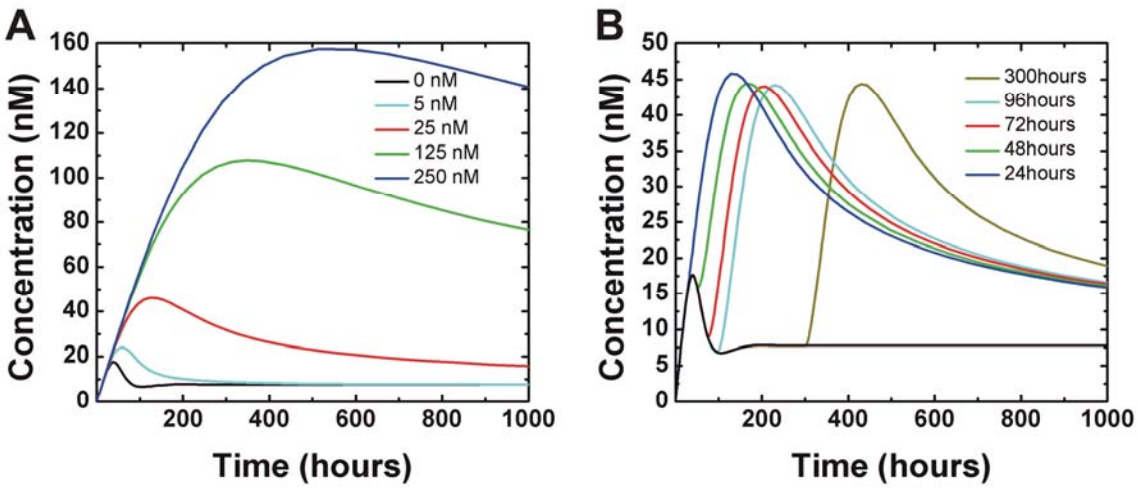

Figure 3.3 p19 Concentration and Timing effect peak mRNA accumulation and infection window. (*A*) The accumulation of mRNA transcripts over time in the presence of 0, 5, 25, 125, and 250 nM p19 produced at a constant rate in the cell. (*B*) mRNA accumulation in the presence of 25 nM p19 introduced at 24, 48, 72, 96, and 300 h.

Modeling Supports Formation of a Transient Ternary siRNA:Dicer:p19 Complex

An alternative model was developed to specifically address the competition of p19 with Dicer for siRNA. This reaction may occur by dissociative binding, with the free siRNA as an obligatory intermediary, or by the formation of a ternary complex between the three participants (Figure 3.5) (for details of the model and its analysis, please see Model Description). As additional model input we estimated the SD and SP complex dissociation rate constants by EMSA to $(4.8 \pm 0.1) \times 10^{-4}$ s^{-1} and $(7.2 \pm 0.1) \times 10^{-4}$, respectively (Figure A5).

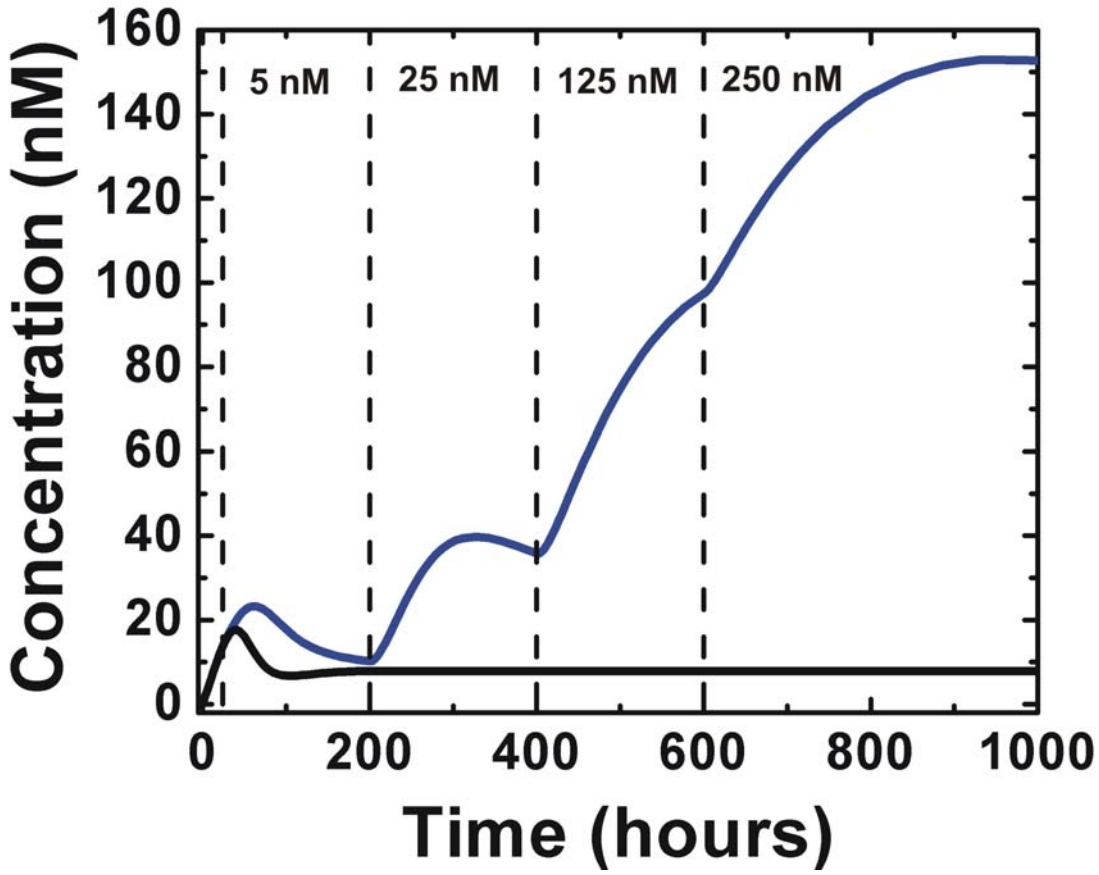

Figure 3.4 Stepwise Introduction of p19 can significantly increase mRNA rising phase. p19 is added to cells at 24, 200, 400, and 600 hours and with increasing concentrations of 5, 25, 125, and 250 nM, respectively (blue curve). mRNA accumulation in the absence of p19 is shown in black. The rising phase of mRNA replication is increased 30-fold over wild-type conditions and 2-fold over p19 added at the onset of infection. Overall infection duration, which is calculated as the time needed to reach the equilibrium suppression level observed in the absence of p19, is increased by over 100-fold.

Based on measured dissociation equilibrium constants for p19 ($K_{D,app}$ = 0.17 ± 0.02 nM) and Dicer ($K_{D,app}$ = 3.7 ± 0.4 nM), we found that dissociative binding alone with free siRNA as an obligatory intermediate cannot reproduce the experimental competition data. In contrast, a model that includes formation of a ternary SDP complex reproduces all experimental data well (Figure 3.5*A*,*B)*; all plots use the following rate constants: $k_3 = 3.27 \times 10^6$ $M^{-1}s^{-1}$, $k_{-3} = 0.0011$ s^{-1}, $k_{-4} = 0.156$ s^{-1}, $k_4 = 2.56 \times 10^5$ $M^{-1}s^{-1}$. Notably, the equilibrium dissociation constant for the formation of the ternary complex from [SP] + [D] is weaker than that of [SD] + [P] (K_D = 0.34 nM and Kd = 608.7 nM, respectively), illustrating the shuttling of siRNA toward the p19 bound state.

3.4 Discussion

Although RNAi is an innate immune response, it has become most extensively used as a tool for functional genomics (32), gene therapy (33-35), vaccine production (36) and therapeutics (37). For such applications, viruses offer a natural model system for regulating RNAi efficiency and identifying points of further development. One mechanism, used by the tombusviridae family of plant pathogens, is to encode the RNA silencing suppressor protein p19. Dimers of p19 bind small interfering RNAs, independent of sequence, to prevent siRNA incorporation into RISC and subsequent silencing of viral infection. p19's ability to bind siRNAs is correlated with the symptom spread and cytotoxicity of this class of viruses, and is found to regulate RNAi effectively also in non-native hosts.

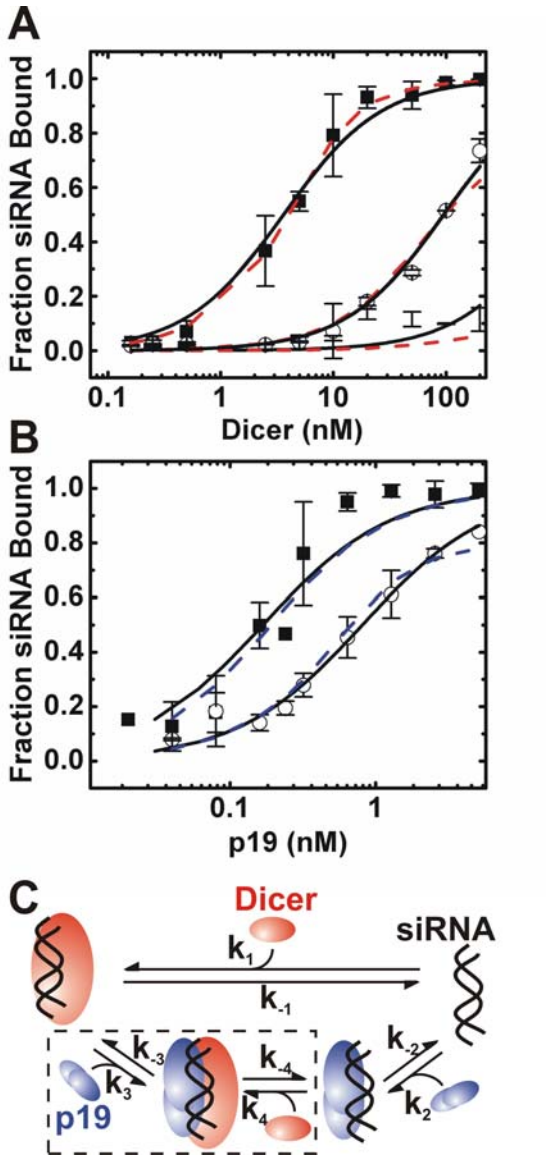

Figure 3.5 Competition of p19 with human Dicer for siRNA binding as detected by EMSA. (*A*) Fraction of siRNA (S) bound to Dicer (D) over increasing Dicer concentrations in the absence (black squares) and presence of p19 (P) at 0.17 nM (open circles) or 2.5 nM (black dots). Black solid lines are hyperbolic fits. Red dashed lines indicate model fits with $k_3 = 3.27 \times 10^6\ M^{-1}s^{-1}$, $k_{-3} = 0.0011\ s^{-1}$, $k_{-4} = 0.156\ s^{-1}$, $k_4 = 2.56 \times 10^5\ M^{-1}s^{-1}$. (*B*) Fraction of siRNA bound to p19 over increasing p19 concentrations in the

(Figure 3.5 continued) absence (black squares) or presence of a saturating Dicer concentration of 140 nM (open circles). Hyperbolic fits are in black. Blue dashed lines indicate model fits with rate constants as indicated above. Representative EMSA gel images are shown in Appendix (Figure A2). (*C*) Two protein competition model.

Here, we illustrate time dependent interactions between p19 and the entire RNAi pathway by modeling exogenous p19 introduction into cells expressing a viral mRNA target. We observe a marked reduction in the maximum accumulation of Dicer bound siRNAs and of mature RISC complexes in the presence of p19 (Figure 3.2). Interestingly, the concentration of free siRNA is increased alongside p19, supporting release of these molecules into the cytoplasm (Figure 3.2). Increasing the concentration of p19 linearly increases the peak mRNA accumulation and has a large effect on infection duration, increasing the time in the rising phase by ~10-fold (Figure 3.3*A*).

Additionally, p19 action was seen to time-invariantly reinitiate mRNA replication after equilibrium mRNA suppression has been reached (Figure 3.3*B*). Allowing for the possibility that p19 could regulate the rising phase of mRNA accumulation, we observed a 30-fold increase in the rising phase of mRNA replication with stepwise addition of p19 and an overall increase in infection duration of over 100-fold (Figure 3.4).

Next, we modeled the interaction of p19 with human Dicer and saw evidence for a ternary complex between the siRNA, Dicer, and p19. Rate constants for this reaction were numerically determined to be $k_3 = 3.27 \times 10^6$ $M^{-1}s^{-1}$ and $k_4 = 2.56 \times 10^5$ $M^{-1}s^{-1}$ for the formation of the ternary complex from either the Dicer bound or p19 bound state, and $k_{-3} = 0.0011$ s^{-1} and $k_{-4} = 0.156$ s^{-1} for dissociation of the complex back into the Dicer:siRNA or p19:siRNA complex, respectively (Figure 3.5).

Taken together, our models support a catch and release mechanism of p19 action, in which p19 can bind siRNAs directly or by facilitating Dicer dissociation. Time-invariance of p19 suggests an active need for Dicer bound siRNAs and RISC complexes to maintain equilibrium suppression. The idea of long-term active RNAi suppression of mRNA was suggested also in experiments showing enhancement of HIV replication in latently infected cells upon knockdown of Dicer or Drosha, another enzyme active in RNAi (38). From our model we can predict the following principles for optimal use of p19 in tuning RNAi regulation.

Principles for p19 Interaction with RNAi-Based Applications

(1) **Proximity-** p19 expressed close to the source of infection maximizes the benefit of siRNA shuttling through its ternary interaction with Dicer.

(2) **Increased concentration**- Higher p19 concentrations produce increased viral mRNA production, longer rising phases and much slower suppression, increasing the observed duration of infection.

(3) **Timing of Incubation**- The incubation time before harvesting cells can significantly affect yield. Optimal incubation times scale linearly with the effective concentration of p19 in the cell.

(4) **Timing of Introduction**- Addition of p19 before full suppression of infection increases the rising phase of mRNA production and the time needed to reach peak mRNA levels. Late introduction of p19 is observed to reinitiate mRNA accumulation even after equilibrium has been reached.

Although the benefits are apparent, there are potential drawbacks concerning the use of p19 in some applications. The effect of equilibrium reactivation may not be specific due to p19's sequence independent binding of siRNAs and its observed interactions with other classes of small RNAs (39). This could be a source of off-target up-regulation of other RNAi suppressed targets including reinitiation of dormant viral satellites, or activation of endogenously suppressed proteins.

p19, additionally, seems to be a much more effective modulator of infection duration, than it is an inducer of mRNA accumulation. Modest gains in viral load were observed in experiments infecting HIV clones into cell lines stably transfected with p19 (40). These results suggest that conventional promoters do not produce p19 in high enough quantities to induce substantial mRNA accumulation. An added factor is the fact that the incubation time necessary to achieve maximal mRNA levels is dependent on p19 concentration, increasing the optimal incubation time 8.7-fold at the highest modeled concentration. A summary of these drawbacks and concerns is given below.

Drawbacks and Concerns of p19

(1) **Dormant viruses**- The effectiveness of p19 is not specific to the gene of interest due to its ability to bind siRNAs and other small RNA, independent of sequence. This can be a source of off-target effects including up-regulation of other RNAi suppressed targets.

(2) **Long Incubation Times**- Maximum efficiency comes at the cost of longer incubation times of greater than 8-fold of the original infection, dependent on p19 concentration.

(3) **Significance of Sustained Dosing**- Sufficiently high sustained dosing of p19 may be a challenge when using conventional promoters used in stable cell transfection. Introduction of a low dose of p19 early in the infection window leads to limited, if any, discernable difference in yield.

We conclude that p19 can significantly increase the yield of a virally introduced gene of interest. This may be of benefit in numerous functional applications that use RNAi as a tool for genetic research, protein production and therapeutics, as long as possible complications are also considered.

3.5 Acknowledgements

I would like to thank Dr. Patrick Nelson and Dr. Trachette Jackson for generously giving of their time for helpful discussions on computational modeling.

3.6 References

1. Carthew RW & Sontheimer EJ (2009) Origins and Mechanisms of miRNAs and siRNAs. *Cell* **136**(4):642-655
2. Chellappan P, Vanitharani R, & Fauquet CM (2005) MicroRNA-binding viral protein interferes with Arabidopsis development. *Proc Natl Acad Sci U S A* **102**(29):10381-10386
3. Baulcombe D (2004) RNA silencing in plants. *Nature* **431**:356-363
4. Ding SW & Voinnet O (2007) Antiviral immunity directed by small RNAs. *Cell* **130**(3):413-426
5. Fire A, *et al.* (1998) Potent and specific genetic interference by double-stranded RNA in Caenorhabditis elegans. *Nature* **391**:806-881.
6. Johansen LK & Carrington JC (2001) Silencing on the spot. Induction and suppression of RNA silencing in the Agrobacterium-mediated transient expression system. *Plant Physiol* **126**(3):930-938
7. Scholthof H (2006) The Tombusvirus-encoded P19: from irrelevance to elegance. *Nat Rev Microbiol* (4):405-411.
8. Silhavy D & Burgyan J (2004) Effects and side-effects of viral RNA silencing suppressors on short RNAs. *Trends Plant Sci* (9):76–83.
9. Umbach JL & Cullen BR (2009) The role of RNAi and microRNAs in animal virus replication and antiviral immunity. *Genes Dev* **23**(10):1151-1164

10. Collingwood MA, *et al.* (2008) Chemical modification patterns compatible with high potency dicer-substrate small interfering RNAs. *Oligonucleotides* **18**(2):187-200

11. Kim DH, *et al.* (2005) Synthetic dsRNA Dicer substrates enhance RNAi potency and efficacy. *Nat Biotechnol* **23**(2):222-226

12. Jaskiewicz L & Filipowicz W (2008) Role of Dicer in posttranscriptional RNA silencing. *Curr Top Microbiol Immunol* **320**:77-97

13. Ji X (2008) The mechanism of RNase III action: how dicer dices. *Curr Top Microbiol Immunol* **320**:99-116

14. Siomi H & Siomi MC (2009) On the road to reading the RNA-interference code. *Nature* **457**(7228):396-404

15. Bergstrom CT, McKittrick E, & Antia R (2003) Mathematical models of RNA silencing: unidirectional amplification limits accidental self-directed reactions. *Proc Natl Acad Sci U S A* **100**(20):11511-11516

16. Marshall WF (2008) Modeling recursive RNA interference. *PLoS Comput Biol* **4**(9):e1000183

17. Bartlett DW & Davis ME (2006) Insights into the kinetics of siRNA-mediated gene silencing from live-cell and live-animal bioluminescent imaging. *Nucleic Acids Res* **34**(1):322-333

18. Goutsias J & Lee NH (2007) Computational and experimental approaches for modeling gene regulatory networks. *Curr Pharm Des* **13**(14):1415-1436

19. Groenenboom MA, Maree AF, & Hogeweg P (2005) The RNA silencing pathway: the bits and pieces that matter. *PLoS Comput Biol* **1**(2):155-165

20. Groenenboom MA & Hogeweg P (2008) The dynamics and efficacy of antiviral RNA silencing: A model study. *BMC Syst Biol* **2**:28

21. Qu F & Morris TJ (2005) Suppressors of RNA silencing encoded by plant viruses and their role in viral infections. *FEBS Lett* **579**(26):5958-5964

22. Roth BM, Pruss GJ, & Vance VB (2004) Plant viral suppressors of RNA silencing. *Virus Res* **102**(1):97-108

23. Voinnet O (2001) RNA silencing as a plant immune system against viruses. *Trends Genet* **17**(8):449-459

24. Chu M, Desvoyes B, Turina M, Noad R, & Scholthof HB (2000) Genetic dissection of tomato bushy stunt virus p19-protein mediated host-dependent symptom induction and systemic invasion. *Virology* (266):79-87.

25. Omarov R, Sparks K, Smith L, Zindovic J, & Scholthof HB (2006) Biological relevance of a stable biochemical interaction between the tombusvirus-encoded P19 and short interfering RNAs. *J Virol* **80**(6):3000-3008

26. Silhavy D*, et al.* (2002) A viral protein suppresses RNA silencing and binds silencing-generated, 21- to 25-nucleotide double-stranded RNAs. *EMBO J.* **21**:3070-3080.

27. Havelda Z, Hornyik C, Valoczi A, & Burgyan J (2005) Defective Interfering RNA Hinders the Activity of a Tombusvirus-Encoded Posttranscriptional Gene Silencing Suppressor. *J Virol* (79):450-457.

28. Dunoyer P, Lecellier CH, Parizotto EA, Himber C, & Voinnet O (2004) Probing the microRNA and small interfering RNA pathways with virus-encoded suppressors of RNA silencing. *Plant Cell* **16**(5):1235-1250

29. Vargason JM, Szittya G, Burgyan J, & Hall TM (2003) Size selective recognition of siRNA by an RNA silencing suppressor. *Cell* (115):799-811.

30. Ye K, Malinina L, & Patel DJ (2003) Recognition of siRNA by a viral suppressor of RNA silencing. *Nature* (426):874-878.

31. Xia Z, Zhu Z, Zhu J, & Zhou R (2009) Recognition mechanism of siRNA by viral p19 suppressor of RNA silencing: a molecular dynamics study. *Biophys J* **96**(5):1761-1769

32. Belles X (Beyond Drosophila: RNAi in vivo and functional genomics in insects. *Annu Rev Entomol* **55**:111-128

33. Barichievy S, Saayman S, Arbuthnot P, & Weinberg MS (2009) RNA interference-based gene expression strategies aimed at sustained therapeutic inhibition of HIV. *Curr Top Med Chem* **9**(12):1065-1078

34. Berkhout B & ter Brake O (2009) Towards a durable RNAi gene therapy for HIV-AIDS. *Expert Opin Biol Ther* **9**(2):161-170

35. Schnettler E, *et al.* (2009) The NS3 protein of rice hoja blanca virus complements the RNAi suppressor function of HIV-1 Tat. *EMBO Rep* **10**(3):258-263

36. Zheng N, *et al.* (2009) Boosted expression of the SARS-CoV nucleocapsid protein in tobacco and its immunogenicity in mice. *Vaccine* **27**(36):5001-5007

37. Tiemann K & Rossi JJ (2009) RNAi-based therapeutics-current status, challenges and prospects. *EMBO Mol Med* **1**(3):142-151

38. Triboulet R, *et al.* (2007) Suppression of microRNA-silencing pathway by HIV-1 during virus replication. *Science* **315**(5818):1579-1582

39. Lakatos L, Szittya G, Silhavy D, & Burgyan J (2004) Molecular mechanism of RNA silencing suppression mediated by p19 protein of tombusviruses. *EMBO J* **23**(4):876-884.

40. de Vries W, *et al.* (2008) Increased virus replication in mammalian cells by blocking intracellular innate defense responses. *Gene Ther* **15**(7):545-552

CHAPTER 4:

IN VITRO PROBING OF MICRO-RNA CONTAINING COMPLEXES IN HUMAN CYTOSOLIC EXTRACT

4.1 Introduction

MicroRNAs (miRNAs) are a large and growing class of ~ 21-25 nucleotide small non-coding RNAs that can act as posttranscriptional gene regulators. miRNAs are usually endogenous transcripts processed first in the nucleus, and then exported into the cytoplasm where they repress messenger RNA translation (1). The current estimation is that 40-70% of all miRNAs are transcribed from introns of protein-coding genes and both introns and exons of non-coding RNAs (2). Initially synthesized as large primary-miRNA (pri-miRNA) transcripts, microRNAs are cleaved in the nucleus by the nuclear enzyme Drosha into smaller imperfectly base-paired stem-loops (pre-miRNAs) (3-5). These pre-miRNAs are then exported to the cytoplasm where they are further processed into mature miRNAs by the RNase III enzyme Dicer (6, 7). Mature miRNA duplexes are loaded into the RNA Induced Silencing Complex (RISC), which retains one strand of the duplex as a guide strand to target specific mRNAs for either destabilization (8) or translational repression (9, 10) (Figure 4.1*A*).

Despite distinct overlaps in processing, miRNAs differ from another well-known class of non-coding RNAs, small interfering RNAs (siRNAs), in both their biogenesis

and ultimate cellular functionality (11) (Figure 4.1*B*). siRNAs are typically ~ 21-22 nucleotide exogenous products cleaved initially in the cytoplasm, by Dicer, from long double-stranded RNA duplexes derived from viruses or transposons (12-14). After cleavage, both small RNAs are incorporated into (different forms of) RISC, to carry out the recognition, cleavage and/or repression of the mRNA targets (15). In contrast to microRNAs, siRNAs direct targeted degradation of their parent mRNA and require complete complementarity for binding (11).

Micro-RNAs, uniquely, require incomplete complementarity in their duplex formation and in binding with a target mRNA to induce repression. Recognition is achieved by small seed sequences, five to eight nucleotides in length, that are fully complementary to regions within the 3' UTR of an mRNA with some non-conserved binding in peripheral flanking sequences (11). Consequently, the stringency for target recognition is reduced, allowing a single miRNA to regulate numerous genes. For example, in humans, known miRNAs represent less than 1% of the transcribed genome, yet they are estimated to regulate >30% of all protein-coding genes (19). Alteration, therefore, in a single miRNA can lead to distinct higher-order regulation of hundreds of genes and alter the expression patterns of large subsets of proteins (20).

Lethal-7 (let-7) is an early emerging class of miRNAs that regulate cellular proliferation and the timing of cell differentiation in various species (21). There are currently nine referenced examples in this class labeled let-7a through let-7i. Cells that poorly express let-7 are seen in certain lung cancers (22), and the seed sequences of these molecules have been mapped to deleted mRNA regions in cancerous cell lines (22, 23).

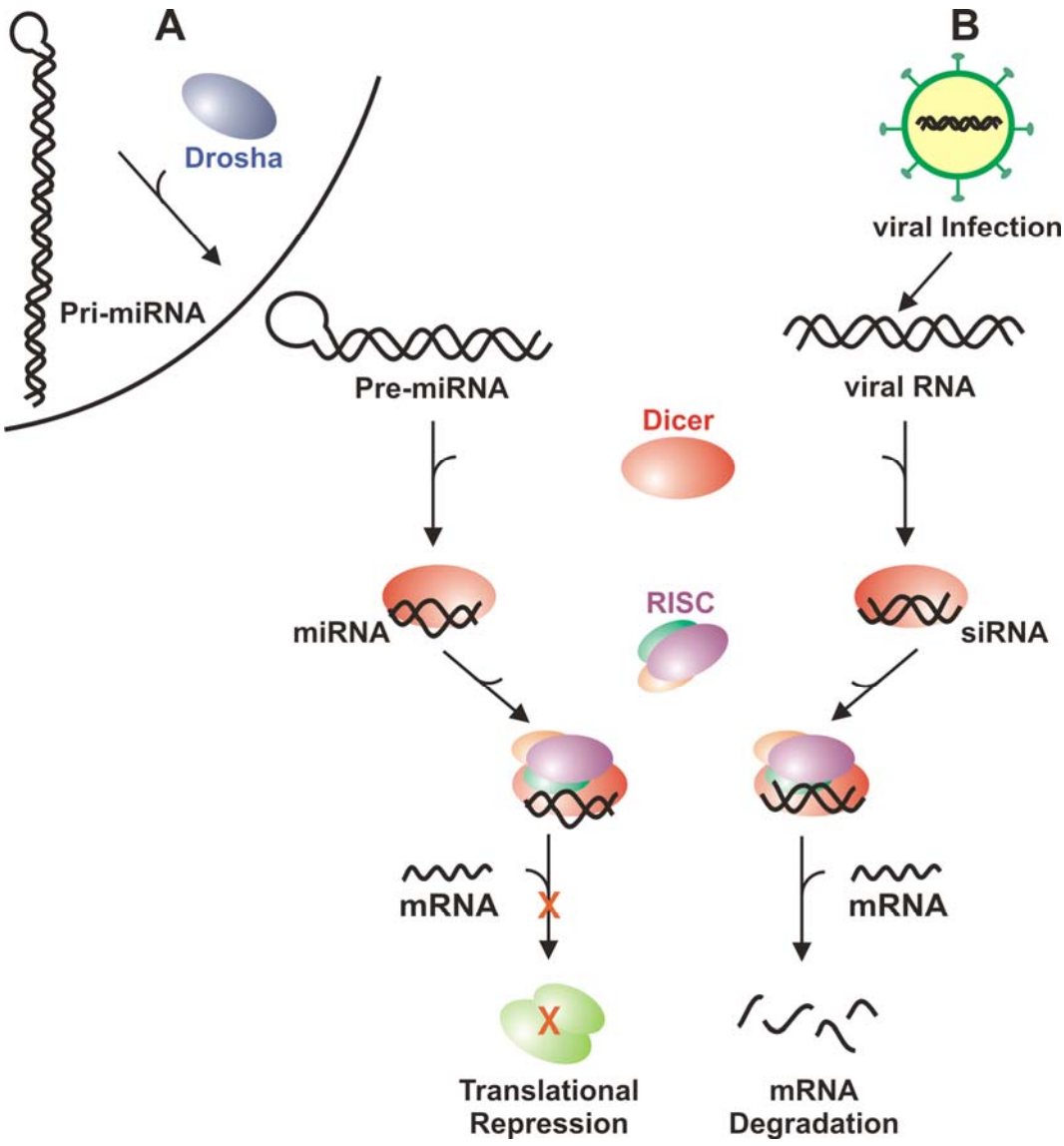

Figure 4.1 MicroRNA and siRNA Pathways. (*A*) MicroRNAs are initially transcribed in the nucleus as longer primary RNA transcripts (pri-miRNA) and cleaved by the nuclear enzyme, Drosha. Drosha cut pre-miRNAs are exported into the cytoplasm for further processing into mature miRNAs by the RNase III enzyme Dicer. In humans, Dicer associated miRNAs recruit RISC complex formation (16, 17), which represses translation of targeted mRNAs. MicroRNAs require selected mismatches in base pairing for functionality (*B*) Small interfering RNAs (siRNAs) are cleaved from long cytosolic

(Figure 4.1 continued) RNA, derived from viral infection or transposons, by the RNase III enzyme Dicer. In humans, the Dicer/siRNA complex is a part of the RISC loading complex (18) and promotes degradation of the mRNA target. siRNAs require full complementarity to promote degradation.

Findings such as these suggest that this miRNA can act as a tumor suppressor as well as a regulator of cell fate (24). The mechanism, however, by which let-7 regulates gene expression still remains poorly understood. Here we specifically 3'-end label let-7a miRNA using the fluorophore Cy3, with the ultimate goal of imaging its cellular localization over time within living cells.

A central obstacle in the path of imaging small molecules *in vivo* is that of reaching a sufficient signal-to-noise ratio. One fluorophore is often not enough to effectively image the inside of a living cell. Typically, to overcome this problem, targets are either immobilized in a single location (i.e., the cell membrane) or they are labeled with multiple fluorophores sufficient to be seen above the auto-fluorescence of the cell. In the case of miRNAs, these techniques are problematic, localization cannot be studied after membrane immobilization, and miRNAs are too small to be labeled sufficiently to counteract its fast diffusion (which leads to blurring when imaging). In order to achieve the desired signal–to-noise ratio a suitable target is needed to concentrate the let-7 fluorescence and ensure specificity.

Only five of the over 100 endogenous targets for let-7a have more than four binding sites in their 3' UTR and, of these, only one target, High Mobility Group protein or HMGA2, has more than six sites (25). High Mobility Group A (HMGA) proteins

generally alter chromatin architecture and thus participate in the transcriptional regulation of gene expression (26). They were originally isolated from mammalian cells, named according to their electrophoretic mobility in polyacrylamide gels, and arbitrarily classified as a specific type of nonhistone proteins, based on the observation that they are ubiquitous in mammalian cells and are associated with isolated chromatin. HMGA2 has been implicated in tumorigenesis due to transcriptional up-regulation and chromosomal translocations in several types of tumors. Additionally, the HMGA2 3' UTR has seven let-7 binding sites and disruption of these sites enhances oncogenic transformation (27, 28). The function of this up-regulation in tumorigenesis is as yet unclear, however, the correlation between over-expression of HMGA2 and tumor growth may explain the higher degree of let-7 regulation. For localization assays, the number of let-7 binding sites within HMGA2 would allow for up to seven single-labeled let-7 miRNAs to be associated with one mRNA, thus increasing the image quality and slowing the apparent tumbling of the miRNAs after association with the larger molecule.

As a precursor to the *in vivo* work, we determine here the potential effect of let-7a labeling on binding and complexation using *in vitro* complex formation assays with human cell extract. Gel-based analysis shows Cy3-labeling biases protein complexes to form with a single-stranded miRNA rather than with the double-stranded form. It is unclear whether this bias will limit *in vivo* binding as the miRNA duplex is unwound before mRNA recognition. Moreover, the extent of complexation is altered upon Cy3 labeling, showing limited ATP dependence and co-migration with complexes containing human Dicer.

4.2 Materials and Methods

Preparation of Let 7 and HMGA2. All RNAs were synthesized by the HHMI Biopolymer/Keck Foundation Biotechnology Resource Laboratory at the Yale University School of Medicine, then deprotected and purified as previously described (29, 30). Sequences were derived from the wild-type let 7a target scan sequence (31) and were as follows: Let-7a Antisense strand 5′-P-UGA GGU AGU AGG UUG UAU AGU U-(Amino C7)-3′; Let-7 Sense strand 5′-P-CUA UAC AAU CUA CUG UCU UUC C-3′, Prelet-7 Antisense strand 5′-P-UGG GAU GAG GUA GUA GGU UGU AUA GUU-(Amino C7)-3′; Prelet-7 Sense strand 5′-P-CUA UAC AAU CUA CUG UCU UUC CUA-3′, where P denotes a 5′-phosphate and (Amino C7) denotes a phosphoramidite of the same name from Glen Research. The antisense strands were also synthesized with only one or no modifications wherein the Amino C7 linker or the unlabeled 5' P was removed. HMGA*2* cDNA (pCMV•SPORT6.1) was provided by the Bartel lab and prepared as previously described (25). cDNA was amplified by PCR from the pCMV•SPORT6.1 plasmid with the forward primer containing the T7 promoter sequence (Forward T7 UTI 2: TAA TAC GAC TCA CTA TAG GG CAG ATA TCC AGC ACA GTG G and Reverse 2UTR: TCG AAG GGC CCT CTA GAC TC) or by direct transcription from a pEF6 plasmid containing HMGA2 subcloned downstream of a T7 promoter. Products were run on a 0.7% Agraose gel and eluted using 1mM EDTA. Transcriptions were done with T7 RiboMax Express Kit (Promega), Maxiscript (Applied Biosystem), and MegaScript (Applied Biosystem) as per manufactures instructions.

EMSA. For radioactive EMSAs, the non-phosphorylated antisense strand was first 5′-^{32}P labeled with T4 polynucleotide kinase (PNK) and γ-^{32}P-ATP at an RNA concentration of 800 nM. PNK was inactivated by heating to 90 °C for 10 min, then the 5′ phosphorylated complementary strand was added in 2-fold molar excess and the reaction slowly cooled to room temperature to anneal the two strands. The miRNA duplex was further purified by polyacrylamide gel electrophoresis on a 20% (v/v) nondenaturing gel. The duplex miRNA was cut out, eluted overnight into 1 mM EDTA at 4 ^{o}C, ethanol precipitated, and dissolved in RNase-free water. Scintillation counting was done on a Beckman LS6500 Multipurpose Scintillation Counter. EMSAs were performed as described previously (32) on 10-cm non-denaturing 4, 12, or 20% (v/v) polyacrylamide gels in 0.5x TBE (44.5 mM Tris-Borate, 1 mM EDTA) and run at 500 V and 4 ^{o}C for 2 h. p19, at varying final concentrations, was added to radio-labeled siRNA duplex (50,000 cpm, < 400 pM of 5′-^{32}P labeled duplex) in 10 μL standard buffer and incubated for 0.5 h. Next, 10 μL non-denaturing loading buffer (10% glycerol, 0.5x TBE, 0.025% bromophenol blue, and 0.025% xylene cyanol) was added and each sample loaded onto a 12% (v/v) polyacrylamide gel.

RISC Assembly Complex Formation. Let7a (synthesized as above) was labeled with Cy3 monoreactive dye, containing NHS-Ester purchased from GE Healthcare (PA23001), by combining up to 30 nmoles of RNA dissolved in 11μl water, 75 μL of 0.1 Sodium tetraborate pH 8.5, and 200 mg of Cy3 dye dissolved in 14 μL of DMSO. Labeling reaction was tumbled overnight at 25 ^{o}C, then ethanol precipitated with (3 vol ETOH, 0.1 vol 3 M NaOAc, and 0.01 vol 100mM NTP) at -20 ^{o}C overnight. Samples

were purified using reverse phase High Pressure Liquid Chromatography and concentrations determined by a Beckman 640B UV spectrophotometer. To observe RISC assembly complexes 15 % (v/v) cytosolic HeLa cell extract (Jena Bioscience) was incubated with 100 nM Cy3 labeled let-7 or < 400 pM radiolabeled miRNA antisense strand or duplex (prepared as above) in a final volume of 10 μL HeLa buffer [8% (v/v) Lysis Buffer (23.7 mM HEPES, pH 7.5, 79 mM potassium acetate, 1.58 mM magnesium acetate, 5 mM DTT, and 1 mg/ml Perabloc SC (Roche)), supplemented with 20% (v/v) 5x RNAi mix (125 mM creatine phosphate, 5 mM ATP, 25 mM DTT), 2% (w/v) creatine kinase, and 20% (v/v) RNA guard RNase Inhibitor (GE Bioscience)] for 0.5 h at 4 ^{o}C, unless otherwise specified. ATP depletion experiments were done by addition of 1 μL of 100 mM glucose and omitting ATP generating system. Multiple transcription products of HMGA2 mRNA were added at 10% (v/v) to Hela cell complexes preformed with radio-labeled let-7 (as described above).

Western Blots for Dicer Detection. RISC assembly complexes were formed as described above, but scaled up 6-fold for western detection. Non-denaturing 12% polyacrylamide gels were soaked in 0.1% (w/v) SDS for 15 min and then electroblotted in Tris-Glycine transfer buffer (25 mM Tris, 25 mM Glycine) onto a PVDF (Polyvinylidene Fluoride) membrane (Immobilon-P Membrane, Millipore) over 75 min at 300 mA, using a Bio-Rad Trans-Blot SD semi-dry transfer cell per the manufacturer's instructions. After transfer, the proteins were fixed to the membrane by incubating in 5-10% (v/v) acetic acid, rinsing with deionized water, and air-drying. The membrane was probed with a rabbit primary antibody against Dicer (Santa Cruz Biotechnology),

followed by a goat anti-rabbit secondary antibody, conjugated with horseradish peroxidase (Zymed, Invitrogen). The blot was developed using a peroxide/enhancer solution (ECL-Plus detection, Amersham), and visualized on a Typhoon 9410 Variable Mode Imager.

4.3 Results

Complex Formation between Radio-labeled Let-7 and HeLa cell Extract Components

Let-7a duplexes were 5` end labeled with radioactive γ-^{32}P-ATP (Figure 4.2*A*). The labeled duplex was then incubated with S100 cytosolic HeLa cell extract and complexes were resolved on polyacrylamide gels. We observed that six bands formed in the presence of extract, which we labeled complex I – complex VI, respectively (Figure 4.2*B*). These miRNA-containing complexes show variations in relative abundance, with complexes I, II, and IV consistently the most prominent and limiting amounts of complexes III and VI (Figure 4.2*C*). These complexes were compared to those formed with a luciferase targeting siRNA duplex of similar size, also 5' end labeled with γ-^{32}P-ATP and incubated with HeLa extract (Figure 4.2*C*). Only three complexes of relatively equal abundance were formed in the presence of the siRNA duplex, consistent with our previous results (Figure 2.4), and were labeled complex D, C2, and C1, respectively (Figure 4.2*C*).

When comparing their evolution over time, miRNA complexes exhibit increased stability, whereas siRNA complexes increased by ~3-fold over a two-hour period (Figure 4.2*C*). Additionally, complex I runs comparably to the siRNA complex C1, at 10 and 120 min incubations, while micro-RNA complex III compared with the siRNA complex C2 at both incubation times (Figure 4.2*C*). Complex V, however, consistently runs lower than the siRNA complex D, whereas complex VI runs higher at both 10 and 120 min. Complex D was shown previously to be the only Dicer-containing siRNA band,

suggesting that complexes V and VI are distinct from the Dicer:siRNA complex (Figure 2.4).

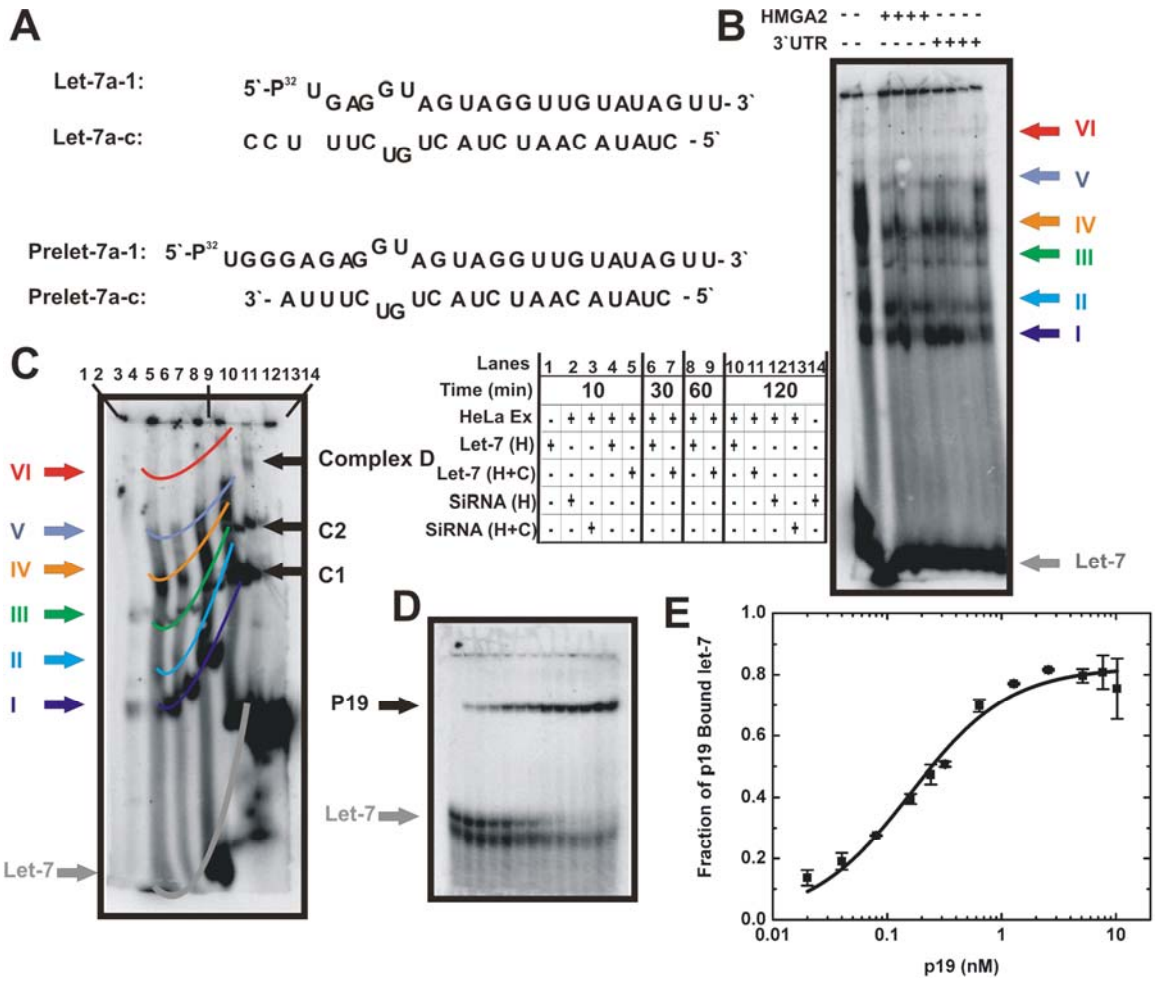

Figure 4.2 Complex Formation of Radio-labeled Let-7a. (*A*) Sequence of let-7a and prelet-7a duplexes (*B*) Complex formation between let-7 duplexes and cytosolic HeLa cell extract. Lanes 3-6 include full-length HMGA2 messenger RNA transcripts. Lanes 7-10 include the 3` UTR only. (*C*) Time-course of miRNA vs siRNA complex formation. Let-7 only (lane1). Complexes formed between radio-labeled siRNA and cytosolic HeLa cell extract after a 10 min incubation (lane 2), plus addition of 100 nM of unlabeled siRNA (lane 3). Let-7 complexes after a 10, 30, 60 and 120 min incubation (lanes 4, 6, 8

(Figure 4.2 continued) and 10), plus addition of 100 nM of unlabeled let-7 duplex (lanes 5, 7 , 9 and 11). siRNA complexes after a 120 min incubation (lane 12), plus addition of 100 nM of unlabeled siRNA (lane 13). SiRNA only (lane 14). (*D*) EMSA assay between p19 and let-7. (*E*) Graph of p19 concentration verses fraction of bound let-7 miRNAs.

Addition of unlabeled let-7 duplexes competed with most complexes as expected, but also shifted relative abundance. Complexes II, IV, V, and VI were completely depleted in the presence of 100 nM of unlabeled let-7 duplex (Figure 4.2*C*). Complex III was retained at approximately the same abundance in the presence or absence of unlabeled let-7 duplex, and the abundance of complex I increased by 2-fold at all time-points upon addition of unlabeled let-7 (Figure 4.2*C*). Similarly, complexes C1 and C2 were retained in the presence of unlabeled siRNA after 120 min, whereas complex D showed complete depletion over the same time frame (Figure 4.2*C*). The similarities between the miRNA complexes I and III and that of siRNA complexes C1 and C2 suggest they may represent similar non-RISC-related complexes formed in the presence of modified small RNAs.

p19 Binds miRNAs with the Same Affinity as siRNAs

Due to the observed differences in complex formation between the siRNA and miRNA duplexes, the effect of sequence as compared to structural changes were probed by binding of a sequence-independent viral protein, p19. p19 is a highly conserved pathogenicity factor encoded by the tombusvirus family of viruses to bind siRNAs and competes with Dicer *in vivo*. We have shown p19 to have a strong affinity for siRNA

duplexes (Figures 2.2 and A2*D*), and it is known to bind independent of sequence (33). Sequence-independence is achieved by homodimers of the protein binding siRNA duplexes in a positively charged surface cleft and stacking on both terminal base pairs to establish a caliper-like size selection for duplexes with 19 base pairs and 2-nucleotide long 3′-overhangs (32, 34, 35). miRNAs, with their inherent mismatches, were initially assumed to be potentially weaker substrates for p19 .

To test for miRNA binding by p19, radioactive electrophoretic mobility shift assays (EMSAs) were performed wherein the miRNA duplex was incubated with purified p19 (Figure 4.2*D*). The apparent equilibrium dissociation constant for the p19:miRNA complex was measured as $K_{D,app}$ = 0.16 ± 0.02 nM (Figure 4.2*D,E*), which is identical, within experimental error, of the dissociation constant measured for the siRNA:p19 complex ($K_{D,app}$ = 0.17 ± 0.03 nM) (Figure A2).

Messenger RNA Addition Produces no Effect on miRNA Complexes

To determine the effect messenger RNA addition has on formation of miRNA complexes in HeLa cell extract, HMGA2 target mRNA was transcribed using a T7 promoter either from a plasmid containing the entire HMGA2 sequence or a PCR product of only the 3'UTR of HMGA2. Radio-labeled miRNA duplexes were incubated, as above, with cytosolic HeLa cell extract to form complexes I-VI, then either full-length HMGA2 or the 3'UTR only was added and analyzed by EMSA to determine migration differences (Figure 4.2*B*). No change in migration was observed due to the addition of mRNA for either full length or 3' UTR HMGA2 constructs (Figure 4.2*B*). We hypothesize that transcripts may be degraded in extract due to a lack of a 5`-end cap, or

that saturating endogenous transcripts are available and contributing to any RISC related complexes currently observed. Additionally, HMGA2 mRNA may simply not bind a miRISC or other complex *in vitro*.

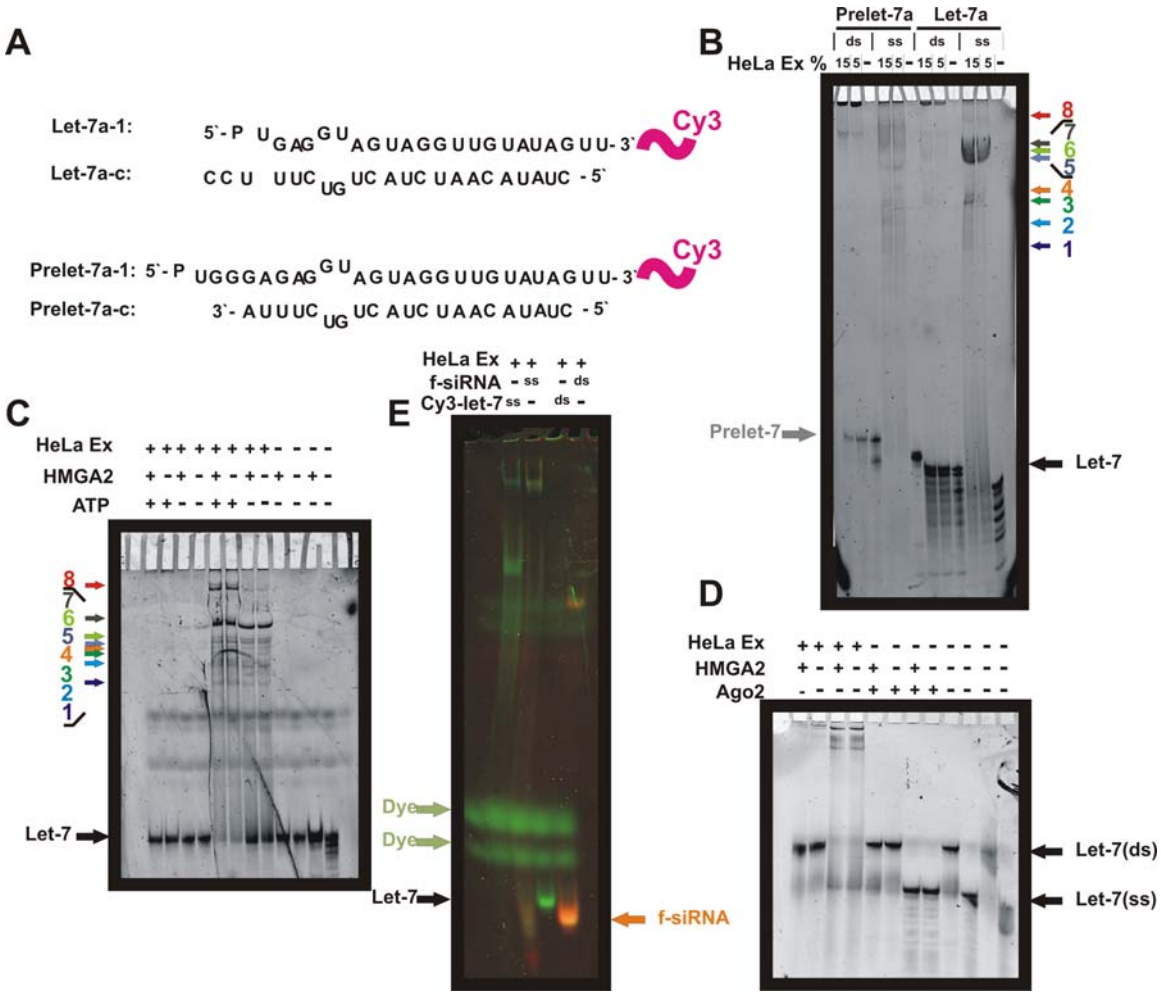

Figure 4.3 Complex Formation of Cy3-labeled Let-7a. (*A*) Position of Cy3 labeling and sequence of let-7a and prelet-7a duplexes (*B*) Complex formation between single or double-stranded Cy3 let-7a and prelet-7. Addition of 15%, 5%, or 0% (v/v) Hela cell extract to double-stranded prelet-7 (lanes 1-3), single-stranded prelet-7 (lanes 4-6), double-stranded let-7 (lanes 7-9), and single-stranded let-7 (lanes 10-12), respectively. (12% non-denaturing gel, run 4 h at 4^{o} C) (*C*) ATP dependence of Cy3 let-7 complexes. Double-stranded let-7 incubated with HeLa cell extract and either (+) an ATP generating

(Figure 4.3 continued) system, with and without HMGA2 3`UTR (lanes1 and 2 respectively), or (-) an ATP generating system, with and without HMGA2 3`UTR (lanes 3 and 4 respectively). Lanes 4-8 contain single-stranded let-7 with additions identical to lanes 1-4, respectively. Duplex (lanes 9-10) or single-stranded let-7 (lanes 11-12) plus or minus HMGA2 mRNA. (12% non-denaturing gel, run 2 h at 4^{o} C) ATP was depleted in extract by addition of glucose and hexokinase. Double and single-stranded let-7 ran similarly for the above gel conditions. (*D*) Double or single-stranded Cy3 let-7, respectively, (+ or -) HMGA2 mRNA and Hela cell extract (lanes 1-4), purified Ago2 protein (lanes 5-8) or no proteins (lanes 9-12). (*E*) Comparison of Cy3 let-7 and fluorescein labeled siRNA complexes in cytosolic HeLa cell extract . Lanes 1-5 contain respectively, dyes only (XCB and BPB), single-stranded Cy3 let-7, single-stranded fluorescein labeled siRNA, double-stranded Cy3 let-7, and double-stranded fluorescein labeled siRNA.

Cy3 labeled Let-7 Bias Complexes Toward Single-Strand Binding

In preparation for *in vivo* fluorescence assays, we next 3` end labeled the antisense strand of the let-7a miRNA with the fluorescent dye Cyanine 3 or (Cy3) (Figure 4.3*A*). We initially characterize the *in vitro* binding and efficacy of the fluorescently tagged miRNA for complex formation. Single-stranded Cy3 labeled let-7 formed eight complexes, in EMSAs containing 15 or 5% (v/v) cytosolic HeLa cell extract and a creatine phosphate ATP generating system (Figure 4.3*B*), complexes were labeled 1-8 respectively. We mimic the natural hairpin precursor to the mature let-7a with an extended 24-mer (prelet-7a). Similarly, Cy3 labeled single-stranded prelet-7a formed

eight complexes, yet bands appeared shifted when compared with let-7 complexes (Figure 4.3*B*). For let-7 and prelet-7a, we observed limited binding between the duplex form of the miRNA and the human cytosolic cell extract (Figure 4.3*B*). To obtain information regarding the ATP dependence of these complexes, ATP was depleted in the HeLa cell extract by addition of glucose and hexokinase and removed by omitting the ATP generating system. Only complex 8 showed a marked dependence on ATP, and was reduced in the ATP(-) extract by 50% (Figure 4.3*C*).

From here we sought to establish the binding ability of a HMGA2 mRNA for Cy3 let-7. No shift was observed in the presence of HMGA2 mRNA and binding was not facilitated by the addition of ATP (Figure 4.3*C*), purified Ago2 protein (Figure 4.3*D*), or HeLa cell extract alone or in combination (Figure 4.3*C*,*D*).

Formation of siRNA complexes was also inhibited by fluorescent labeling. Double-stranded fluorescein labeled siRNA formed only one complex in extract as compared to three seen for the radio-labeled species (Figure 4.3*E*). Single-stranded fluorescein labeled siRNA formed a much slower running complex comparable to the microRNA complex 8 (Figure 4.3*E*).

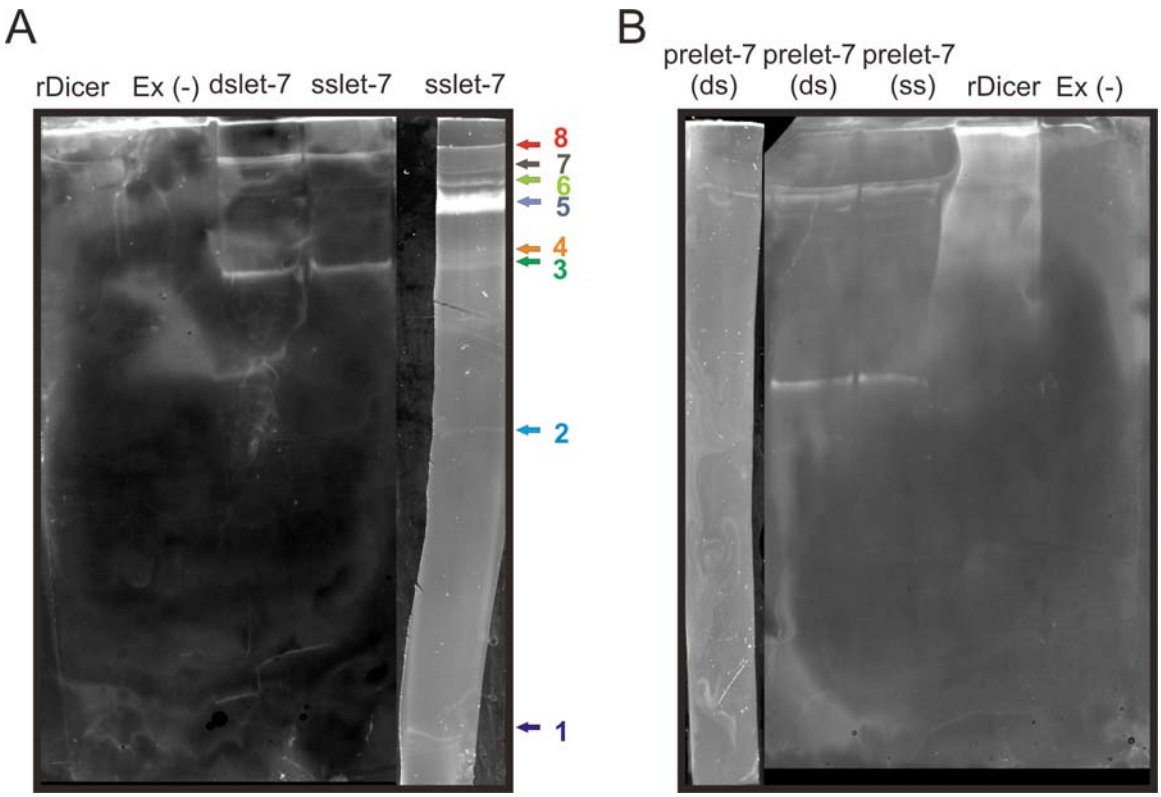

Figure 4.4 Western blots against Dicer. (*A*) Lanes 1-4 contain recombinant human Dicer (Genlantis Inc), a no protein control, double-stranded let-7 with HeLa cell extract, and single-stranded let-7 with HeLa cell extract imaged by western blots against Dicer. Lane 5 is a duplicate of lane 4, excised before western detection and imaged for Cy3. (*B*) Lane 1 contains double-stranded prelet-7 with HeLa cell extract imaged for Cy3. Lanes 2-5 contain double-stranded prelet-7 with HeLa cell extract, single-stranded prelet-7 with HeLa cell extract, recombinant human Dicer (Genlantis Inc), and a no protein control imaged by western blot. Western and Cy3 images were aligned using ImageJ software.

Western Blots show Dicer Co-migration with Single-stranded Complexes

To determine if specifically complex 8 or any of the Cy3 let-7 single-stranded complexes contain the enzyme Dicer Western blots were performed. Single-stranded let-7 complexes were scaled up for Western detection and formed as stated above. Dicer ran in two bands for both single- and double-stranded let-7, corresponding to complex 3 and complex 8 in the Cy3 scan (Figure 4.4*A*). Identical Dicer bands were formed for double-stranded let-7 as for the single-stranded case despite there being no visible double-stranded complexes in previous gels. Conversely, double-stranded prelet-7 formed a single band in a scaled up lane image for Cy3 (Figure 4.4*B*). This complex corresponded to the slower migrating of the two Dicer bands visible in the Western. Again two Dicer bands were seen in the presence of single- or double-stranded prelet-7 without any visible band running parallel to the faster migrating Dicer band (Figure 4.4*B*).

4.4 Discussion

The family of let-7 micro-RNAs is important for cell differentiation and the timing of cell fate in a host of organisms. They down-regulate a potentially tumor-causing protein, HMGA2, which contains seven let-7 binding sites in the 3`untranslated region of its mRNA (27). We observe by EMSA six complexes formed when mixing radio-labeled let-7a duplexes and human cytosolic extract *in vitro* (Complexes I-VI). All complexes are relatively stable over time and do not appear to be affected by either the full-length mRNA or the 3`UTR of HMGA2 mRNA targets (Figure 4.2*B,C*).

When comparing with the three complexes formed in the presence of siRNA duplexes (complexes D, C2, and C1), microRNA complexes I and III show overlap in migration with complexes C1 and C2, respectively, suggesting non-specific RNA binding (Figure 4.2*C*). Addition of unlabeled miRNAs or siRNAs competes off all complexes except C2, III, and I; complex I alone increases in relative abundance in the presence of unlabeled miRNA at all times observed (Figure 4.2*C*). The siRNA-containing complex D does not appear to overlap with any of the miRNA complexes and is the only siRNA complex that contains the enzyme Dicer (Figure 2.4*C*).

Despite stark differences in complex formation, sequence, and structure of si and miRNAs, we measure identical binding affinities with the viral RNA silencing suppressor protein 19 (p19). p19 binds siRNAs independent of sequence, but is thought, based on crystallographic (32, 34) and MD simulation evidence (35), to recognize the structure and length of an siRNA by stacking on terminal tryptophans. This binding prevents incorporation of the siRNA into the RISC machinery and suppresses RNAi. Variation in siRNA length by as little as 2 nucleotides has been shown to significantly reduce p19's binding affinity. miRNAs were assumed to be potentially weaker binding partners for p19 owing to differences in structure. We observe a binding affinity between p19 and let-7a miRNA identical to that between p19 and a luciferase targeting siRNA, which is consistent with structural data observing minimal RNA duplex disruption due to sequence mismatches (36).

This finding has dual significance in that it shows that differences in base pairing may not be the only factor contributing to the observed differences in gel electrophoretic mobility between the complexes formed with siRNA and miRNA in HeLa cytosolic cell

extract. Secondly, although miRNA:p19 binding has been observed *in vivo* (33), the mechanism of p19's functionality and its usefulness as an RSS is challenged when miRNAs compete for p19 binding with p19's siRNA targets. Also, the ternary complex between p19, Dicer, and siRNA, defined in Chapter 2, is ever more important for explaining the specific shuttling of siRNAs to p19 proteins in the presence of a constant miRNA competitor (Figure 2.3).

With regards to miRNA action, there are still many unanswered questions such as: Where do miRNA/mRNA complexes localize *in vivo*? Do they end up in punctate P-bodies, diffuse in the cytosol, or aggregate as large or small clusters? Do miRNAs remain associated with mRNAs over long or short times? Once associated with RISC, how often are miRNAs turned over? Is there any heterogeneity in the mechanism of action of a specific miRNA between cells (or even within a single cell)? And how does p19 binding effect miRNA localization?

All these questions can be addressed with appropriate *in vivo* localization for which we will choose a fluorescence detection assay that lends itself well to intercellular miRNA localization for a number of reasons. The first is that single-labeled miRNAs diffuse too quickly for accurate detection *in vivo*, but binding to an mRNA would associate the fluorescence with a larger molecule that would diffuse much more slowly. Also, HMGA2's seven let-7 seed sequences would multiply the photon count, lighting the complexes up like a Christmas tree and thus making them clearly distinguishable above the cellular autofluorescence and any background from freely diffusing miRNAs.

Cy3 was initially chosen for let-7 labeling and compared *in vitro* to radio-labeled constructs. Cy3 labeling reduces duplex binding in extract (Figure 4.3*B*) but promotes

binding of single-stranded let-7, leading to eight identifiable complexes (1-8) (Figure 4.3*B,C*). Amongst the complexes forming with single-stranded miRNA, only complex 8 shows a dependence on ATP and is depleted in ATP(-) extract. Complex 8 also co-migrated with Dicer bands in Western blots (Figure 4.4*A*). Similar results were found for a Cy3 labeled precurser let-7 (prelet-7) (Figure 4.4*B*).

HMGA2 messenger RNA binding was not observed for single or double-stranded Cy3 let-7, and was not enhanced in the presence of ATP, Ago2 protein (a known miRNA binding component of RISC), or HeLa cell extract (Figure 4.3*C,D*). Messenger RNA transcripts without a 5` cap may be degraded in extract or may be competed away by mRNAs present in the commercial extract used here due to insufficient RNase treatment.

ATP may facilitate RISC incorporation of single stranded miRNAs in the presence of Cy3, however, as the miRNA duplex is widely considered the biologically active form, a more conservative interpretation is that Cy3 labeling sterically interferes with RISC protein binding and biases complex formation toward the single stranded miRNA. Although Western blot analysis showed complex 8 to co-migrate with Dicer, raising the intriguing possibility that Dicer may be binding single-stranded miRNA directly, this does not reflect its *in vivo* activity. Alternative fluorophore and labeling strategies will be explored for subsequent assays *in vitro* and *in vivo* to rule out the more trivial explanations for our findings.

4.5 Acknowledgements

I would like to thank Melanie Sabbagh, Charity Haynes, and Aniruda Ratham for their contributions to the reported characterization of Cy3 labeled let-7.

4.6 References

1. Davidson-Moncada J, Papavasiliou FN, & Tam W (MicroRNAs of the immune system: roles in inflammation and cancer. *Ann N Y Acad Sci* **1183**:183-194
2. Rodriguez A, Griffiths-Jones S, Ashurst JL, & Bradley A (2004) Identification of mammalian microRNA host genes and transcription units. *Genome Res* **14**(10A):1902-1910
3. Lee Y, *et al.* (2004) MicroRNA genes are transcribed by RNA polymerase II. *EMBO J* **23**(20):4051-4060
4. Denli AM, Tops BB, Plasterk RH, Ketting RF, & Hannon GJ (2004) Processing of primary microRNAs by the Microprocessor complex. *Nature* **432**(7014):231-235
5. Han J, *et al.* (2004) The Drosha-DGCR8 complex in primary microRNA processing. *Genes Dev* **18**(24):3016-3027
6. Ketting RF, *et al.* (2001) Dicer functions in RNA interference and in synthesis of small RNA involved in developmental timing in C. elegans. *Genes Dev* **15**(20):2654-2659
7. Grishok A, *et al.* (2001) Genes and mechanisms related to RNA interference regulate expression of the small temporal RNAs that control C. elegans developmental timing. *Cell* **106**(1):23-34
8. Yekta S, Shih IH, & Bartel DP (2004) MicroRNA-directed cleavage of HOXB8 mRNA. *Science* **304**(5670):594-596

9. Du T & Zamore PD (2005) microPrimer: the biogenesis and function of microRNA. *Development* **132**(21):4645-4652

10. Filipowicz W, Bhattacharyya SN, & Sonenberg N (2008) Mechanisms of post-transcriptional regulation by microRNAs: are the answers in sight? *Nat Rev Genet* **9**(2):102-114

11. Carthew RW & Sontheimer EJ (2009) Origins and Mechanisms of miRNAs and siRNAs. *Cell* **136**(4):642-655

12. Ding SW & Voinnet O (2007) Antiviral immunity directed by small RNAs. *Cell* **130**(3):413-426

13. Ji X (2008) The mechanism of RNase III action: how dicer dices. *Curr Top Microbiol Immunol* **320**:99-116

14. Siomi H & Siomi MC (2009) On the road to reading the RNA-interference code. *Nature* **457**(7228):396-404

15. Liu J, *et al.* (2004) Argonaute2 is the catalytic engine of mammalian RNAi. *Science* **305**(5689):1437-1441

16. Chendrimada TP, *et al.* (2005) TRBP recruits the Dicer complex to Ago2 for microRNA processing and gene silencing. *Nature* **436**(7051):740-744

17. Gregory RI, Chendrimada TP, Cooch N, & Shiekhattar R (2005) Human RISC couples microRNA biogenesis and posttranscriptional gene silencing. *Cell* **123**(4):631-640

18. Wang HW, *et al.* (2009) Structural insights into RNA processing by the human RISC-loading complex. *Nature structural & molecular biology* **16**(11):1148-1153

19. Lewis BP, Burge CB, & Bartel DP (2005) Conserved seed pairing, often flanked by adenosines, indicates that thousands of human genes are microRNA targets. *Cell* **120**(1):15-20

20. Chen K & Rajewsky N (2007) The evolution of gene regulation by transcription factors and microRNAs. *Nat Rev Genet* **8**(2):93-103

21. Reinhart BJ*, et al.* (2000) The 21-nucleotide let-7 RNA regulates developmental timing in Caenorhabditis elegans. *Nature* **403**(6772):901-906

22. Calin GA*, et al.* (2004) Human microRNA genes are frequently located at fragile sites and genomic regions involved in cancers. *Proc Natl Acad Sci U S A* **101**(9):2999-3004

23. Takamizawa J*, et al.* (2004) Reduced expression of the let-7 microRNAs in human lung cancers in association with shortened postoperative survival. *Cancer Res* **64**(11):3753-3756

24. Pasquinelli AE*, et al.* (2000) Conservation of the sequence and temporal expression of let-7 heterochronic regulatory RNA. *Nature* **408**(6808):86-89

25. Mayr C, Hemann MT, & Bartel DP (2007) Disrupting the pairing between let-7 and Hmga2 enhances oncogenic transformation. *Science* **315**(5818):1576-1579

26. Kumar MS*, et al.* (2008) Suppression of non-small cell lung tumor development by the let-7 microRNA family. *Proc Natl Acad Sci U S A* **105**(10):3903-3908

27. Young AR & Narita M (2007) Oncogenic HMGA2: short or small? *Genes Dev* **21**(9):1005-1009

28. Meyer B*, et al.* (2007) HMGA2 overexpression in non-small cell lung cancer. *Mol Carcinog* **46**(7):503-511

29. Walter NG (2002) Probing RNA structural dynamics and function by fluorescence resonance energy transfer. *Curr. Protocols Nucleic Acid Chem*), pp 11.10.11-11.10.23.

30. Hoerter JA & Walter NG (2007) Chemical modification resolves the asymmetry of siRNA strand degradation in human blood serum. *RNA* **13**(11):1887-1893

31. Friedman RC, Farh KK, Burge CB, & Bartel DP (2009) Most mammalian mRNAs are conserved targets of microRNAs. *Genome Res* **19**(1):92-105

32. Vargason JM, Szittya G, Burgyan J, & Hall TM (2003) Size selective recognition of siRNA by an RNA silencing suppressor. *Cell* (115):799-811.

33. Lakatos L, Szittya G, Silhavy D, & Burgyan J (2004) Molecular mechanism of RNA silencing suppression mediated by p19 protein of tombusviruses. *EMBO J* **23**(4):876-884.

34. Ye K, Malinina L, & Patel DJ (2003) Recognition of siRNA by a viral suppressor of RNA silencing. *Nature* (426):874-878.

35. Xia Z, Zhu Z, Zhu J, & Zhou R (2009) Recognition mechanism of siRNA by viral p19 suppressor of RNA silencing: a molecular dynamics study. *Biophys J* **96**(5):1761-1769

36. Nemecek D, Vaisocherova H, Stepanek J, & Turpin P Y (2005) Structural features of a central mismatch in oligonucleotide hybrid duplexes visualized via Raman spectroscopy: model system for evaluation of potential "antisense" drugs. *Biopolymers* **79**(1):1-8

Chapter 5:

SUMMARY AND FUTURE DIRECTIONS

5.1 Summary

RNA, now considered as a primary effector of gene regulation, interferes in the progression of an invading virus to suppress or silence viral infection (1-6). RNA interference (RNAi) is initiated by double-stranded RNA, produced during viral replication and cleaved in the cytoplasm by the RNAse III enzyme Dicer. Dicer produces small-interfering RNA (siRNA) that act as guides for the cellular RNAi machine, RISC, to degrade complementary viral messenger RNAs (mRNA) (7-10). The effect of mRNA degradation reduces viral protein production, cytotoxicity, symptom spread, and ultimately halts the progression of infection.

As a countermeasure to RNAi, most effective viruses have evolved elaborate mechanisms of invasion. One of the earliest viral strategies observed was the production of an RNAi suppressor protein, or RSS, to short-circuit mRNA degradation and recover infection phenotype (11-13). The tombusviridae class of viruses produce an RSS, termed p19, as their primary defense against RNAi, which binds Dicer-produced siRNAs independent of sequence to prevent incorporation into RISC and subsequent degradation (14). p19 measures the siRNA duplex length through stacking interactions of

tryptophans on the terminal bases, and is commonly described as sequestering siRNAs away from the RNAi machinery (15-17).

Here, we characterize the interaction between p19 and the RNAi pathway to further elucidate its mechanism. We observe that p19 binds reversibly to siRNAs with a fast association ($(1.69 \pm 0.07) \times 10^8$ $M^{-1}s^{-1}$) and dissociation (0.062 ± 0.002 s^{-1}) rate constant, suggesting the possibility of a multi-turnover mechanism for its mode of action against RNAi (Figure 2.2). Competition between the Dicer enzyme and p19 shows higher than expected vulerability of siRNA:Dicer complexes to p19, and a lower than expected effect of Dicer on siRNA:p19 binding than expected from a simple free-siRNA capture mechanism, (Figure 2.3). This result suggests the presence of a ternary complex between siRNA, Dicer, and p19. Only the assumption of such a transient ternary complex intermediate can explain the observed efficient shuttling of an siRNA toward the p19 bound state. A simple model based on this mechanism yields evidence for an >20-fold bias in dissociation equilibrium constant for the ternary complex to dissociate into the siRNA:p19 complex rather than the siRNA:Dicer complex. Additionally, we observe p19 to compete strongly with human Dicer and to a lesser extent with fully mature RNAi complexes, suggesting p19's interaction with Dicer as the primary entry point for suppression of the RNAi pathway (Figure 2.4).

Computational modeling is employed to describe the impact of exogenously introduced p19 on the expression of a messenger RNA targets. We find p19 action to be concentration dependent and able to significantly increase the peak amount of mRNA produced and extend the length of the viral replication phase (Figure 3.3*A*). Our model also predicts p19 to time invariantly reinitiate viral replication after steady-state

suppression has been reached (Figure 3.3*B*). This time invariance allows p19 to be potentially used as a tool to extend mRNA rising phase duration for a gene of interest (Figure 3.4).

Exogenous viral infection is only one of many sources of double-stranded RNA that can activate RNAi. Endogenously produced transcripts are also cleaved by Dicer into microRNAs (miRNAs) that are bound by RISC and induce translational repression as opposed to cleavage of mRNA targets. miRNAs differ from siRNAs in that they are neither fully complementary in their duplex form nor in their binding to mRNA targets. Underscoring these differences in mechanism, we observe distinctly different complexes formed in the presence of miRNAs as opposed to siRNAs in human cell extract (Figure 4.2*B,C*). Interestingly, miRNAs and siRNAs show an identical affinity for binding p19 (Figure 4.2*D,E*), suggesting that the ternary complex between siRNAs, Dicer, and p19 is ever more important for specifically shuttling siRNAs to p19 proteins in the presence of a constant miRNA competitor (Figures 2.3 and 4.2).

Viral counter-suppression by p19 can act as a model system for the use of an RSS in RNAi-suppression and, analogous to immunosuppressants in modern organ transplant surgery, p19 can be used as an offset to the RNAi response for applications such as plant-based vaccines and genetic therapy. From our experimentation and mathematical modeling we postulate the following principles for optimization of p19 and its impact on RNAi efficiency.

Principles for p19 Interaction with RNAi-Based Applications

(1) **Proximity**- p19 expressed close to the source of infection maximizes the benefit of siRNA shuttling through its ternary interaction with Dicer.

(2) **Increased concentration**- Higher p19 concentrations produce increased viral mRNA production, longer rising phases, and slower suppression, thus increasing the observed duration of infection.

(3) **Timing of Incubation**- Optimal incubation times scale linearly with the effective concentration of p19 in the cell.

(4) **Timing of Introduction**- Addition of p19 before full suppression of infection increases the rising phase of mRNA production and the time needed to reach peak mRNA levels. Late introduction of p19 is observed to reinitiate mRNA accumulation even after equilibrium has been reached.

Drawbacks and Concerns

(1) **Dormant viruses**- The effectiveness of p19 is not specific to the gene of interest due to its ability to bind siRNAs and other small RNA, independent of sequence. This feature can be a source of off-target effects including up-regulation of other normally RNAi suppressed targets such as transposons.

(2) **Long Incubation Times**- Maximum efficiency comes at the cost of longer incubation times of greater than 8-fold the original infection.

(3) **Significance of Sustained Dosing-** Sufficient sustained dosing of p19 may be a challenge for conventional promoters used in stable cellular transfection. Introduction of a low dose of p19 early in the infection window leads to limited, if any, discernable difference in yield.

Some of these principles are consistent with prior experimental studies suggesting the RNAi pathway actively suppresses viral infection by showing viral production can be reinitiated by knockdown of Dicer or Drosha (18). We observe, in the absence of p19, relatively high levels of viral siRNAs that remain bound to Dicer and RISC even after the infection has been suppressed, supporting active repression of viral mRNA by the RNAi pathway (Figure 3.2). Other predictions remain to be experimentally tested. For application specific goals, p19 and other RSS's offer an alternative approach for the regulation of RNAi and provide a platform for controlling dosing. Understanding and modeling relevant biophysical properties in the presence of RSSs, as advanced here, is therefore anticipated to become critical for broader and safer use of RNAi therapeutics in human disease control.

5.2 Future Directions

Kinetic Characterization of eukaryotic RSS's and their Applications to Therapeutics

While RNAi is a powerful host immune response, triggered by emergent viruses or transposons, virus-encoded RNA silencing suppressor proteins or RSS's represent a central mechanism for sustained viral infection in the presence of active RNAi. Due to their high conservation and the reduction of viral phenotype in the absence of RSSs, suppressor proteins may represent ideal drug targets for stemming symptom spread and cytotoxcity.

RSS's are found primarily in plant viruses where they must contend with host amplification of siRNAs by RNA dependent RNA Polymerases (RdRps). Studies show that the relative strengths of these two factors, along with other plant defense components, can critically influence the outcome of virus infections (20). Human and other eukaryotic viral RNAi suppressors that do not combat RdRps seem to be further specialized for human cells and exhibit increased viability for conventional gene therapy (19).

To target human cells, the techniques described in Chapter 2 could be employed for kinetics testing and future biochemical and biophysical characterization of various RSS proteins. Additionally, the ternary complex between the RSS p19, siRNA, and human Dicer could be experimentally isolated by HPLC or anti-p19 antibody shift assays to confirm our computational findings and provide for an avenue to test the stability and find conditions for disruption of such a complex.

Modeling Extension(s)

As RNAi is gaining momentum as a potential therapeutic strategy, with drug design on the horizon, it is difficult to predict the direct outcome of genetic silencing by experimental means only, due to the lack of known contributing enzymes and kinetic constants. Here modeling will become a key tool in interpreting the interplay between RNAi components and human diseases. Accuracy of results from mathematical and computer models of RNAi are in this case complicated by the presence of uncertainties in the experimental data that are used to estimate parameter values.

Ranked Sensitivity Analysis (RSA) is a method for dealing with uncertainty by sampling the entire parameter space for each variable. This approach overcomes uncertainty limitations and provides a global sensitivity coefficient to rank the effect of multiple variations on the system output. RSA has been used successfully on HIV (21), compartmental ordinary differential equation (22), and agent-based models (23) to determine sensitivity, but has not as yet been used to study the RNA interference pathway.

Principle Component Analysis (PCA) is a more sophisticated formal sensitivity analysis that evaluates the relationship between parameters and solutions, not only the variation in the output. The use of PCA on HIV models was developed at the University of Michigan, and offers new insights into nontrivial relationships between model parameters (24). Again, this analysis has not been applied to RNA interference modeling.

Future work using this two-tiered approach to careful sensitivity analysis would give confidence weighting to experimentally derived parameters as well as assign priority to parameters most vital to the predicted outcome, yielding a filtered set of complex scenarios that can be further tested by experiment.

Single molecule investigations of HMGA2:Let7 binding

Single molecule studies have provided new methods for observing previously unattainable information on the dynamics, behavior, and the mechanisms of action between individual molecules, as well as heterogeneity among different molecules within a population (25). Overcoming the limitations of bulk measurements, single molecule techniques would allow HMGA2/let-7 binding to be characterized for each of HMGA2's seven let-7 binding sites. Previous studies have shown each of the seven binding sites to be relevant and contributing to HMGA repression (26). Single molecule techniques are well suited to measure the binding kinetics of all let-7 binding sites of HMGA2 and their interaction with microRNA loaded RISC. Continuing members of the Walter lab will be pursuing this question to uncover detailed information regarding the HMGA2/let-7 interaction.

Fluorescent localization of Let7 targeting in vivo

After their incorpoaration into RISC, little is known about what happens to an siRNA/miRNA and its mRNA target. It is not known whether the mRNA is degraded, permanently sequestered into p-bodies, or recycled for further use. To probe these mechanistic features of the RNAi pathway, continuing members of the Walter lab will

pursue the *in vivo* and *in vitro* characterization studies begun in Chapter 4. Variations on the labeling of 3'-Cy3-labeled let-7a should be generated and characterized.

5.3 References

1. Fire A, *et al.* (1998) Potent and specific genetic interference by double-stranded RNA in Caenorhabditis elegans. *Nature* 391:806-881.
2. Castanotto D & Rossi JJ (2009) The promises and pitfalls of RNA-interference-based therapeutics. *Nature* 457(7228):426-433
3. Carthew RW & Sontheimer EJ (2009) Origins and Mechanisms of miRNAs and siRNAs. *Cell* 136(4):642-655
4. Lee SK & Kumar P (2009) Conditional RNAi: towards a silent gene therapy. *Adv Drug Deliv Rev* 61(7-8):650-664
5. Grimm D (2009) Small silencing RNAs: state-of-the-art. *Adv Drug Deliv Rev* 61(9):672-703
6. Umbach JL & Cullen BR (2009) The role of RNAi and microRNAs in animal virus replication and antiviral immunity. *Genes Dev* 23(10):1151-1164
7. Collingwood MA, *et al.* (2008) Chemical modification patterns compatible with high potency dicer-substrate small interfering RNAs. *Oligonucleotides* 18(2):187-200
8. Kim DH, *et al.* (2005) Synthetic dsRNA Dicer substrates enhance RNAi potency and efficacy. *Nat Biotechnol* 23(2):222-226

9. Ji X (2008) The mechanism of RNase III action: how dicer dices. *Curr Top Microbiol Immunol* 320:99-116

10. Siomi H & Siomi MC (2009) On the road to reading the RNA-interference code. *Nature* 457(7228):396-404

11. Qu F & Morris TJ (2005) Suppressors of RNA silencing encoded by plant viruses and their role in viral infections. *FEBS Lett* 579(26):5958-5964

12. Roth BM, Pruss GJ, & Vance VB (2004) Plant viral suppressors of RNA silencing. *Virus Res* 102(1):97-108

13. Voinnet O (2001) RNA silencing as a plant immune system against viruses. *Trends Genet* 17(8):449-459

14. Scholthof H (2006) The Tombusvirus-encoded P19: from irrelevance to elegance. *Nat Rev Microbiol* (4):405-411.

15. Vargason JM, Szittya G, Burgyan J, & Hall TM (2003) Size selective recognition of siRNA by an RNA silencing suppressor. *Cell* (115):799-811.

16. Ye K, Malinina L, & Patel DJ (2003) Recognition of siRNA by a viral suppressor of RNA silencing. *Nature* (426):874-878.

17. Xia Z, Zhu Z, Zhu J, & Zhou R (2009) Recognition mechanism of siRNA by viral p19 suppressor of RNA silencing: a molecular dynamics study. *Biophys J* 96(5):1761-1769

18. Triboulet R*, et al.* (2007) Suppression of microRNA-silencing pathway by HIV-1 during virus replication. *Science* 315(5818):1579-1582

19. de Vries W*, et al.* (2008) Increased virus replication in mammalian cells by blocking intracellular innate defense responses. *Gene Ther* 15(7):545-552

20. Qu F, *et al.* (2005) RDR6 has a broad-spectrum but temperature-dependent antiviral defense role in Nicotiana benthamiana. *J Virol* 79(24):15209-15217

21. M. BS, N. AA, B. GH, & O. KJ (2001) Predicting the unpredictable: Transmission of drug-resistant HIV. *Nature* 7(9):1016-1020.

22. Ellwein LM, Tran HT, Zapata C, Novak V, & Olufsen MS (2008) Sensitivity Analysis and Model Assessment: Mathematical Models for Arterial Blood Flow and Blood Pressure. *Cardiovascular Engineering* 8(2):94-108.

23. Marino S, Hogue IB, Ray CJ, & Kirschner DE (2008) A methodology for performing global uncertainty and sensitivity analysis in systems biology. *J Theor Biol* 254(1):178-196

24. Bortz DM & Nelson PW (2004) Sensitivity analysis of a nonlinear lumped parameter model of HIV infection dynamics. *Bull Math Biol* 66(5):1009-1026

25. Walter NG, Huang CY, Manzo AJ, & Sobhy MA (2008) Do-it-yourself guide: how to use the modern single-molecule toolkit. *Nat Methods* 5(6):475-489

26. Mayr C, Hemann MT, & Bartel DP (2007) Disrupting the pairing between let-7 and Hmga2 enhances oncogenic transformation. *Science* 315(5818):1576-1579

Appendix A

Rawlings et al, Figure A1

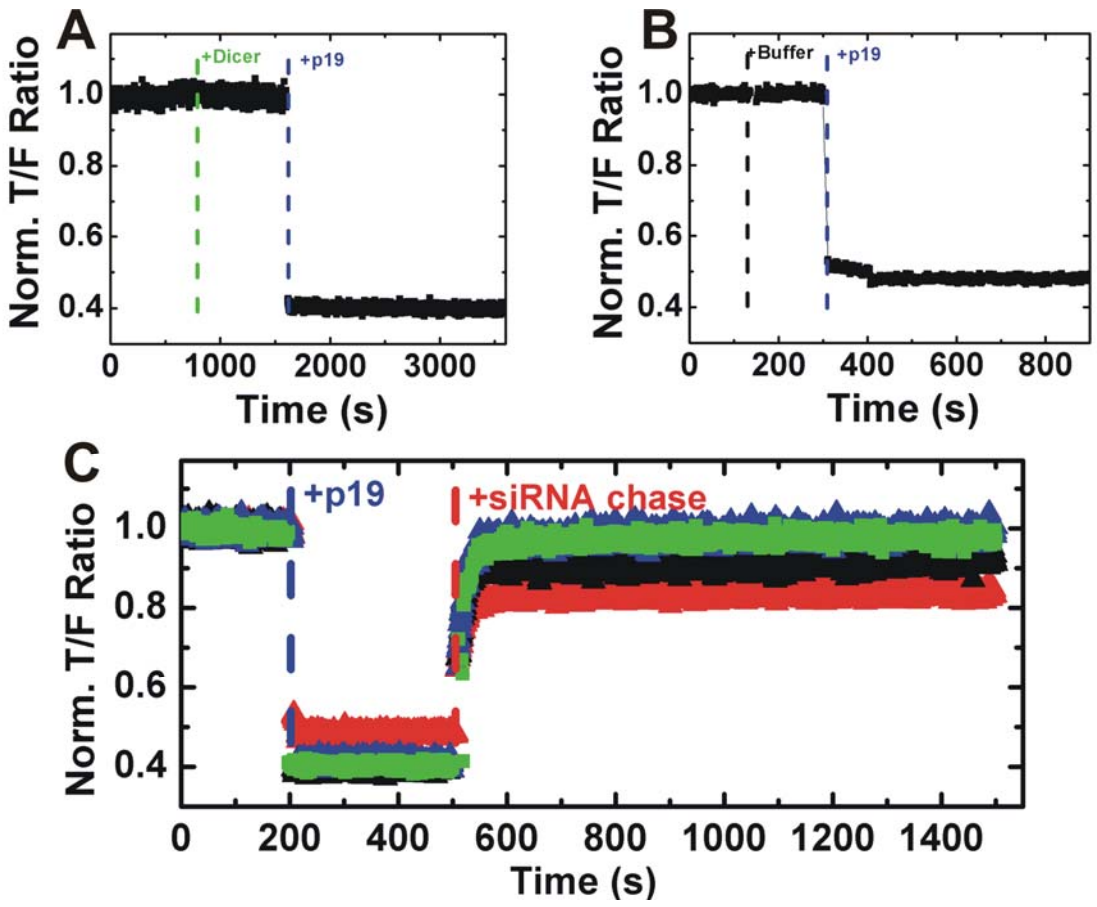

Figure A1 Concentration dependence of siRNA:p19 dissociation kinetics. (*A, B*) Doubly-labeled siRNA (50 nM) after addition of Dicer (5nM green dotted line) or Buffer (black dotted line) respectively, followed by addition of p19 (500 nM, blue dotted line). (*C*) Doubly-labeled siRNA (50 nM) was bound by p19 (500 nM, blue dotted line) after which excess unlabeled siRNA was added at concentrations of 500 nM (red), 750 nM (black), 1.5 μM (green), 3 μM (blue), respectively.

Rawlings et al, Figure A2

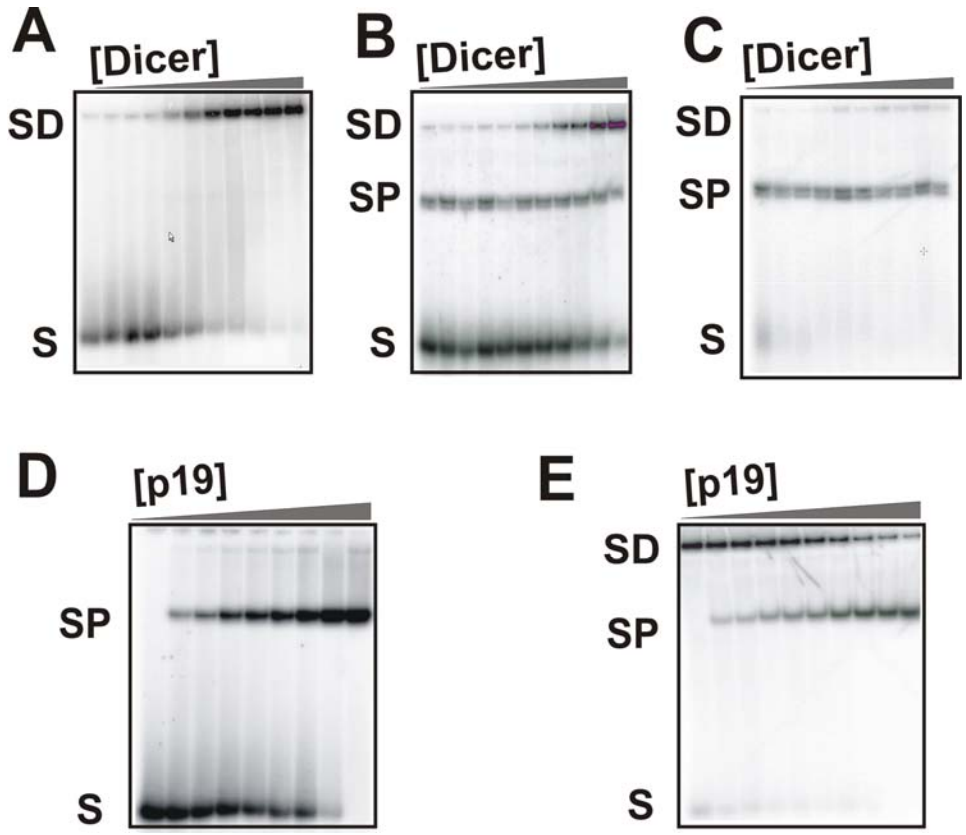

Figure A2 Competition between p19 and human Dicer for siRNA binding as shown by EMSAs. siRNA (S) labeled with [γ–^{32}P] ATP are bound to (*A*). Recombinant human Dicer (D) (Genlantis Inc.) where Dicer concentrations are 0, 0.16, 0.25, 0.5, 2.5, 5, 10, 16, 50 ,100, 200 nM, respectively. Samples were incubated for 30 min before loading onto a 12% nondenaturing polyacrylamide gel. (*B*). siRNA pre-incubated with [p19] = 0.16 nM for 30 min followed by Dicer addition as described above. (*C*). siRNA pre-incubated with [p19] = 2.56 nM for 30 min followed by Dicer addition as described above. (*D*). p19 only (P) where p19 concentrations are 0, 0.02, 0.04, 0.08, 0.16, 0.32, 0.64, 1.28, 2.56, 5.12 nM, respectively. Samples were incubated for 30 min before loading onto a 12% nondenaturing polyacrylamide gel. (*E*). siRNA pre-incubated with [Dicer] = 140 nM for 30 min followed by p19 addition as described in *D*.

Rawlings et al, Figure A3

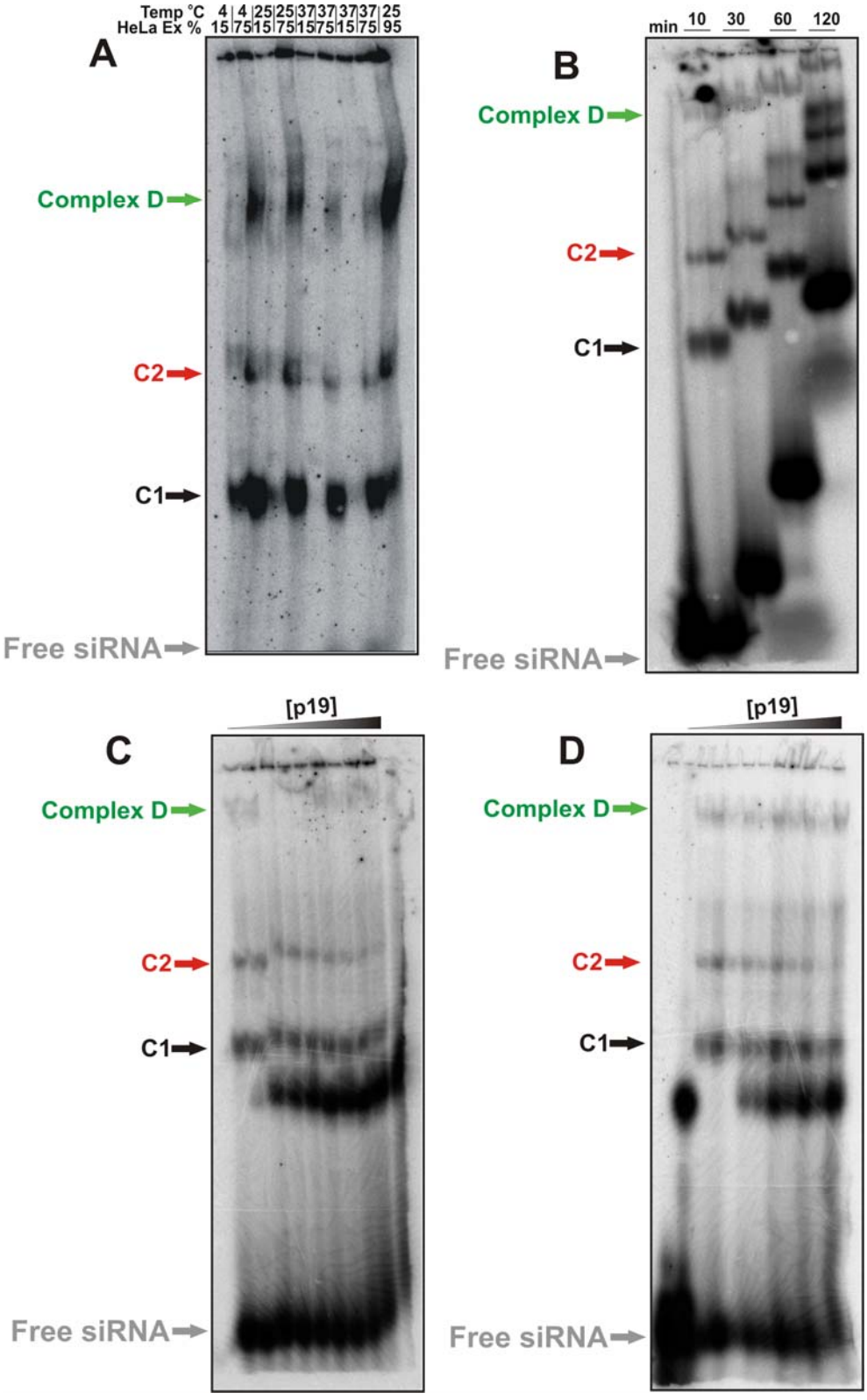

Figure A3 Comparison of siRNA complex formation for different HeLa cell extract concentrations and temperatures. (*A*) (lanes 1-2) 15% or 75% HeLa extract conditions incubated with siRNA for 1 h at 4 ^{o}C, (lanes 3-4) incubated at 25 ^{o}C, (lanes 5-8) incubated at 37 ^{o}C, and (lane 9) 93% HeLa cell extract in the absence of an ATP generating system and in supplied buffer (20 mM HEPES-Na pH 7.9, 42 mM ammounium sulfate, 0.2 mM EDTA, 0.5 mM DTT and 20% glycerol). The effect of incubation temperature and HeLa extract concentration on complex formation was limited. The same migration patterns are seen under all conditions. (*B*) Formation of complexes D, C2, and C1 after 10, 30, 60 and 120 min incubation of siRNA in 50% cytosolic HeLa cell extract. Samples were loaded onto a running 4% native polyacrylamide gel, leading to the indicated differences in migration. (*C*) Formation of complexes after 2.5 h incubation of siRNA in 50% cytosolic HeLa cell extract, and increasing concentrations of p19. (*D*) Formation of complexes after 2 h incubation of siRNA in 50% cytosolic HeLa cell extract, followed by the addition of increasing concentrations of p19 and further incubation for 30 min.

Rawlings et al, Figure A4

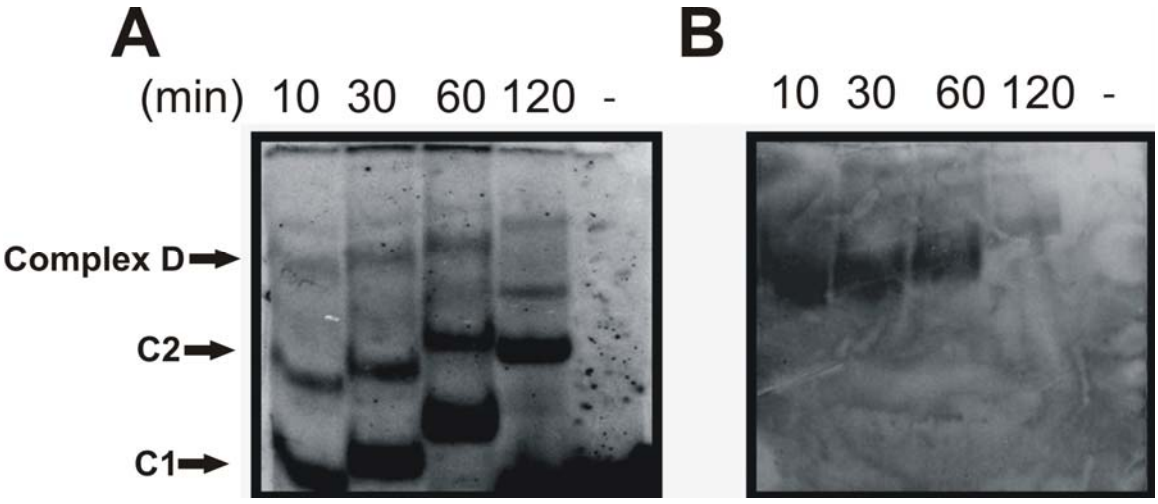

Figure A4 Western blot detection of Dicer (*A*) A scaled-up version of the time course gel in (Figure 2.4*B*), imaged for radio-labeled siRNA, yields sufficient complexes for Western blot detection of Dicer. (*B*) Western blot of a similar gel to (*A*) probed with a rabbit primary antibody against Dicer, followed by a goat anti-rabbit secondary antibody, conjugated with horseradish peroxidase. Samples were loaded onto a running gel, leading to the observed differences in migration

Rawlings et al, Figure A5

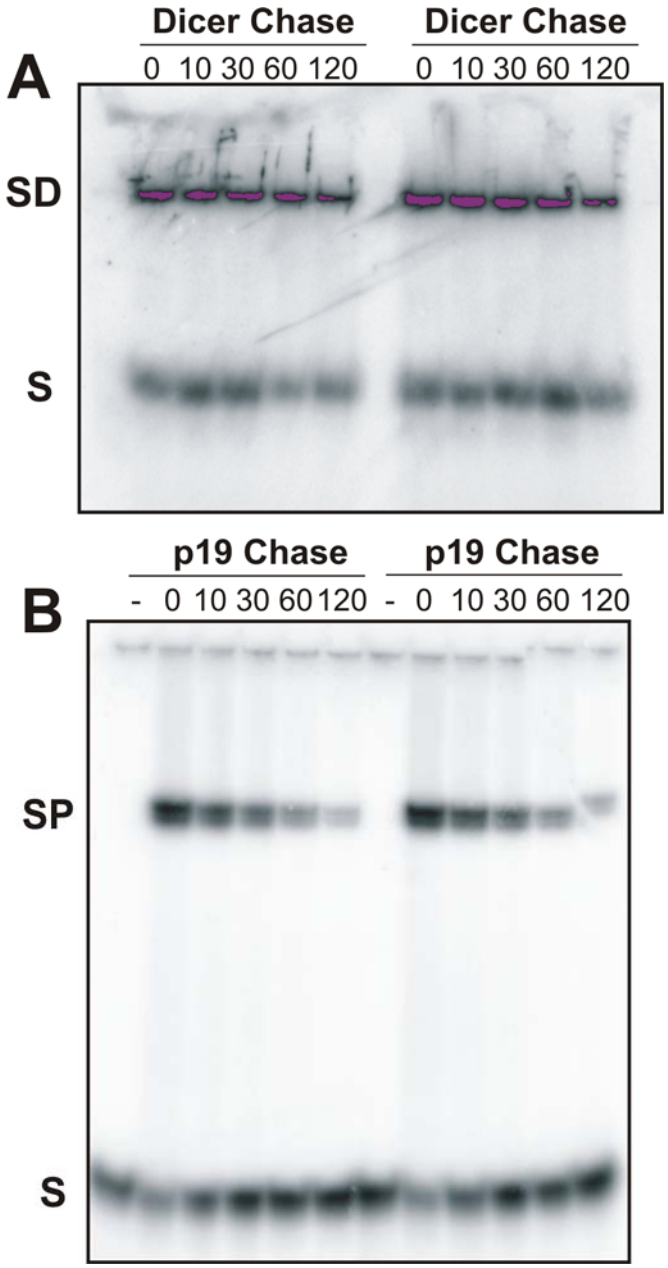

Figure A5 Gel-based dissociation chase assays. Duplicate gel chase experiments were done in standard buffer with (*A*) 70 nM recombinant Dicer or (*B*) 10 nM of p19 added to 5′-^{32}P labeled siRNA before addition of 750 nM unlabeled siRNA chase at 0, 10, 30, 60 and 120 min.

Rawlings et al, Figure A6

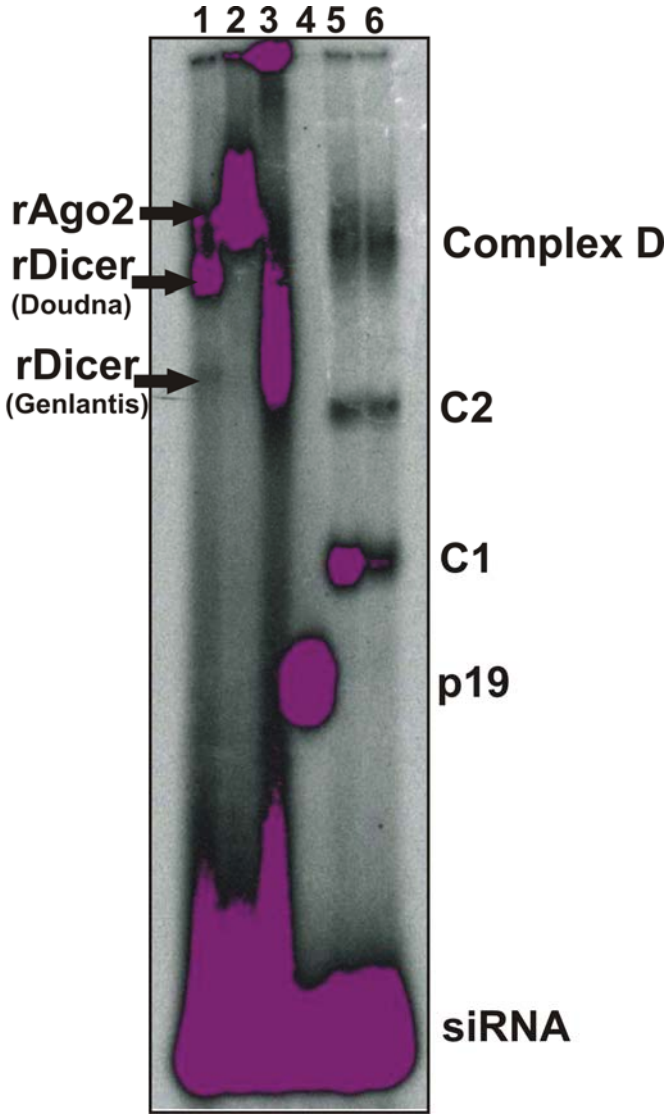

Figure A6 Size comparison of protein-siRNA binding complexes. [γ–^{32}P] ATP labeled siRNA bound to: (lane 1) purified rDicer provided for analytical purposes from the J. Doudna lab. (lane 2): purified recombinant Ago2 protein provided for analytical purposes from the J. Doudna lab. (lane 3): rDicer (Genlantis Inc), (lane 4) purified p19, (lane 5-6) 15% Hela extract. All lanes were incubated 30 min before loading. Nondenaturing 4% (w/v) polyacrylamide gel electrophoresis was used to resolve these complexes as described above.

Appendix B

Model Description

Grouped RNA Interference with p19: For the model described schematically in (Figure B1) (below), changes in viral protein expression levels were monitored in the absence and presence of the RSS p19. Changes in free p19 protein over time depend on terms representing the natural rates of production (rx rt / rdm), degradation (rdp [p19]), and the extent of siRNA binding (v∗[siRNA] [P]). Production of p19 is governed by its transcription rate (rx), its messenger RNA degradation rate (rdm), and its translation rate (rt), which are assumed to have reached equilibrium on a faster time-scale than that of repression. The p19 protein is degraded by the first order rate constant (rdp) and bound to siRNAs by the second order rate constant (v∗).

$$p19'[\tau] = \frac{r_x r_t}{r_{dm}} - r_{dp}[p19] - v_*[siRNA][p19] \qquad \textbf{[1]}$$

The amount of usable siRNA in the system, i.e. the fraction able to associate with RISC, is reduced by the amount of siRNA bound to p19. Production of siRNA is dependent on the catalytic rate of Dicer (kcatD) and is degraded by a first order rate constant (rds).

$$siRNA'[\tau] = k_{catD}[Dicer] - r_{ds}[siRNA] - v_*[siRNA][p19] \qquad \textbf{[2]}$$

The viral protein of interest that serves as a reporter of RNAi suppression and p19 enhancement is described as:

$$viral'[\tau] = \frac{r_x r_t}{\frac{k_{catR}}{K_{DR}}[RISC][siRNA] + r_{dm}} - r_{dp}[viral]$$

where (kcatR) is the catalytic rate for RISC cleavage of mRNA. The additional term in the denominator of Equation 3 is a quasi-steady state assumption used in previous work (1, 2) to describe RISC mediated degradation of viral messenger RNA (mRNA). It assumes that the active concentration of siRNA-loaded RISC is approaching its steady state value at the rate (kcatR). This contributes to the rate of degradation of the viral mRNA as described by the concentration of RISC, siRNA, and the dissociation constant for RISC binding (K_{DR}). The proteins that are not regulated by the RNAi pathway are represented as constants at steady state.

$$[Dicer] = \frac{r_x r_t}{r_{dp} r_{dm}} \quad [4] \qquad [RISC] = \frac{r_x r_t}{r_{dp} r_{dm}} \quad [5]$$

Equations (1-3) are rescaled as described in Marshall 2008 (2) at steady state to yield:

$$P = \frac{1}{1 + v\frac{kcat_D S}{r_{dp}^2}} \quad [6] \qquad S = \frac{1}{\beta + \frac{vP}{r_{dp}}} \quad [7] \qquad V = \frac{1}{1 + \alpha S} \quad [8]$$

where v is a scaler multiple of v_* equal to (rx rt/rdm rdp) v_*. The value of the viral protein at steady state is dependent on the form of S. As shown in the absence of the RNA interfering pathway where S = 0, due to no Dicer cleavage, V = 1, or the unsuppressed protein level. Substituting Equation 6 into Equation 7 we get two solutions for S where only S_2 is biological relevant:

$$S_1 = \frac{k_{catD}v - r_{dp}v - r_{dp}^2\beta - \sqrt{4k_{catD}r_{dp}^2v\beta + \left(-k_{catD}v + r_{dp}v + r_{dp}^2\beta\right)^2}}{2k_{catD}v\beta}$$

$$S_2 = \frac{k_{catD}v - r_{dp}v - r_{dp}^2\beta + \sqrt{4k_{catD}r_{dp}^2v\beta + \left(-k_{catD}v + r_{dp}v + r_{dp}^2\beta\right)^2}}{2k_{catD}v\beta}$$

[9]

Substituting S_2 into Equation 8 yields:

$$V = \frac{1}{1 + \frac{y\left(k_{catD}v - rdpv - rdp^2\beta + \sqrt{4k_{catD}rdp^2v\beta + (-k_{catD}v + rdpv + rdp^2\beta)^2}\right)}{2k_{catD}v}}$$

[10]

where y equals the efficiency of the RNAi pathway in a specific cell line (2).

Using Equation 10 above and the values of y = 1.2 derived for HEK293 cells (2) and an experimentally derived catalytic rate for Dicer (kcatD = 11.4 mol/s) (3) the effect of p19 was plotted versus (v) and (rdp). We see a higher than expect dependence on protein

degradation (rdp) showing increased degradation correlating with increased viral production requiring a ratio of rdp = .5 kcatD to reproduce experimental data (4) and rdp values on the order of 10^2 mol/s to optimize protein production.

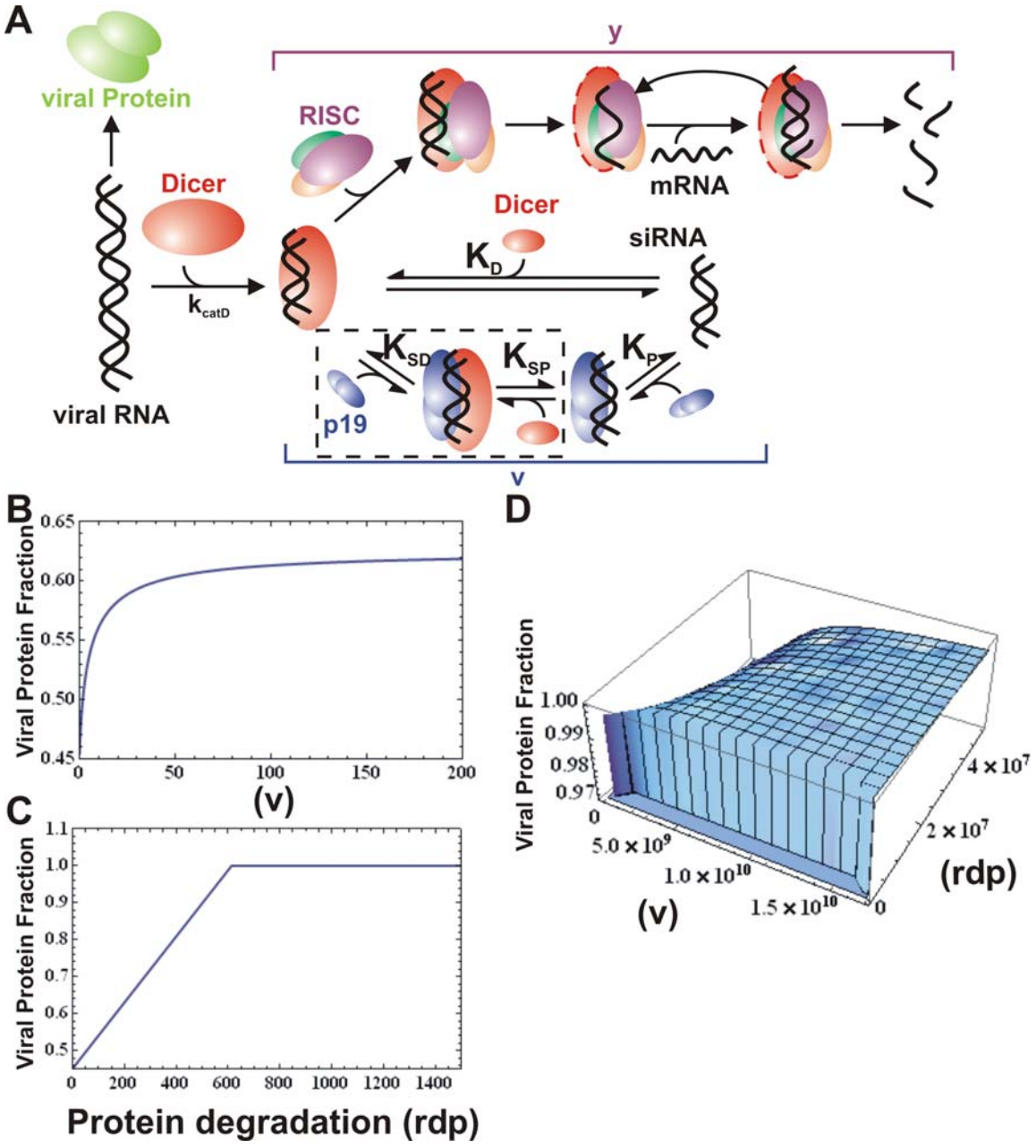

Figure B1 The interaction of p19 with RNAi at Steady State. (*A*) Model Schematic (*B*) Viral protein level over (v) assuming rdp = 0.5 kcatD = 5.7 mol/s and Viral protein level over (rdp) assuming v = 1.69 x 10^8 . (*C*) 3D plot of Viral protein level over (v) and (rdp)

References

1. Groenenboom MA, Maree AF, & Hogeweg P (2005) The RNA silencing pathway: the bits and pieces that matter. *PLoS Comput Biol* 1(2):155-165
2. Marshall WF (2008) Modeling recursive RNA interference. *PLoS Comput Biol* 4(9):e1000183
3. Ma E, MacRae IJ, Kirsch JF, & Doudna JA (2008) Autoinhibition of human dicer by its internal helicase domain. *J Mol Biol* 380(1):237-243
4. de Vries W, *et al.* (2008) Increased virus replication in mammalian cells by blocking intracellular innate defense responses. *Gene Ther* 15(7):545-552

Appendix C

Grouped RNA Interference with p19

```
Clear["Global`*"]

Protein Production is described by:
Production=(rx rt)/rdm;
Degradation= rdp *p19;
Binding = v (siRNA)*p19;

dp19dt=Production-Degradation-Binding;
dsiRNAdt=kcatD (Dicer)-rds (siRNA)-Binding;
dvirusdt= (rx rt)/(rdm +kcatR/KDR RISC siRNA)-rdp virus;
Dicer=(rx rt)/(rdm rdp);
RISC=(rx rt)/(rdm rdp);
p19= (rx rt)/(rdm rdp) P;
virus=(rx rt)/(rdm rdp) V;
siRNA=(rx rt kcatD)/(rdm rdp^2) S;
\[CapitalTau]=t/rdp;
a =(rx rt)/(rdm rdp);
b=(rx rt kcatD)/(rdm rdp^2);

1/a*1/rdp*dp19dt//FullSimplify//Expand
1-P-(kcatD P rt rx S v)/(rdm rdp^3)

p1=Solve[dp19dt==0,P]
s1=Solve[b*rdp*dsiRNAdt==0,S]
v1=Solve[a*rdp*dvirusdt==0,V]
(*p2=Expand[1/P/.p1]/.(rt rx)/(rdm rdp^3)->ao/rdp^2
Pss=Simplify[1/p2]*)
{{P->(rdm rdp^3)/(rdm rdp^3+kcatD rt rx S v)}}
{{S->(rdm rdp^2)/(rdm rdp rds+P rt rx v)}}
{{V->(KDR rdm^3 rdp^3)/(KDR rdm^3 rdp^3+kcatD kcatR rt^2 rx^2 S)}}

Preduce=1/(1+(kcatD rt rx S v)/(rdm rdp^3))/.(rt rx)/(rdm rdp^3)->ao/rdp^2/.ao  v->v
Sreduce=1/(rds/rdp+(P rt rx v)/(rdm rdp^2))/.(rt rx)/(rdm rdp^2)->ao/rdp/.rds/rdp-
>\[Beta]/.ao v->v
Vreduce=1/(1+(kcatD kcatR rt^2 rx^2 S)/(KDR rdm^3 rdp^3))/.(kcatD kcatR rt^2
rx^2)/(KDR rdm^3 rdp^3)->\[Alpha]
1/(1+(kcatD S v)/rdp^2)
1/((P v)/rdp+\[Beta])
1/(1+S \[Alpha])

Sreduce2=Sreduce/.P->Preduce
1/(v/(rdp (1+(kcatD S v)/rdp^2))+\[Beta])
```

```
Ssolve=Solve[S==Sreduce2, S]//Flatten
{S->(kcatD v-rdp v-rdp^2 \[Beta]-Sqrt[4 kcatD rdp^2 v \[Beta]+(-kcatD v+rdp v+rdp^2
\[Beta])^2])/(2 kcatD v \[Beta]),S->(kcatD v-rdp v-rdp^2 \[Beta]+Sqrt[4 kcatD rdp^2 v
\[Beta]+(-kcatD v+rdp v+rdp^2 \[Beta])^2])/(2 kcatD v \[Beta])}

Vp1=Vreduce/.Ssolve[[1]]/.\[Alpha]->\[Beta] y
Vp2=Vreduce/.Ssolve[[2]]/.\[Alpha]->\[Beta] y
1/(1+(y (kcatD v-rdp v-rdp^2 \[Beta]-Sqrt[4 kcatD rdp^2 v \[Beta]+(-kcatD v+rdp
v+rdp^2 \[Beta])^2]))/(2 kcatD v))
1/(1+(y (kcatD v-rdp v-rdp^2 \[Beta]+Sqrt[4 kcatD rdp^2 v \[Beta]+(-kcatD v+rdp
v+rdp^2 \[Beta])^2]))/(2 kcatD v))
(*ylabel=Normalized Fraction of Viral Protien;
xlabel= v (Binding rate constant 1/M00 *second)*)
(*Plot[Evaluate[Vp1/.y->1.22/.\[Beta]->1/.rdp00->.01 kcatD], {v, 0, 200000}]
kcaD =.19 fmol/min (Ma Doudna 2008) so 11.4 moles/s*)
kcatD=11.4;
Vp=1/(1+y);
Plot[Evaluate[Vp2/.y->1.2/.\[Beta]->1/.rdp->.5 kcatD], {v, 0, 200},Frame-
>True,PlotRange->{{0,2 10^2},{.45,.65}},AxesLabel->{v ,P}]

Plot[Evaluate[Vp2/.y->1.22/.\[Beta]->1/.v->1.69 10^8], {rdp, 0, 200 10^4},Frame-
>True,AxesLabel->Automatic,PlotRange->{{0,15 10^2},{.45,1.1}}]

Plot3D[Vp2/.y->1.22/.\[Beta]->1,{v, 0, 1.69 10^10},{rdp, 0, 5 10^7},LabelStyle-
>Directive[Black,Bold,16]]
```

Dissociative Equilibrium Shift

Clear["Global`*"]
There are five species in this Model S,Di,P, SD, SP
And eight potential rate constants k1-k8

The Reaction are as follows
S + Di <-> SD [k1 on , k2 off]
S + P <->SP [k3 on , k4 off]

The Differential Equations are
S=So -SP[t] -SD[t];

Di=Dio -SD[t];
P= Po -SP[t];

SD'[t]=Collect[k1*S* Di -k1*KDd SD[t] ,{SD[t],SP[t]}]
SP'[t]=Collect[k3*S* P -k3*KDp SP[t] ,{SP[t],SD[t]}]

Dio k1 So+k1 SD[t]^2-Dio k1 SP[t]+SD[t] (-Dio k1-k1 KDd-k1 So+k1 SP[t])
k3 Po So-k3 Po SD[t]+(-k3 KDp-k3 Po-k3 So+k3 SD[t]) SP[t]+k3 SP[t]^2

Non-dimensionalize SD[t]=SD $^{*}_{\mathbf{SD}}$, SP[t]=SP $^{*}_{\mathbf{SP}}$, t=t τ
u=SD'[t]/.{SD[t]->x X , SP[t]->y Y, t->t τ};
v=SP'[t]/.{SD[t]->x X , SP[t]->y Y, t->t τ};
w=u*(τ/X)//Expand
z=v*(τ/Y)//Expand
-Dio k1 x τ-k1 KDd x τ-k1 So x τ+(Dio k1 So τ)/X+k1 x^2 X τ+k1 x y Y τ-(Dio k1 y Y τ)/X
-k3 KDp y τ-k3 Po y τ-k3 So y τ+k3 x X y τ+(k3 Po So τ)/Y-(k3 Po x X τ)/Y+k3 y^2 Y τ
If we could let τ=1 /k1 and X=Dio, Y=Po
s=w/.{τ->1 /k1, X->Dio, Y->Po }
q=Collect[z/.{τ->1 /k1, X->Dio, Y->Po }/.{k3/k1->ε},ε]
So-Dio x-KDd x-So x+Dio x^2-Po y+Po x y
(So-Dio x-KDp y-Po y-So y+Dio x y+Po y^2) ε
Now the Nondementionalized equations SD'[t]=s and SP'[t]=q. They depend on known constants Po, Dio, So, and KDd,KDp
At Steady state both s = q= 0 so we will solve for x
f=Solve[s==0,x]
{{x->(Dio+KDd+So-Po y-)/(2 Dio)},{x->(Dio+KDd+So-Po y+)/(2 Dio)}}
s1=Solve[s==0,y]
{{y->(-So+Dio x+KDd x+So x-Dio x^2)/(Po (-1+x))}}
{{y->(-So+Dio x+KDd x+So x-Dio x^2)/(Po (-1+x))}}
s2=y/.s1
Solve[s2*==x*140,x

{{y->(-So+Dio x+KDd x+So x-Dio x^2)/(Po (-1+x))}}
{(-So+Dio x+KDd x+So x-Dio x^2)/(Po (-1+x))}
Plot[s2/.{Dio->do,So->so,KDd->kd,KDp->kp,Po->po},{x,0,1}]

.17/140
2*.17
0.00121429
0.34
Expand[-4 Dio (So-Po y)+(-Dio-KDd-So+Po y)^2]
Dio^2+2 Dio KDd+KDd^2-2 Dio So+2 KDd So+So^2+2 Dio Po y-2 KDd Po y-2 Po So y+Po^2 y^2
We get two values for x or (SD)as a function of y or (SP) so we can plug the two values of x into the equation for y'[t]=q. Then solve for y in terms of only constants.
j1=q/.f[[1]];
j2=q/.f[[2]];
r1=Solve[j1==0,y];
r2=Solve[j2==0,y];
The solutions for y are quite long but we get three values of y for x_1 and three values of y for x_2. So in total we have six steady states. Summarized below:
x_1=A (y), and so y11=a,y12=b,y13=c,
x_2=B (y),and so y21=d,y22=e,y23=g
The steady states are:
[A (a),a],[A (b),b],[A (c),c],
[B (d),d],[B (e),e],[B (g),g]
If we replace the known constant with numbers we get
kd=3.67;kp=.17;
do=140;so=.3810;po=.17;
h1=r1/.{Dio->do,So->so,KDd->kd,KDp->kp,Po->po};
h2=r2/.{Dio->do,So->so,KDd->kd,KDp->kp,Po->po};
For[i=1 ,i<7,i++,
If [i<4,
M[i,1]=f[[1]]/.h1[[i]]/.{Dio->do,So->so,KDd->kd,KDp->kp,Po->po},
M[i,1]=f[[2]]/.h2[[i-3]]/.{Dio->do,So->so,KDd->kd,KDp->kp,Po->po}]]
For[i=1 ,i<7,i++,
If [i<4,
M[i,2]=y/.h1[[i]],
M[i,2]=y/.h2[[i-3]]]]
p=Array[M,{6,2}]
{{{x->0.0068067 -1.05058*10^{-17} I},0.128883 +8.88178*10^{-15} I},{{x->-0.0496608+1.05344*10^{-18} I},47.8008 -8.88178*10^{-16} I},{{x->0.00577486 +1.26077*10^{-17} I},1.00119 -1.06581*10^{-14} I},{{x->1.02639 -2.79191*10^{-19} I},0.128883 +8.88178*10^{-15} I},{{x->1.02497 +2.50639*10^{-20} I},47.8008 -8.88178*10^{-16} I},{{x->1.02637 +3.34352*10^{-19} I},1.00119 -1.06581*10^{-14} I}}
Next we must evaluate the stability of these steady states and look into there relavance. Negative values of x or y would mean negative concentrations and are meaningless.

Values of SD or SP complex greater than 1 (the amount of So) are meaningless as well. Only the first and third steady state satifies this so we will evaluate their stability. Tangent question is this true for all values of Po? (Change Po above in h1 and h2 to see how p changes) See below for full matrix.
For stability we must find the Jacobian of the system and evaluate it at the steady state. ({
{∂s/∂x, ∂s/∂y},
{∂q/∂x, ∂q/∂y}
})xss,yss

s
q
So-Dio x-KDd x-So x+Dio x^2-Po y+Po x y
(So-Dio x-KDp y-Po y-So y+Dio x y+Po y^2) ε
J=({
{D[s,x], D[s,y]},
{D[q,x], D[q,y]}
})
{{-Dio-KDd-So+2 Dio x+Po y,-Po+Po x},{(-Dio+Dio y) ε,(-KDp-Po-So+Dio x+2 Po y) ε}}
Evaluate at the steady state (1)
M[1,1]
Jss1=J/.M[1,1]/.y->M[1,2]/.{Dio->do,So->so,KDd->kd,KDp->kp,Po->po}
{{-142.742-1.43173*10^{-15} I,-0.168843-1.78599*10^{-18} I},{(-121.956+1.24345*10^{-12} I) ε,(-0.343242+1.54899*10^{-15} I) ε}}
If the Trace of Jss (a-d) is less than zero and the determanent of Jss1 (ad-bc)is greater than zero the steady state is Stable.
Tr[Jss1]
Det[Jss1]
(-142.742-1.43173*10^{-15} I)-(0.343242 -1.54899*10^{-15} I) ε
(28.4036 -1.0885*10^{-14} I) ε
Steady state (1) is Stable for Po = 0.17nM
SD=x X = .0068 Dio = .0068 140 nM =0.952 nM
SP=y Y= .13 Po = .13 .17nM =0.0221 nM
Evaluate at the steady state (3)
M[3,1]
M[3,2]
{x->0.00577486 +1.26077*10^{-17} I}
1.00119 -1.06581*10^{-14} I
Jss2=J/.M[3,1]/.y->M[3,2]/.{Dio->do,So->so,KDd->kd,KDp->kp,Po->po}
{{-142.883+1.71827*10^{-15} I,-0.169018+2.14331*10^{-18} I},{(0.166793 -1.49214*10^{-12} I) ε,(-0.191114-1.85869*10^{-15} I) ε}}
If the Trace of Jss (a-d) is less than zero and the determanent of Jss2 (ad-bc)is greater than zero the steady state is Stable.
Tr[Jss2]
Det[Jss2]
(-142.883+1.71827*10^{-15} I)-(0.191114 +1.85869*10^{-15} I) ε

(27.3351 +1.30477*10^{-14} I) ε
Steady state (3) is Stable for Po = 0.17nM
SD=x X = .0057 Dio = .0057 140 nM =0.812 nM
SP=y Y= 1.02 Po = 1 .17nM =0.17 nM
****
Now do we get simular steady states for Po=0, 0.04,0.08,0.16,0.24,0.32,0.64, 1.28, 2.15, 5.12

*Values of y or (SP)
Makes a matrix Y1 with three rows corresponding to the three values of y associated with x1 -> y1, y2, y3, with 9 columns corresponding to y at each value of Po .

```
  Y1= ({
  {y1 (po1), y1 (po2)...},
  {y2 (po1)
   y3 (po1), y2 (po2)...
   y3 (po2)...}
 } )
```

Do the same with Y2 equaling the x2-> y4, y5, y6,

```
     Y2= ({
  {y4 (po1), y4 (po2)...},
  {y5 (po1)
   y6 (po1), y5 (po2)...
   y6 (po2)...}
 } )
```

For Po=0 the value of y is 1/0 an indeterminant so I leave it off.

```
kd=3.67;kp=.17;
do=140;so=1;
po1={ 0.04,0.08,0.16,0.24,0.32,0.64, 1.28, 2.15, 5.12};
For[j=1 ,j<10,j++,
 For[i=1 ,i<4,i++,
  Y1[i,j]=y/.r1[[i]]/.{Dio->do,So->so,KDd->kd,KDp->kp,Po->po1[[j]]};
  Y2[i,j]=y/.r2[[i]]/.{Dio->do,So->so,KDd->kd,KDp->kp,Po->po1[[j]]}]];
```

Use Y1 and Y2 to get the values of x1 (X1) and x2 (X2)for all values of y six steady states for each value of Po (60 in total)

```
X1= ({
    {x1[y1 (po1)], x1[y1 (po2)]...},
    {x1[y2 (po1)]
     x1[y3 (po1)], x1[y2 (po2)]...
     x1[y3 (po2)]...}
  } ) where X2 is similar with x2[y4 (po1)]...
For[j=1 ,j<10,j++,
 For[i=1 ,i<4,i++,
  X1[i,j]=x/.f[[1]]/.y->Y1[i,j]/.{Dio->do,So->so,KDd->kd,KDp->kp,Po->po1[[j]]};
  X2[i,j]=x/.f[[2]]/.y->Y2[i,j]/.{Dio->do,So->so,KDd->kd,KDp->kp,Po->po1[[j]]}; ]]
```

Make a combination matrix with 60 rows and 4 columns which are:

[Po , x, y, Stability] The stability column will say (true or false)

```
Clear[W]
```

Column 1 with only the Po value in use.

```
n=1;
For[k=n;j=0,j<10,j++
  If[k<55,
   For[k=n,k<n+6,k++,
    H[k,1]=po1[[j]]];
   n=k]]
```

Column 2 and 3 with steady values [x,y] respectively

```
n=1;
For[k=n;j=0,j<10,j++
  If[k<55,
   For[k=n,k<n+3,k++,
    If[k==n,
     H[k,2]=X1[1,j];
     H[k+3,2]=X2[1,j];
     H[k,3]=Y1[1,j];
     H[k+3,3]=Y2[1,j]];
    If[k==n+1,
     H[k,2]=X1[2,j];
     H[k+3,2]=X2[2,j];
     H[k,3]=Y1[2,j];
     H[k+3,3]=Y2[2,j]];
    If[k==n+2,
     H[k,2]=X1[3,j];
     H[k+3,2]=X2[3,j]];
    H[k,3]=Y1[3,j];
    H[k+3,3]=Y2[3,j]];
   n=k+3]]
```

Column 4 The stability condition for each steady state. For the Jacobian evaluated at each steady state if the Trace is less than zero and the Determinant is greater than zero the condition is stable (True)

```
For[k=1,k<55,k++,
 W[k]=J/.{x->H[k,2],y->H[k,3]}/.{Dio->do,So->so,KDd->kd,KDp->kp,Po->H[k,1],ε-
>1};
 If[Re[Tr[W[k]]]<0 && Re[Det[W[k]]]>0&&Re[H[k,2]]>0&&Re[H[k,2]]>0,
  H[k,4]="True";,
  H[k,4]="False"];]
```

The Full matrix for Stability Sorted by stability (*negative values of x and y are automatically considered False because they are not biologically relavent)

```
c1=Sort[Array[H,{54,4}],StringLength[#1[[4]]]<StringLength[#2[[4]]]&]//MatrixForm
```

Explicit Time-Dependence of RNA Interference

```
function  proof10

   tspan = [0; 200
   u0 = [0,0,0,0,25,0,0,25,0,0];

[d1,d2,SD,S,D,P,SP,Ago,RISC,mRNA]

[t,u] = ode15s (@f,tspan,u0);
```

```
figure;
% subplot (2,2,4),
plot (t,u (:,1),t,u (:,2),t,u (:,3),t,u (:,4),t,u (:,7),t,u
(:,9),t,u (:,10));
legend('dsRNA_
1','dsRNA_2','SD','siRNA','SP','RISC','mRNA');
xlabel ('Time (hours)');
ylabel ('Concentration (nM)')
% title ('k5=3.6E-6 ; k1=3.6E-6 [nM-1hour-1]');
% title ('kt=792; k1=.01476;k3= 608.4 ;k4 =363.6; *k5 = 0 *
;Kd=3.67;Vmax = kt*u (5);Km = 2800;');
title ('proof5 [Po]=25 nM; dds2/t=10 nM/hour')
% save newstruct.mat u
% save time t
```

```
fid = fopen ('Proof10_p19=0.txt', 'w');
% fprintf (fid,
'tspan\tdsRNA_1\tdsRNA_2\tSD\tsiRNA\tSP\tRISC\tmRNA\n');
% allTheData = [t,u (:,1),u (:,2),u (:,3),u (:,4),u (:,7),u
(:,9),u (:,10)];
% dlmwrite ('Proof10_p19=0.txt', allTheData, '-append'); %
default adds commas
% % dlmwrite ('Proof10_p19=0.txt', allTheData, '\t'
% fclose (fid);
```

```
function dudt = f (t,u)
kt=792;         % hour-1       (0.22 molecules/second = 792
molecules/hour)
k1=.01476;      % nM-1 hour-1 (4.1E-6 nM-1 s-1 = .01476 nM-1
hour-1)
k3= 608.4;      % nM-1 hour-1 (.169 nM-1s-1 = 608.4nM-1 hour-
1)
k4 =363.6;      % hour-1       (.101 s-1= 363.6 hour-1)
k5 = 0.04446;   % nM-1 hour-1 (1.235 nM-1s-1 = .04446 nM-1
hour-1)
Kd=3.67;        % nM
Vmax = kt;%*u (5);% nM / hour   (kt * Do)
Km = 2800;      % nM
k6 = .001;      % nM-2 hour-1
k7 = .001;      % nM-2 hour-1
k8 = .1;        % nM-1 hour-1
h  = .6;      % nM / hour
```

```
j  = .10;
dudt = [Vmax*(u (2)/(Km+u (2)))-Vmax*(u (1)/(Km+u (1)));
          Vmax*(u (10)/(Km+u (10)))-Vmax*(u (2)/(Km+u
          (2)))+ k7*u (9)*u (10);
          Vmax*(u (10)/(Km+u (10)))+Vmax*(u (1)/(Km+u
          (1)))+Vmax*(u (2)/(Km+u (2)))+k1*u (4)*u (5)-
          k1*Kd*u (3)-k5*u (3)*u (6)-k6*u (3)*u (8);
          -k3*u (4)*u (6)+k4*u (7)-k1*u (4)*u (5)+k1*Kd*u
          (3);
          0;
          0;
          k3*u (4)*u (6)-k4*u (7)+k5*u (3)*u (6);
          0;
          k6*u (3)*u (8)-k8*u (9);
          h- k7*u (9)*u (10)];

            % u (1) = d1      % u (6) = P
            % u (2) = d2      % u (7) = SP
            % u (3) = SD      % u (8) = Ago
            % u (4) = S       % u (9) = RISC
            % u (5) = D       % u (10) = mRNA
```

Ternary Complex Formation

```
function  datadicer8o
global k5 k6 k7 k8 k1;
tspan = [0 .25 .5 .75 1 2];
D=[0; 0.16; 0.25; 0.5; 2.5; 5; 10; 20; 50; 100;

200;400;800;1000;10000];
```

```
data1= [0.01551 0.02897 0.03184 0.06967 0.36631 0.54888
0.79121 0.93095 0.93917 0.98475 0.99714];     % Experimental
data for fraction of SD bound from Dicer gel shift assay (no
p19)
error1=[0.00759 0.00741 0.00692 0.03871 0.12943 0.03561
0.15126 0.04014 0.05066 0.00882 2.46E-04];    % Error for
data1
data2= [0.02166 0.01851 0.02311 0.02302 0.02179 0.03181
0.07124 0.18036 0.28608 0.51479 0.73466];     % Experimental
data for fraction of SD bound from Dicer-p19 gel shift assay
(p19=0.16 nM)
error2=[0.00459 0.00259 7.10E-04 1.52E-04 9.77E-05 0.00209

0.10068 0.01508 0.01057 4.17E-04 0.04317]; % Error for data2
```

```
St=.3825; % St=Total concentration of [S] in nM.
    Pt=0.16;   % Pt=Amount of free Dicer p19
SPo=(.4183)*St; % SPo is the determined fraction from
'datafit1.m' the SP fraction 's' at [P]=.16 nM .4183
;[P]=2.56 nM .9376
So=St-SPo;
SDo=0;
SDPo=0;
if Pt<=SPo
    Po=0;
else
     Po=Pt-SPo;
end
k1bar=[.92];
k5bar=[0];
k6bar=[0];
k7bar=[0];
k8bar=[0];

% k1bar=[0:.02:.1];
% k5bar=[11.76];
% k6bar=[4];
% k7bar=[560];
% k8bar=[.92];
tic
for a=1:length (k1bar)
for i=1:length (k5bar)
for j=1:length (k6bar)
for l=1:length (k7bar)
```

```
for n=1:length (k8bar)
    k1=k1bar (a);
    k5=k5bar (i);
    k6=k6bar (j);
    k7=k7bar (l);
    k8=k8bar (n);
    for r=1:1:length (D)          % Increment Dicer conc
        u0 = [0,0,SDo,So,D (r),Po,SPo,SDPo];
%[d1,d2,SD,S,D,P,SP,SDP]
        [t,u] = ode15s (@f,tspan,u0);
    for m=1:1:6;          % Increment time
        q (r,m,i,j,l,n,a)=u (m,3)/(u (m,7)+u (m,3)+u (m,4)+u
(m,8)); % Create matrix "s" containing the value of
SD/(SP+SD+S) where each column is a different time point and
each row is a different Dicer initial concentration.
           if r<=length (data2)
            R (r,m,i,j,l,n,a)= (data2 (r)-q
(r,m,i,j,l,n,a))^2;
        end
        for s=3:1:length (u0);
            U (r,s,m,i,j,l,n,a)=u (m,s);
        end
    end
    end
end
end
end
end
end
save q0 q
save U0 U
save R0 R
toc
```

```
%%
tic
% Loop to determine the best fit for k5-8 by added the
residuals of an entire time point over all Dicer
      % concentrations. min_k5-8 will print out.
     min_residual_fit=1000;

for m=1:1:length (tspan)
    for a=1:length (k1bar)
    for i=1:length (k5bar)
    for j=1:length (k6bar) % Defines the range for k6
    for l=1:length (k7bar) % Defines the range for k7
    for n=1:length (k8bar) % Defines the range for k8
        sum_fit _res=0;
        for r=1:1:length (data2)
        sum_fit _res=sum_fit _res+R (r,m,i,j,l,n,a);
        end
        if sum_fit _res< min_residual _fit
            min_residual _fit=sum_fit _res;
```

```
            min_residual=R (:,m,i,j,l,n,a);
            min_t=tspan (m);
            min_k1=k1bar (a);
            min_k5=k5bar (i);
            min_k6=k6bar (j);
            min_k7=k7bar (l);
            min_k8=k8bar (n);
            v=[i,j,l,n,m,a];
        end
    end
    end
    end
    end
    end
end
save sum_fit _res sum_fit _res
save v0 v
min_residual
dicerfit=[min_t, min_k1, min_k5, min_k6, min_k7, min_k8]
save dicerfit0 dicerfit
toc
```

```
%% TO fit for k1 with Dicer only
k1bar=[.92];
for a=1:1:length (k1bar)
     k1=k1bar (a);
for r=1:1:length (D)
     k5=min_k5; k6=min_k6; k7=min_k7; k8=min_k8; % k1=.45;
u0 = [0,0,0,St,D (r),0,0,0];  %[d1,d2,SD,S,D,P,SP,SDP] in
the pressence of SP
[t,u] = ode15s (@f,tspan,u0);
for m=1:1:6;
qo (r,a,m)= u (m,3)/(u (m,7)+u (m,3)+u (m,4)); % Same as 's'
if r<=length (data1)
Ro (r,a,m)= (data1 (r)-qo (r,a,m))^2;
end
        for s=3:1:length (u0);
            Uo (m,s,r,a)=u (m,s);
        end
end
end
end
save qo qo
save Ro Ro

tic
% Loop to determine the best fit for k5-8 by added the
residuals of an entire time point over all Dicer
      % concentrations. min_k5-8 will print out.
     min_residual_fit=1000;

for m=1:1:length (tspan)
    for a=1:length (k1bar)
```

```
        sum_fit _res=0;
        for r=1:1:length (data1)
        sum_fit _res=sum_fit _res+Ro (r,a,m);
        end
        if sum_fit _res< min_residual _fit
            min_residual _fit=sum_fit _res;
            min_residual=Ro (:,a,m);
            min_to=tspan (m);
            min_k1o=k1bar (a);

            vo=[a,m];
        end
    end
end
save sum_fit _res sum_fit _res
save vo vo
min_residual
dicerfito=[min_to, min_k1o]
save dicerfito dicerfito
toc

%%
figure
axes1 = axes
('Parent',figure,'FontSize',20,'FontName','Arial');
% Uncomment the following line to preserve the Y-limits of
the axes
% ylim ([0 500]);
box ('on');
hold ('all');

plot (D,qo (:,vo (1),vo
(2)),'k','Parent',axes1,'LineWidth',3); %2:.2:length (k1bar)
errorbar (D (1:length
(data1))',data1,error1,'MarkerSize',10,'Marker','o','LineSty
le','none',...
         'LineWidth',1,...
         'Color',[0 0 0],...
         'Parent',axes1);
%%
%%
plot (D,q (:,v (5),v (1),v (2),v (3),v (4),v
(6)),'r','Parent',axes1,'LineWidth',3);
errorbar (D (1:length
(data2))',data2',error2','MarkerSize',25,'Marker','.','LineS
tyle','none',...
         'LineWidth',1,...
         'Color',[1 0 0],...
        'Parent',axes1);

xlabel ('Dicer Concentration
(nM)','FontSize',24,'FontName','Arial');
```

```
ylabel ('Fraction Dicer bound
siRNA','FontSize',24,'FontName','Arial');
title ('open=S+D only (fit black), closed=S+D+P (fit red),
S=1nM, k2=2, k4=2, k5=0','FontSize',12,'FontName','Arial')

hold;
figure
plot (D,U (:,3:8,3,v (1),v (2),v (3),v (4),v
(6)),'LineWidth',3);
legend ('SD','S','D','P','SP','SDP');
xlabel ('Dicer Concentration
(nM)','FontSize',24,'FontName','Arial');
ylabel ('Concentration
(nM)','FontSize',24,'FontName','Arial');
% title ('open=S+D only (fit black), closed=S+D+P (fit red),
S=1nM, k2=2, k4=2, k5=0','FontSize',12,'FontName','Arial')
%%

% D2 = transpose (D)=D' these are equal (All data must be
column vectors to
     % write to file.)

% comment out the next 2 if origin blows up
fid = fopen ('Dicer Best Fit.txt', 'w');
fprintf (fid,
'D\tdata1\terror1\tfit1\tdata2\terror2\tfit2\n');

allTheData = [D,data1',error1', qo (:,vo (1),vo
(2)),data2',error2', q (:,v (5),v (1),v (2),v (3),v (4),v
(6))];
dlmwrite ('Dicer Best Fit.txt', allTheData, '-append'); %
default adds commas
% dlmwrite ('Dicer Best Fit.txt', allTheData, '/t');% No
names with tabs
fclose (fid);

% ------------------------------------------------------------
----------------

function dudt = f (t,u)  % function du/dt = f (t,u)
global k5 k6 k7 k8 k1;
% k1=.45;    % nM-1 hour-1 (4.1E-6 nM-1 s-1 = .01476 nM-1
hour-1)
k2=1.71;   % hour-1 Dicerchase
k3= 608.4; % nM-1 hour-1 (.169 nM-1s-1 = 608.4 nM-1 hour-1)
k4 = 2;    % hour-1 (.06 s-1= 216 hour-1 or .03 min-1 = 2
hour-1)
% k5 =0;    % nM-1 hour-1 (1.235 nM-1s-1 = .04446 nM-1 hour-
1)
Kd=96;     % nM
KD=0.17;   % nM  k4/KD=k3

dudt = [0;0;
```

```
            k1*u (4)*u (5)-k2*u (3)-k5*u (3)*u (6)+k6*u (8);
            -k4/KD*u (4)*u (6)+k4*u (7)-k1*u (4)*u (5)+k2*u
(3);
            -k1*u (4)*u (5)+k2*u (3)-k8*u (7)*u (5)+k7*u (8);
            -k4/KD*u (4)*u (6)+k4*u (7)-k5*u (3)*u (6)+k6*u
(8);
             k4/KD*u (4)*u (6)-k4*u (7)-k8*u (7)*u (5)+k7*u
(8);
             k5*u (3)*u (6)-k6*u (8)+k8*u (7)*u (5)-k7*u
(8);];

% Can not put 'end' to close the function if you are using
global variables*
```

```
                % u (1) = d1        % u (5) = D
                % u (2) = d2        % u (6) = P
                % u (3) = SD
                % u (4) = S         % u (7) = SP
```